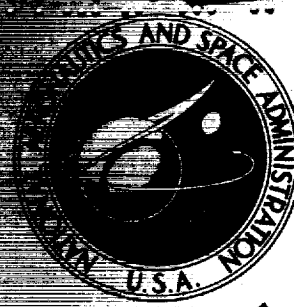


REF ID: A66 12754

**NASA CONTRACTOR
REPORT**



UB
NASA CR-278

**CASE FILE
COPY**

CLASSIFICATION CHANGE
UNCLASSIFIED

By Authority of *NPSP* *12-5-69*

**MEASUREMENTS OF FLOW CHARACTERISTICS
IN A BASIC VORTEX TUBE**

by Arthur Travers and Bruce V. Johnson

Prepared under Contract No. NASw-847 by
UNITED AIRCRAFT CORPORATION
East Hartford, Conn.

for

Declassified by authority of NASA
Classification Change Notices No. **193**
Date **28 FEB 1970**

NATIONAL AERONAUTICS AND SPACE ADMINISTRATION - WASHINGTON, D. C. - JANUARY 1966

1. The first part of the document is a list of names and addresses of the members of the committee. The names are listed in alphabetical order, and the addresses are given in full. The list is as follows:

Mr. J. H. Smith, 123 Main Street, New York, N. Y.
Mr. J. K. Jones, 456 Elm Street, Boston, Mass.
Mr. W. L. Brown, 789 Oak Street, Chicago, Ill.
Mr. R. M. Green, 101 Pine Street, Philadelphia, Pa.
Mr. S. P. White, 202 Cedar Street, Baltimore, Md.
Mr. T. Q. Black, 303 Maple Street, Washington, D. C.
Mr. U. R. Grey, 404 Birch Street, St. Louis, Mo.
Mr. V. S. Blue, 505 Spruce Street, Kansas City, Mo.
Mr. W. T. Red, 606 Ash Street, Omaha, Neb.
Mr. X. Y. Purple, 707 Hickory Street, Denver, Colo.
Mr. Z. A. Gold, 808 Walnut Street, Portland, Ore.
Mr. B. C. Silver, 909 Chestnut Street, San Francisco, Cal.
Mr. D. E. Bronze, 1010 Broadway, New York, N. Y.
Mr. F. G. Iron, 1111 Madison Avenue, New York, N. Y.
Mr. H. I. Steel, 1212 Park Avenue, New York, N. Y.
Mr. J. L. Lead, 1313 Fifth Avenue, New York, N. Y.
Mr. K. M. Tin, 1414 Sixth Avenue, New York, N. Y.
Mr. N. O. Copper, 1515 Seventh Avenue, New York, N. Y.
Mr. P. Q. Nickel, 1616 Eighth Avenue, New York, N. Y.
Mr. R. S. Zinc, 1717 Ninth Avenue, New York, N. Y.
Mr. T. U. Silver, 1818 Tenth Avenue, New York, N. Y.
Mr. V. W. Gold, 1919 Eleventh Avenue, New York, N. Y.
Mr. X. Y. Iron, 2020 Twelfth Avenue, New York, N. Y.
Mr. Z. A. Steel, 2121 Thirteenth Avenue, New York, N. Y.
Mr. B. C. Lead, 2222 Fourteenth Avenue, New York, N. Y.
Mr. D. E. Tin, 2323 Fifteenth Avenue, New York, N. Y.
Mr. F. G. Copper, 2424 Sixteenth Avenue, New York, N. Y.
Mr. H. I. Nickel, 2525 Seventeenth Avenue, New York, N. Y.
Mr. J. L. Zinc, 2626 Eighteenth Avenue, New York, N. Y.
Mr. K. M. Silver, 2727 Nineteenth Avenue, New York, N. Y.
Mr. N. O. Gold, 2828 Twentieth Avenue, New York, N. Y.
Mr. P. Q. Iron, 2929 Twenty-first Avenue, New York, N. Y.
Mr. R. S. Steel, 3030 Twenty-second Avenue, New York, N. Y.
Mr. T. U. Lead, 3131 Twenty-third Avenue, New York, N. Y.
Mr. V. W. Tin, 3232 Twenty-fourth Avenue, New York, N. Y.
Mr. X. Y. Copper, 3333 Twenty-fifth Avenue, New York, N. Y.
Mr. Z. A. Nickel, 3434 Twenty-sixth Avenue, New York, N. Y.
Mr. B. C. Zinc, 3535 Twenty-seventh Avenue, New York, N. Y.
Mr. D. E. Silver, 3636 Twenty-eighth Avenue, New York, N. Y.
Mr. F. G. Gold, 3737 Twenty-ninth Avenue, New York, N. Y.
Mr. H. I. Iron, 3838 Thirtieth Avenue, New York, N. Y.
Mr. J. L. Steel, 3939 Thirty-first Avenue, New York, N. Y.
Mr. K. M. Lead, 4040 Thirty-second Avenue, New York, N. Y.
Mr. N. O. Tin, 4141 Thirty-third Avenue, New York, N. Y.
Mr. P. Q. Copper, 4242 Thirty-fourth Avenue, New York, N. Y.
Mr. R. S. Nickel, 4343 Thirty-fifth Avenue, New York, N. Y.
Mr. T. U. Zinc, 4444 Thirty-sixth Avenue, New York, N. Y.
Mr. V. W. Silver, 4545 Thirty-seventh Avenue, New York, N. Y.
Mr. X. Y. Gold, 4646 Thirty-eighth Avenue, New York, N. Y.
Mr. Z. A. Iron, 4747 Thirty-ninth Avenue, New York, N. Y.
Mr. B. C. Steel, 4848 Fortieth Avenue, New York, N. Y.
Mr. D. E. Lead, 4949 Forty-first Avenue, New York, N. Y.
Mr. F. G. Tin, 5050 Forty-second Avenue, New York, N. Y.
Mr. H. I. Copper, 5151 Forty-third Avenue, New York, N. Y.
Mr. J. L. Nickel, 5252 Forty-fourth Avenue, New York, N. Y.
Mr. K. M. Zinc, 5353 Forty-fifth Avenue, New York, N. Y.
Mr. N. O. Silver, 5454 Forty-sixth Avenue, New York, N. Y.
Mr. P. Q. Gold, 5555 Forty-seventh Avenue, New York, N. Y.
Mr. R. S. Iron, 5656 Forty-eighth Avenue, New York, N. Y.
Mr. T. U. Steel, 5757 Forty-ninth Avenue, New York, N. Y.
Mr. V. W. Lead, 5858 Fiftieth Avenue, New York, N. Y.
Mr. X. Y. Tin, 5959 Fifty-first Avenue, New York, N. Y.
Mr. Z. A. Copper, 6060 Fifty-second Avenue, New York, N. Y.
Mr. B. C. Nickel, 6161 Fifty-third Avenue, New York, N. Y.
Mr. D. E. Zinc, 6262 Fifty-fourth Avenue, New York, N. Y.
Mr. F. G. Silver, 6363 Fifty-fifth Avenue, New York, N. Y.
Mr. H. I. Gold, 6464 Fifty-sixth Avenue, New York, N. Y.
Mr. J. L. Iron, 6565 Fifty-seventh Avenue, New York, N. Y.
Mr. K. M. Steel, 6666 Fifty-eighth Avenue, New York, N. Y.
Mr. N. O. Lead, 6767 Fifty-ninth Avenue, New York, N. Y.
Mr. P. Q. Tin, 6868 Sixtieth Avenue, New York, N. Y.
Mr. R. S. Copper, 6969 Sixty-first Avenue, New York, N. Y.
Mr. T. U. Nickel, 7070 Sixty-second Avenue, New York, N. Y.
Mr. V. W. Zinc, 7171 Sixty-third Avenue, New York, N. Y.
Mr. X. Y. Silver, 7272 Sixty-fourth Avenue, New York, N. Y.
Mr. Z. A. Gold, 7373 Sixty-fifth Avenue, New York, N. Y.
Mr. B. C. Iron, 7474 Sixty-sixth Avenue, New York, N. Y.
Mr. D. E. Steel, 7575 Sixty-seventh Avenue, New York, N. Y.
Mr. F. G. Lead, 7676 Sixty-eighth Avenue, New York, N. Y.
Mr. H. I. Tin, 7777 Sixty-ninth Avenue, New York, N. Y.
Mr. J. L. Copper, 7878 Seventieth Avenue, New York, N. Y.
Mr. K. M. Nickel, 7979 Seventy-first Avenue, New York, N. Y.
Mr. N. O. Zinc, 8080 Seventy-second Avenue, New York, N. Y.
Mr. P. Q. Silver, 8181 Seventy-third Avenue, New York, N. Y.
Mr. R. S. Gold, 8282 Seventy-fourth Avenue, New York, N. Y.
Mr. T. U. Iron, 8383 Seventy-fifth Avenue, New York, N. Y.
Mr. V. W. Steel, 8484 Seventy-sixth Avenue, New York, N. Y.
Mr. X. Y. Lead, 8585 Seventy-seventh Avenue, New York, N. Y.
Mr. Z. A. Tin, 8686 Seventy-eighth Avenue, New York, N. Y.
Mr. B. C. Copper, 8787 Seventy-ninth Avenue, New York, N. Y.
Mr. D. E. Nickel, 8888 Eightieth Avenue, New York, N. Y.
Mr. F. G. Zinc, 8989 Eighty-first Avenue, New York, N. Y.
Mr. H. I. Silver, 9090 Eighty-second Avenue, New York, N. Y.
Mr. J. L. Gold, 9191 Eighty-third Avenue, New York, N. Y.
Mr. K. M. Iron, 9292 Eighty-fourth Avenue, New York, N. Y.
Mr. N. O. Steel, 9393 Eighty-fifth Avenue, New York, N. Y.
Mr. P. Q. Lead, 9494 Eighty-sixth Avenue, New York, N. Y.
Mr. R. S. Tin, 9595 Eighty-seventh Avenue, New York, N. Y.
Mr. T. U. Copper, 9696 Eighty-eighth Avenue, New York, N. Y.
Mr. V. W. Nickel, 9797 Eighty-ninth Avenue, New York, N. Y.
Mr. X. Y. Zinc, 9898 Ninetieth Avenue, New York, N. Y.
Mr. Z. A. Silver, 9999 One hundredth Avenue, New York, N. Y.

2. The second part of the document is a list of the names and addresses of the members of the committee. The names are listed in alphabetical order, and the addresses are given in full. The list is as follows:

Mr. J. H. Smith, 123 Main Street, New York, N. Y.
Mr. J. K. Jones, 456 Elm Street, Boston, Mass.
Mr. W. L. Brown, 789 Oak Street, Chicago, Ill.
Mr. R. M. Green, 101 Pine Street, Philadelphia, Pa.
Mr. S. P. White, 202 Cedar Street, Baltimore, Md.
Mr. T. Q. Black, 303 Maple Street, Washington, D. C.
Mr. U. R. Grey, 404 Birch Street, St. Louis, Mo.
Mr. V. S. Blue, 505 Spruce Street, Kansas City, Mo.
Mr. W. T. Red, 606 Ash Street, Omaha, Neb.
Mr. X. Y. Purple, 707 Hickory Street, Denver, Colo.
Mr. Z. A. Gold, 808 Walnut Street, Portland, Ore.
Mr. B. C. Silver, 909 Chestnut Street, San Francisco, Cal.
Mr. D. E. Bronze, 1010 Broadway, New York, N. Y.
Mr. F. G. Iron, 1111 Madison Avenue, New York, N. Y.
Mr. H. I. Steel, 1212 Park Avenue, New York, N. Y.
Mr. J. L. Lead, 1313 Fifth Avenue, New York, N. Y.
Mr. K. M. Tin, 1414 Sixth Avenue, New York, N. Y.
Mr. N. O. Copper, 1515 Seventh Avenue, New York, N. Y.
Mr. P. Q. Nickel, 1616 Eighth Avenue, New York, N. Y.
Mr. R. S. Zinc, 1717 Ninth Avenue, New York, N. Y.
Mr. T. U. Silver, 1818 Tenth Avenue, New York, N. Y.
Mr. V. W. Gold, 1919 Eleventh Avenue, New York, N. Y.
Mr. X. Y. Iron, 2020 Twelfth Avenue, New York, N. Y.
Mr. Z. A. Steel, 2121 Thirteenth Avenue, New York, N. Y.
Mr. B. C. Lead, 2222 Fourteenth Avenue, New York, N. Y.
Mr. D. E. Tin, 2323 Fifteenth Avenue, New York, N. Y.
Mr. F. G. Copper, 2424 Sixteenth Avenue, New York, N. Y.
Mr. H. I. Nickel, 2525 Seventeenth Avenue, New York, N. Y.
Mr. J. L. Zinc, 2626 Eighteenth Avenue, New York, N. Y.
Mr. K. M. Silver, 2727 Nineteenth Avenue, New York, N. Y.
Mr. N. O. Gold, 2828 Twentieth Avenue, New York, N. Y.
Mr. P. Q. Iron, 2929 Twenty-first Avenue, New York, N. Y.
Mr. R. S. Steel, 3030 Twenty-second Avenue, New York, N. Y.
Mr. T. U. Lead, 3131 Twenty-third Avenue, New York, N. Y.
Mr. V. W. Tin, 3232 Twenty-fourth Avenue, New York, N. Y.
Mr. X. Y. Copper, 3333 Twenty-fifth Avenue, New York, N. Y.
Mr. Z. A. Nickel, 3434 Twenty-sixth Avenue, New York, N. Y.
Mr. B. C. Zinc, 3535 Twenty-seventh Avenue, New York, N. Y.
Mr. D. E. Silver, 3636 Twenty-eighth Avenue, New York, N. Y.
Mr. F. G. Gold, 3737 Twenty-ninth Avenue, New York, N. Y.
Mr. H. I. Iron, 3838 Thirtieth Avenue, New York, N. Y.
Mr. J. L. Steel, 3939 Thirty-first Avenue, New York, N. Y.
Mr. K. M. Lead, 4040 Thirty-second Avenue, New York, N. Y.
Mr. N. O. Tin, 4141 Thirty-third Avenue, New York, N. Y.
Mr. P. Q. Copper, 4242 Thirty-fourth Avenue, New York, N. Y.
Mr. R. S. Nickel, 4343 Thirty-fifth Avenue, New York, N. Y.
Mr. T. U. Zinc, 4444 Thirty-sixth Avenue, New York, N. Y.
Mr. V. W. Silver, 4545 Thirty-seventh Avenue, New York, N. Y.
Mr. X. Y. Gold, 4646 Thirty-eighth Avenue, New York, N. Y.
Mr. Z. A. Iron, 4747 Thirty-ninth Avenue, New York, N. Y.
Mr. B. C. Steel, 4848 Fortieth Avenue, New York, N. Y.
Mr. D. E. Lead, 4949 Forty-first Avenue, New York, N. Y.
Mr. F. G. Tin, 5050 Forty-second Avenue, New York, N. Y.
Mr. H. I. Copper, 5151 Forty-third Avenue, New York, N. Y.
Mr. J. L. Nickel, 5252 Forty-fourth Avenue, New York, N. Y.
Mr. K. M. Zinc, 5353 Forty-fifth Avenue, New York, N. Y.
Mr. N. O. Silver, 5454 Forty-sixth Avenue, New York, N. Y.
Mr. P. Q. Gold, 5555 Forty-seventh Avenue, New York, N. Y.
Mr. R. S. Iron, 5656 Forty-eighth Avenue, New York, N. Y.
Mr. T. U. Steel, 5757 Forty-ninth Avenue, New York, N. Y.
Mr. V. W. Lead, 5858 Fiftieth Avenue, New York, N. Y.
Mr. X. Y. Tin, 5959 Fifty-first Avenue, New York, N. Y.
Mr. Z. A. Copper, 6060 Fifty-second Avenue, New York, N. Y.
Mr. B. C. Nickel, 6161 Fifty-third Avenue, New York, N. Y.
Mr. D. E. Zinc, 6262 Fifty-fourth Avenue, New York, N. Y.
Mr. F. G. Silver, 6363 Fifty-fifth Avenue, New York, N. Y.
Mr. H. I. Gold, 6464 Fifty-sixth Avenue, New York, N. Y.
Mr. J. L. Iron, 6565 Fifty-seventh Avenue, New York, N. Y.
Mr. K. M. Steel, 6666 Fifty-eighth Avenue, New York, N. Y.
Mr. N. O. Lead, 6767 Fifty-ninth Avenue, New York, N. Y.
Mr. P. Q. Tin, 6868 Sixtieth Avenue, New York, N. Y.
Mr. R. S. Copper, 6969 Sixty-first Avenue, New York, N. Y.
Mr. T. U. Nickel, 7070 Sixty-second Avenue, New York, N. Y.
Mr. V. W. Zinc, 7171 Sixty-third Avenue, New York, N. Y.
Mr. X. Y. Silver, 7272 Sixty-fourth Avenue, New York, N. Y.
Mr. Z. A. Gold, 7373 Sixty-fifth Avenue, New York, N. Y.
Mr. B. C. Iron, 7474 Sixty-sixth Avenue, New York, N. Y.
Mr. D. E. Steel, 7575 Sixty-seventh Avenue, New York, N. Y.
Mr. F. G. Lead, 7676 Sixty-eighth Avenue, New York, N. Y.
Mr. H. I. Tin, 7777 Sixty-ninth Avenue, New York, N. Y.
Mr. J. L. Copper, 7878 Seventieth Avenue, New York, N. Y.
Mr. K. M. Nickel, 7979 Seventy-first Avenue, New York, N. Y.
Mr. N. O. Zinc, 8080 Seventy-second Avenue, New York, N. Y.
Mr. P. Q. Silver, 8181 Seventy-third Avenue, New York, N. Y.
Mr. R. S. Gold, 8282 Seventy-fourth Avenue, New York, N. Y.
Mr. T. U. Iron, 8383 Seventy-fifth Avenue, New York, N. Y.
Mr. V. W. Steel, 8484 Seventy-sixth Avenue, New York, N. Y.
Mr. X. Y. Lead, 8585 Seventy-seventh Avenue, New York, N. Y.
Mr. Z. A. Tin, 8686 Seventy-eighth Avenue, New York, N. Y.
Mr. B. C. Copper, 8787 Seventy-ninth Avenue, New York, N. Y.
Mr. D. E. Nickel, 8888 Eightieth Avenue, New York, N. Y.
Mr. F. G. Zinc, 8989 Eighty-first Avenue, New York, N. Y.
Mr. H. I. Silver, 9090 Eighty-second Avenue, New York, N. Y.
Mr. J. L. Gold, 9191 Eighty-third Avenue, New York, N. Y.
Mr. K. M. Iron, 9292 Eighty-fourth Avenue, New York, N. Y.
Mr. N. O. Steel, 9393 Eighty-fifth Avenue, New York, N. Y.
Mr. P. Q. Lead, 9494 Eighty-sixth Avenue, New York, N. Y.
Mr. R. S. Tin, 9595 Eighty-seventh Avenue, New York, N. Y.
Mr. T. U. Copper, 9696 Eighty-eighth Avenue, New York, N. Y.
Mr. V. W. Nickel, 9797 Eighty-ninth Avenue, New York, N. Y.
Mr. X. Y. Zinc, 9898 Ninetieth Avenue, New York, N. Y.
Mr. Z. A. Silver, 9999 One hundredth Avenue, New York, N. Y.

MEASUREMENTS OF FLOW CHARACTERISTICS
IN A BASIC VORTEX TUBE

By Arthur Travers and Bruce V. Johnson

[REDACTED]

Distribution of this report is provided in the interest of information exchange. Responsibility for the contents resides in the author or organization that prepared it.



[REDACTED]

NOTICE

This document should not be returned after it has satisfied your requirements. It may be disposed of in accordance with your local security regulations or the appropriate provisions of the Industrial Security Manual for Safe-Guarding Classified Information.

Prepared under Contract No. NASw-847 by
UNITED AIRCRAFT CORPORATION
East Hartford, Conn.

for

NATIONAL AERONAUTICS AND SPACE ADMINISTRATION

[REDACTED]

... ..

10

1990

[REDACTED]

Measurements of Flow Characteristics

in a Basic Vortex Tube

TABLE OF CONTENTS

	<u>Page</u>
SUMMARY	1
CONCLUSIONS	1
INTRODUCTION	2
EQUIPMENT AND PROCEDURES	3
Equipment	3
Procedures	5
DISCUSSION OF TEST RESULTS WITH PLAIN END WALLS	6
Particle-Trace Results	6
Flow Visualization Results	7
Streamline Patterns	9
DISCUSSION OF TEST RESULTS WITH SUCTION END WALLS	9
End-Wall Suction Distributions	10
Particle-Trace Results	10
Flow Visualization Results	12
REFERENCES	15
LIST OF SYMBOLS	16
APPENDIX - SUPPLEMENTARY FLUID INJECTION STUDIES	18
TABLE I	22
FIGURES	23 -67

[REDACTED]

[REDACTED]

in a Basic Vortex Tube

SUMMARY

An experimental study was conducted to determine the characteristics of confined vortex flows generated in a cylindrical tube by water injection through a single slot extending along the entire length of the tube. Two configurations were tested: a vortex tube with plain end walls and a vortex tube with suction end walls designed to control the interaction between the flow in the end-wall boundary layers and the primary flow. The flow characteristics were determined from photographs of neutrally buoyant plastic particles and dye which were injected as tracer materials.

The flow patterns in the vortex tube with plain end walls were found to be in general agreement with those predicted by a previously developed theory for interacting primary and end-wall boundary layer flows in a vortex tube. It was determined that the primary-flow tangential velocity distributions and the magnitudes of the axial velocities induced in the primary flow by its interaction with the end-wall boundary layers could be reduced by controlling the end-wall boundary layers with distributed end-wall suction.

CONCLUSIONS

1. Distributed suction at the end walls of a vortex tube may be used to control the variation of tangential velocity with radius in the primary-flow region outside the end-wall boundary layers and may be used to minimize the passage of flow from the end-wall boundary layers to the primary flow which would normally occur at small radii without distributed suction.

2. Essentially laminar flow exists at intermediate radii in a vortex tube under certain flow conditions for configurations with either plain or distributed-suction end walls, even though substantial turbulence may exist near the outer periphery of the vortex tube due to the vortex tube injection configuration and/or to the boundary layer on the peripheral wall. For the configuration with plain end walls, essentially laminar flow was observed for low radial inflow velocities in the primary flow and for low radial outflow velocities at intermediate radii in the primary flow.

[REDACTED]

For the configurations with distributed-suction end walls, essentially laminar flow was observed only for low radial inflow velocities in the primary flow.

INTRODUCTION

Determination of the feasibility of gaseous nuclear rocket concepts involving vortex flow for containment of nuclear fuel requires detailed knowledge of confined vortex characteristics over a wide range of conditions. Theoretical studies indicate that one of the major factors influencing the flow in vortex tubes is friction between the flow and the tube end walls. According to theory, this friction produces a secondary flow (the end-wall boundary layers) in which the radial velocity may be of the same order of magnitude as the tangential velocity in the primary flow and orders of magnitude larger than the radial velocity in the primary flow. Theory further indicates that radial variations in the quantity of secondary flow will exist and will be accompanied by axial velocities in the primary-flow region both into and out of the end-wall boundary layers at different radii.

Anderson, in theoretical investigations of confined vortex flows (Refs. 1 and 2), found very strong coupling between the primary and secondary-flow regions with a large amount of flow interchange for some flow conditions. Measurement of flow characteristics in vortex tubes by Cwen, Hale, Johnson and Travers (Ref. 3), Kendall (Ref. 4) and Johnson, Travers and Hale (Ref. 5) substantiate the general characteristics of vortex flows predicted by theory for confined vortices with turbulent end-wall boundary layers (Ref. 2). The importance of the end-wall boundary layers is illustrated by the experimental results, which indicate that more than 90 percent of the total thru-flow entered the end-wall boundary layers in some cases. Reference 5 presented streamline patterns for a test condition in which a recirculation cell existed within the vortex tube. In this recirculation cell flow left the end-wall boundary layer at small radii, moved radially outward and then re-entered the end-wall boundary layer at a larger radius such that the total measured radial flow rate in the end-wall boundary layers at some radii was greater than the total thru-flow. It is evident from these results that substantial axial flow may occur in the primary-flow region of a vortex tube.

The axial velocities in the primary-flow region of the vortex tube are undesirable when the vortex flow is to be utilized for containment of nuclear fuel, and a technique to eliminate or reduce these velocities is needed. Since a secondary flow forms along a stationary wall adjacent to any rotating flow, convection toward the wall will always occur at some radii. Suggestions for preventing the flow from subsequently leaving the boundary layer at other radii have been made in Ref. 6 by Mack (who proposed wall suction) and in Refs. 5 and 7. Results from a momentum-integral analysis discussed in Ref. 5 indicate that increased friction by protrusions from the wall or by wall suction would be equally effective in preventing secondary

flow from re-entering the primary flow. Both of these suggested techniques require that an established secondary flow exist at the outer radius of the region for which the axial flow is to be eliminated by secondary-flow control. The secondary-flow control method utilizing increased wall friction has been investigated experimentally and found to be effective in decreasing the average axial velocities and controlling the circulation distribution within the vortex tube (see Ref. 5).

The objectives of the present investigation were (1) to investigate additional flow conditions with the basic vortex tube geometry employed for the tests reported in Ref. 5; (2) to determine if the distributed-suction technique is effective in controlling the vortex flow characteristics; and (3) to guide concurrent analytical work (Ref. 7).

EQUIPMENT AND PROCEDURES

All equipment and procedures employed, except those related to the suction end walls, are identical to the equipment and procedures employed in the tests described in Ref. 5. However, a description of pertinent information from Ref. 5 is repeated to avoid the necessity of continued reference to that report.

Equipment

Vortex Tube

A transparent-wall vortex tube utilizing water as the working fluid was employed in tests to determine confined vortex flow characteristics. Important dimensional information and features are shown in Figs. 1 and 2. The vortex was driven by the tangential injection of fluid through a single slot extending the full length of the tube. Additional fluid was added and/or removed through the end walls; the flow which was not removed through the end walls was removed through a perforated plate (peripheral bypass screen) located on the peripheral wall of the vortex tube. The three fluid injection and withdrawal configurations employed in the tests are shown in Fig. 3. Fluid was removed from ports located at the center of each end wall (hereafter called thru-flow) in configuration 1. Fluid and dye were injected through the 1-in. dia porous tube and through 1/4-in. ducts located at the center of each end wall in configurations 2 and 3, respectively. Thru-flow injection configurations for other tests with localized fluid injection through the peripheral wall and through the end walls are described in Appendix I.

During the test program, the vortex tube assembly was modified from the configuration shown in Figs. 1 and 2 in order to obtain particle-trace data at radii near the peripheral wall. In the modification, the tube assembly was reoriented

[REDACTED]

to move the injection slot from the bottom of the tube to the rear of the tube, as viewed from the operator's control position. Test cases 1 and 2 (see Table I) were run with the configuration shown in Figs. 1 and 2. Cases 3 through 9 were run with the modified vortex tube.

Both plain and suction end walls were employed during the test program. The plain end walls consisted of smooth lucite plates with the thru-flow ports located at the center of each plate. The suction end walls consisted of a perforated plastic screen (3% open area, 0.024-in. dia holes, 0.030 thick), backed with eleven annular plenums. Thru-flow ports were located at the center of each of these end walls. Figure 4 shows the suction end walls both with and without the porous plastic screen, along with pertinent dimensional information. The flow through each plenum was adjusted and measured independently.

Flow Measuring Instrumentation

Measurements of the total flow injected into the vortex tube were made by a turbine flow meter located upstream of the injection slot. The thru-flow rate was determined in a similar manner by monitoring the water flow entering or leaving the center of each end wall. The flow withdrawn through each plenum of the suction end walls was measured with rotameters.

Optical Apparatus

Tangential velocities were determined from time-exposure photographs of neutrally buoyant polystyrene spheres injected into the flow. A sketch of the optical apparatus used to photograph the particles is shown in Fig. 5. The mercury vapor lamp was powered by a 1-kw, d-c power supply. The chopping disc contained 20 or 40 slots, depending on the flashing rate desired, and was driven by a variable-speed d-c shunt motor which allowed the flashing rate to be varied from 60 to 3000 flashes per sec. Intermittent illumination of the suspended particles caused them to appear as a series of streaks on a time exposure. This technique permitted quantitative evaluation of the flow patterns and velocities within a confined vortex without the influence of probes which would tend to disturb the flow.

To select test particles, small quantities of expandable polystyrene spheres were heated and then dispersed in water; those which remained suspended after 30 minutes were drawn off, dried and sized. Particles selected in this manner were almost neutrally buoyant. The particles used in these tests ranged in diameter from 0.033 to 0.078 in. Typical photographs of several particle traces are presented in Fig. 6. The notations on these photographs are discussed in the procedures section.

Flow visualization was also provided by injection of fluorescent dyes. Time-exposure photographs of the dye patterns were taken through the side wall of the vortex tube with lighting through the entire end wall as shown in Fig. 5 (the

chopping wheel was not used). Exposure for these photographs was 1 sec. Micro-flash photographs of dye patterns were taken through the side and end walls of the vortex tube with illumination through an adjustable slit (usually 1/4 in. wide) shown in Fig. 7. The light source employed for these photographs was a 0.1 micro-second flash.

Procedures

Operational

For operation of the vortex tube, water was pumped from a storage tank through the vortex tube and control valves. For tests with plain end walls, the desired flow conditions were obtained by separate adjustment of the valves downstream of the thru-flow ports and valves downstream of the bypass plenum. This provided independent control of the jet and thru-flow Reynolds numbers. For tests with suction end walls, adjustments were also made in the valves controlling the flow passing through each of the eleven annular plenums located in each end wall.

Particle Data Reduction

Particle photographs similar to the upper and lower photographs of Fig. 6 were used to obtain the local axial and tangential velocities within the 10-in. dia water vortex tube. The photographs were read with the aid of a phototelereader and the resulting data were then further reduced to velocity data with the aid of a digital computer. As described below, two data reduction procedures were employed. The single-trace method gave satisfactory tangential velocity results. However, small reading errors were introduced in this method due to photograph misalignment in the telereader and parallax which led to errors in axial velocity of the same order of magnitude as the low axial velocities in the primary-flow region of the basic vortex. A second but more cumbersome technique, a multiple-trace method, eliminated most of these errors in measurement of axial velocities.

Typical particle traces and the location of points employed in the evaluation of the velocities within the vortex tube are shown in Fig. 6. For both trace methods, the axial and radial locations of the particle traces were established from the distances noted on the photographs and from three locating pins (two of which are visible near the top of each photograph in Fig. 6). The tangential velocity was then calculated from the arc distance between points 3 and 4 (points 3 and 4 were arbitrary locations where the dashed particle trace could be clearly seen, as noted on the upper photograph in Fig. 6), the number of dashes between these two points, and the known light flashing rate. In the single-trace method, the axial velocity was then determined from the axial distance between points 1 and 2 and the previously determined tangential velocity (points 1 and 2 were employed rather than 3 and 4 for axial-velocity determination to reduce parallax errors). The direction of particle motion could be determined from the photographs since only

half of the vortex tube was illuminated while particle photographs were being taken. For the multiple-trace method, the distance Δz between each set of traces in the bottom photograph of Fig. 6 was determined and combined with the measured radius and tangential velocity to evaluate the local axial velocity.

DISCUSSION OF TEST RESULTS WITH PLAIN END WALLS

Four flow conditions were studied in the vortex tube with plain end walls to determine the characteristics of this configuration. These tests are an extension of the studies reported in Ref. 5. In addition to defining the basic flow patterns, the tests with plain end walls serve as a basis for evaluation of the effectiveness of the suction end walls. The four test cases chosen for determination of the characteristics of the primary flow (region of flow excluding the end-wall boundary layers) comprise the following: two weak vortex cases each containing a recirculation cell in which the primary radial flow moved inward at large and small radii and outward at intermediate radii (cases 1 and 2 - see Table I); a very weak vortex case (case 3, with zero thru-flow) in which the radial velocity in most of the primary-flow region was radially outward; and a case with fluid injected through a porous tube located along the centerline which increased the radial outflow velocity (case 4). The jet injection velocity was constant for all flow conditions (the differences in jet Reynolds number were caused by differences in water temperature). Table I lists the flow conditions and geometry employed in test cases 1 through 4.

Particle-Trace Results

Circulation distributions calculated from the tangential-velocity data obtained from particle-trace photographs are presented in Figs. 8 and 9 for flow conditions with thru-flow radial Reynolds numbers of 30 and 0, respectively. A fourth-order least-squares curve was fitted to the experimental data and brackets indicating plus and minus one standard deviation of the data points from the least-squares curves are shown on the figures. Cases 1 and 2 were investigated with the vortex tube assembly shown in Fig. 2. The remainder of the tests were made with the modified vortex tube assembly described previously.

The circulation distributions for cases 1 through 4 are presented in Fig. 10 with the three cases from Ref. 5 shown for comparison. The effect of thru-flow radial Reynolds number on circulation level may be observed for seven thru-flow radial Reynolds numbers ranging in value from -3 to 185. The slope of the circulation curves between radii of 2 and 4 in. increases with decreasing thru-flow radial Reynolds numbers but decreases with decreasing Reynolds number in the central region of the vortex tube ($r < 2$ in.). Figure 11 presents the tangential velocity profiles for the above seven cases.

Flow oscillations and low axial velocities, similar to those reported in Ref. 5, occurred in these tests. This led to scatter in the particle velocity data (± 0.01 ft/sec) which was the same order of magnitude or larger than the small axial velocities which were to be determined and prohibited plotting of axial velocity profiles which convey any pertinent information. (See Fig. 44, Ref. 5, for axial velocity profiles presented with the above mentioned scatter.)

Flow Visualization Results

Time Sequence Photographs

Photographs of the vortex tube with thru-flow radial Reynolds numbers of 60, 30 and -3 are shown in Figs. 12, 13 and 14 for selected times after the cessation of dye injection. At a thru-flow radial Reynolds number of 60 (Fig. 12), the dye was injected into the boundary layer on each end wall at the periphery of the vortex tube and was carried radially inward for some distance by the end-wall boundary layer flow; a portion of the dye then re-entered the primary flow at a radius less than 3.0 in. As the dye spread axially, it formed a set of fronts which moved toward the midplane of the vortex tube from both end walls. At 6.25 min after dye injection, the fronts from both end walls closely approached each other, outlining the shape of two recirculation cells. A narrow annulus of dye near the outer radius of the left dye front can be seen starting to overlap the right dye pattern. At 7.75 min the left cell had cross-fed dye to the right recirculation cell. After 20.75 min most of the dye in the left dye cell has been lost by convection to the right dye cell and to the left wall boundary layer. Note that the dye pattern was well defined and did not diffuse rapidly for $r < 3.0$ in. According to Ref. 5 this indicates a ratio of turbulent to laminar viscosity less than one.

Figure 13 shows the same process occurring for a thru-flow radial Reynolds number of 30; however, the recirculation cells appear to be more diffuse than for the $Re_{r,t} = 60$ case, and the radius of the radial stagnation surface (outer radius of dye pattern where $V_r = 0$) has increased from a radius of 3.0 in. to 3.5 in. The cross-feeding of dye from the left dye cell to the right dye cell proceeds more rapidly than for the $Re_{r,t} = 60$ case.

For case 4, which had a thru-flow radial Reynolds number of -3 (Fig. 14), water was continuously injected through a 1-in. dia porous tube located along the centerline. This water was momentarily colored by pulsed injection of dye to permit flow visualization. The dye moved radially in an irregular motion, and after 1.5 min it had reached the outer wall at some axial stations, indicating a rapid radial outflow.

The radius of the radial stagnation surface for cases 1 and 2 and for a case taken from Ref. 5 (thru-flow radial Reynolds number of 96) are plotted in Fig. 15

along with the comparable theoretical curve (calculated from the analytical results of Ref. 2). The change in the radius of the radial stagnation surface with thru-flow Reynolds number is in good agreement with the theory; however, the values are lower.

Microflash Photographs

Photographs of dye patterns were taken through the side and end walls of the vortex tube by use of 0.1-microsecond duration light flashes (see Fig. 7 for details of the camera arrangement). Photographs at thru-flow radial Reynolds numbers of 60 and 30, presented in Figs. 16 and 17, were taken after several pulses of dye had been injected into the vortex tube. For both cases, the dye near the peripheral wall was very diffuse, indicating a turbulent flow, which was probably the result of both the injection geometry of the slot through which the fluid to drive the vortex was injected and the turbulent boundary layer which formed on the concave peripheral wall of the vortex tube. (It should be noted that the horizontal streaks between radii of 4 and 5 in. result from light reflections, not dye filaments.) The upper photographs in both figures show that a turbulent region also existed near the end walls. The bottom photographs in each figure and the dye photographs in Figs. 12 and 13 indicate the existence of a radial stagnation surface ($r = 3.0$ and 3.5 , respectively) inside of which there exists cell flow with essentially laminar dye patterns. The cell pattern for a thru-flow Reynolds number of 30 appears to be more diffuse than the cell pattern for a thru-flow Reynolds number of 60.

Microflash photographs of dye patterns taken at a thru-flow radial Reynolds number of 0 are presented in Figs. 18a and 18b. The photographs in Fig. 18a, taken through the vortex tube end wall, show the existence of a series of small vortices distributed in two annular arrays at radii of approximately 2 and 3 in. These secondary vortices apparently form as a result of the shear of the fluid with high angular momentum outside of this region on the low angular momentum, inner fluid (see Fig. 10 for circulation distributions). Although the axes of these secondary vortices appear to be parallel to the axis of rotation of the general flow field, they apparently do not extend the full length of the vortex tube since the photographs taken through the side wall of the vortex tube (Fig. 18b) indicate a non-uniform dye distribution in the axial direction at about the radii of the secondary vortices. These secondary vortices therefore appear to be associated with the existence of small three-dimensional recirculation cells. Apparently as a result of these small cells, the flow is turbulent even in the central region of the vortex tube in contrast to the laminar flows which occur for higher thru-flow radial Reynolds numbers. The secondary vortices described here are similar to those discussed in Ref. 8.

Streamline Patterns

Low Positive Thru-Flow Radial Reynolds Numbers (Cases 1 and 2)

The streamline patterns for case 2 ($Re_{r,t} = 30$) are illustrated in the sketch shown in Fig. 19. The streamline pattern for case 1 would be similar. The streamlines were drawn on the basis of information obtained from photographs of dye patterns and the observed movement of neutrally buoyant particles. They indicate that flow moved inward to a radius of 3.5 in. where a radial stagnation surface was formed, implying that the entire radial flow corresponding to $Re_{r,t} = 30$ was in the end-wall boundary layers at this radius. Flow left the end-wall boundary layers between $r = 1.75$ in. and 2.5 in. and re-entered the end-wall boundary layers between $r = 2.5$ and 3.5 in., indicating a radial outflow region (i.e., a recirculation cell) from $r = 1.75$ in. to 3.5 in. Note that the left cell cross-fed fluid to the right cell as shown in the photographs of the dye patterns in Fig. 13. At radii less than 1.75 in. the flow left the end-wall boundary layers and entered the high-axial-velocity central core located inside the thru-flow exhaust radius.

Zero and Negative Thru-Flow Radial Reynolds Numbers (Cases 3 and 4)

The circulation profiles for cases 3 and 4 (Fig. 10), along with the photographs of the dye patterns for case 4 (Fig. 14), indicate that the radial velocity in the central region of the vortex was outward. A sketch of the streamlines for case 3 ($Re_{r,t} = 0$), presented in Fig. 20, illustrates how flow left the end-wall boundary layer between radii of 0 and 3.5 in. and re-entered the end-wall boundary layer between 3.5 and 5 in., thereby tracing out a recirculation cell. The region of radial outflow extends from a radius of zero to nearly 5.0 in. The streamlines for case 4, in which fluid was added at the centerline, would be similar with the exception that the radial velocities would be increased.

DISCUSSION OF TEST RESULTS WITH SUCTION END WALLS

As stated previously, the flow patterns in a basic vortex tube with smooth, flat end walls have axial velocities in the primary-flow region which are undesirable when nuclear fuel is to be contained within the vortex. As discussed in Ref. 7, it is impossible to eliminate convection into the end-wall boundary layers near the peripheral wall by the application of distributed friction or distributed suction at the end walls. However, at radii less than those at which the maximum secondary flow occurs it is possible to control the boundary layer by these techniques and prevent outflow into the primary-flow region, thus eliminating convection in the central region of the vortex. The purpose of the present tests with end-wall suction was to decrease or eliminate the axial velocities in the central portion of the primary-flow region for several different radial flow rates in the

[REDACTED]

primary flow. The desired patterns in the primary-flow region included radial flow inward, radial flow outward, and the intermediate condition of no radial flow, which results in solid-body rotation of the primary flow. Distributed end-wall suction has been employed in the tests described in this report to provide the required flow control. Tests using distributed-friction end walls are described in Ref. 5.

End-Wall Suction Distributions

In each test, the suction distribution for a particular desired primary-flow characteristic was established by injecting dye into the vortex tube near the end walls and observing the dye movement; the suction distribution was progressively altered until there was a minimum of dye interchange between the primary and secondary-flow regions. The resulting suction flow distributions for cases 5 through 8 are presented in Fig. 21. For cases 5 and 6 there was radial flow inward, for case 7, the primary-flow radial Reynolds number was approximately zero (solid-body rotation), and for case 8 there was radial flow outward. To provide the radial out-flow, fluid was injected through 1/4-in. dia ports located at the center of each end wall (thru-flow configuration 3, Fig. 3) at an equivalent radial Reynolds number of -3. From Fig. 21, the sum of the thru-flow and suction flow withdrawn through the entire end wall can be seen to be much larger for the cases with radial flow inward than for the flow conditions with solid-body rotation or radial flow outward.

The effect of increased jet Reynolds numbers (case 9 with suction distribution E) on the total suction flow required is shown in Fig. 22. The ratio of the total suction flow withdrawn through the end walls for each of the two cases in Fig. 22 is approximately equal to the ratio of the injection jet velocities.

Particle-Trace Results

Tangential Velocity and Circulation Distributions

Typical circulation distributions are shown for a primary flow with the radial velocity inward in Fig. 23 and outward in Fig. 24. Approximately 30 percent of the total data points employed in establishing the solid curves (faired by the least-squares technique) are shown. Those data points not plotted lie close to the curve and could not be shown as individual points. For the data presented in Fig. 23, the standard deviation of the data points from a fifth-order least-squares curve through the data is $0.028 \text{ ft}^2/\text{sec}$. The shape of the circulation profile is similar to that for a moderate-strength vortex without flow control -- see, for example, the curve for $Re_{r,t} = 185$ in Fig. 10. For the data in Fig. 24, the standard deviation of the data points from a fifth-order least-squares curve is $0.022 \text{ ft}^2/\text{sec}$.

[REDACTED]

Data obtained at radii greater than 4 in. for case 6 indicated that the circulation level was greater than the value of 0.75 ft²/sec at r_1 to which the profiles had been faired in Ref. 5, although an equal injection mass-flow rate was used for this and the previous cases. Tangential velocity data for $r = 4.3$ to 4.7 in. indicate that the value of the product $V_\phi r$ at these radii is also a function of the thru-flow Reynolds number and not constant as previously believed. Therefore, the profiles are not extrapolated to a fixed circulation level at $r_1 = 5$ in. but are drawn to the largest radius for which data are available.

A composite set of circulation data curves for the four test conditions at $Re_{t,j} = 118,600$ is shown in Fig. 25. In most cases the circulation distribution can be adequately described by an equation of the form $V_\phi r \propto r^{n_\Gamma}$. When the primary-flow radial Reynolds number is constant at all radii, theoretical solutions with a line source or sink at the centerline indicate that $n_\Gamma = 2 - Re_{r,p}$ if $Re_{r,p}$ is less than unity (see Ref. 7). Thus, theoretically, n_Γ is less than two for radial inflow, equal to two for solid-body rotation, and larger than two for radial outflow. Approximate values of n_Γ and the resulting indicated values of $Re_{r,p}$ for the cases in which the $Re_{r,p}$ is less than unity are shown in the Table in Fig. 25.

The tangential velocity distributions for cases with suction distributions A through D are shown in cartesian coordinates on Fig. 26. The average tangential velocity for suction distribution C is seen to be close to that for solid-body rotation (i.e., velocity increasing linearly with r).

Circulation data obtained with suction distribution E is shown in Fig. 27. The standard deviation of the data points from a fifth-order least-squares curve through the data for this case is 0.043, which is approximately the same fraction of the absolute circulation as for the cases with $Re_{t,j} = 118,600$. To indicate the effect of increased tangential Reynolds number on the circulation distribution, the circulation profiles for suction distributions D and E are compared in Fig. 28. Note that, although the circulation level is higher at all radii for $Re_{t,j} = 346,000$ than for $Re_{t,j} = 118,600$, the circulation varies approximately as r^3 for both cases. The thru-flow radial Reynolds number is -3 in each case.

The effectiveness of end-wall suction in tailoring the primary-flow tangential velocity distributions is indicated in Fig. 29, in which the tangential velocity profiles for cases with approximately equal total radial flow at r_1 with plain and suction end walls are shown for comparison. Note again that the slope of the tangential velocity profile with end-wall suction distribution C corresponds to solid-body rotation. The tangential velocity for case 2 with plain end walls, discussed previously, starts to decrease with decreasing radius for $r < 4$ in., as does V_ϕ for the case with suction end walls, but for case 2 the tangential velocity increases with decreasing radius at $r < 3$ in. to a value higher than the jet injection velocity. This indicates that the effective primary-flow Reynolds number was approximately zero at $r = 4$ in. for both cases, but that this Reynolds number then became larger than zero inside of $r = 4$ in. for case 2 as a result of outflow

[REDACTED]

With radial outflow (suction distribution D), illustrated in Fig. 39, the region with large radial mixing appears to encompass most of the vortex tube. This mixing may be the result of secondary vortexes similar to those shown in Fig. 18 for the vortex tube with plain end walls. Because of the opacity of the suction end walls, it was impossible to secure a good photograph of these secondary vortexes for the present case.

Data obtained at radii greater than 4 in. for case 6 indicated that the circulation level was greater than the value of 0.75 ft²/sec at r_1 to which the profiles had been faired in Ref. 5, although an equal injection mass-flow rate was used for this and the previous cases. Tangential velocity data for $r = 4.3$ to 4.7 in. indicate that the value of the product $V_\phi r$ at these radii is also a function of the thru-flow Reynolds number and not constant as previously believed. Therefore, the profiles are not extrapolated to a fixed circulation level at $r_1 = 5$ in. but are drawn to the largest radius for which data are available.

A composite set of circulation data curves for the four test conditions at $Re_{t,j} = 118,600$ is shown in Fig. 25. In most cases the circulation distribution can be adequately described by an equation of the form $V_\phi r \propto r^{n_\Gamma}$. When the primary-flow radial Reynolds number is constant at all radii, theoretical solutions with a line source or sink at the centerline indicate that $n_\Gamma = 2 - Re_{r,p}$ if $Re_{r,p}$ is less than unity (see Ref. 7). Thus, theoretically, n_Γ is less than two for radial inflow, equal to two for solid-body rotation, and larger than two for radial outflow. Approximate values of n_Γ and the resulting indicated values of $Re_{r,p}$ for the cases in which the $Re_{r,p}$ is less than unity are shown in the Table in Fig. 25.

The tangential velocity distributions for cases with suction distributions A through D are shown in cartesian coordinates on Fig. 26. The average tangential velocity for suction distribution C is seen to be close to that for solid-body rotation (i.e., velocity increasing linearly with r).

Circulation data obtained with suction distribution E is shown in Fig. 27. The standard deviation of the data points from a fifth-order least-squares curve through the data for this case is 0.043, which is approximately the same fraction of the absolute circulation as for the cases with $Re_{t,j} = 118,600$. To indicate the effect of increased tangential Reynolds number on the circulation distribution, the circulation profiles for suction distributions D and E are compared in Fig. 28. Note that, although the circulation level is higher at all radii for $Re_{t,j} = 346,000$ than for $Re_{t,j} = 118,600$, the circulation varies approximately as r^3 for both cases. The thru-flow radial Reynolds number is -3 in each case.

The effectiveness of end-wall suction in tailoring the primary-flow tangential velocity distributions is indicated in Fig. 29, in which the tangential velocity profiles for cases with approximately equal total radial flow at r_1 with plain and suction end walls are shown for comparison. Note again that the slope of the tangential velocity profile with end-wall suction distribution C corresponds to solid-body rotation. The tangential velocity for case 2 with plain end walls, discussed previously, starts to decrease with decreasing radius for $r < 4$ in., as does V_ϕ for the case with suction end walls, but for case 2 the tangential velocity increases with decreasing radius at $r < 3$ in. to a value higher than the jet injection velocity. This indicates that the effective primary-flow Reynolds number was approximately zero at $r = 4$ in. for both cases, but that this Reynolds number then became larger than zero inside of $r = 4$ in. for case 2 as a result of outflow

from the boundary layer. This outflow was eliminated by suction distribution C which made it possible to maintain solid-body rotation throughout the primary flow.

Suction-to-Tangential-Velocity Ratios

The variation of the ratio of end-wall suction velocity to local tangential velocity with radius is presented in Figs. 30 through 32 for suction distributions A through E. Distributions of the ratio of suction velocity to local tangential velocity for the two cases with radial inflow (Fig. 30) are similar in shape but the ratio for suction distribution A is slightly higher at radii less than 2.5 in. The suction was commenced at a larger radii with radial outflow and solid-body rotation (Figs. 31 and 32) than with radial inflow (Fig. 30). The suction velocity ratios for radial outflow at two different jet Reynolds numbers (Fig. 32) are approximately identical, which indicates that the required ratio of wall-suction velocity to local tangential velocity is independent of circulation level.

It is of interest to compare the distribution of flow withdrawn through the end walls for suction distribution C with the results of the analysis of Ref. 7 for solid-body rotation. For the analysis, the skin-friction coefficient is expressed as $C_{ft} = C_{ft,0} + \xi (2U_{z,w} / V_\phi)$, where $C_{ft,0}$ is a friction coefficient for a smooth, flat wall (independent of radius), $2U_{z,w} / V_\phi$ is analogous to the flat-plate asymptotic skin-friction coefficient, and ξ is a parameter which describes the effectiveness of suction in increasing the skin-friction coefficient. A second parameter required in the analysis (denoted K_7) is the ratio of the average angular momentum per unit mass in the secondary flow to that in the primary flow. The theoretical variation of the ratio of the secondary flow in the end-wall boundary layer to the boundary layer flow at the radius where flow control is commenced is shown in Fig. 33 for solid-body rotation and values of $\xi / K_7 = 1.10, 1.25, 1.50$ and 2.00 . The experimental data have been made nondimensional with respect to $r_6 = 4.5$ in. and the sum of the thru-flow and suction flow through the end wall to facilitate the comparison. The comparison indicates the equivalent ξ / K_7 value probably changes from approximately 1.2 at $r/r_6 = 0.9$ to about 2.0 at $r/r_6 = 0.4$. This could indicate that the boundary layer profiles change with radius and/or suction velocity ratio and are not constant as assumed in the analysis. Further investigations, both theoretical and experimental, are required to clarify this point.

Flow Visualization Results

Time Sequence Photographs

Photographs of dye patterns in the vortex tube at various times after dye injection are shown in Figs. 34, 35 and 36 for suction distributions B, C, and D, respectively. For suction distribution B (primary flow radially inward, Fig. 34), the dye was injected at the peripheral wall and flowed radially inward to the


central region. Radial velocities were determined by evaluating the rate of change in diameter of the cylindrical dye region with time at the axial midplane and were used to calculate a primary-flow radial Reynolds number, $Re_{r,p} = -V_r r / \nu$. The primary-flow radial Reynolds number changed from 104 at $r = 5$ in. to 5 at 3 in., to a minimum value of 2 at 2.3 in. and to 2.5 at 1.0 in. Results from Ref. 5 for a case without flow control and a thru-flow radial Reynolds number of 103 indicate behavior similar to that indicated in Fig. 34 between $r = 5$ in. and $r = 2$ in., but a larger increase in $Re_{r,p}$ at radii less than 2 in. to values greater than 5. The distribution of flow withdrawn through the end walls (Fig. 21) shows that suction was commenced at approximately 3.5 in. for both cases with radial inflow. However, the primary-flow radial Reynolds number determined from the time sequence of dye photographs indicates the minimum flow in the primary-flow region at a radius of 2.2 in. Since the outer suction radius and the minimum primary-flow radius do not coincide, it would indicate wall suction was applied at radii greater than appropriate for this minimum primary-flow rate (see Ref. 7).

For the case with solid-body rotation (Fig. 35), the dye was injected for about 4 sec through 1/4-in. dia ports located at the center of each end wall; then all injection at these ports was stopped. Although the dye diffused rapidly outward, a fraction remained in the vortex tube for a relatively long time (22.75 min). For the case with radial outflow (Fig. 36), dye was injected for about 4 sec through 1/4-in. dia ports located at the center of each end wall (thru-flow injection configuration 2). After the dye was shut off, clear water was continuously injected during the photograph sequence at an equivalent thru-flow Reynolds number of -3. The dye patterns obtained are similar to those with solid-body rotation.

Microflash Photographs

Typical microflash photographs taken at various times after dye injection for suction distributions B, C, and D are presented in Figs. 37, 38, and 39, respectively. The photographs for suction distribution B (radial inflow) in Fig. 37 indicate stratified dye filaments which appear laminar at radii less than 2 in. Between radii of 2 and 3.5 in. small double vortexes with their axes extending circumferentially, also reported in Ref. 5, are superimposed upon the principal rotating flow. These small vortexes appear to be well-defined local perturbations which cause very little mixing of the dye. A pair of vortexes remained well-defined for one or two rotations of the primary flow.

For the case with solid-body rotation (suction distribution C) illustrated in Fig. 38, the dye was not stratified as for suction distribution B, although there were no large-scale turbulent eddies observable at radii less than 3.5 in. However, there must have been a relatively large amount of turbulent mixing within the vortex since the time sequence photographs indicate that the dye mixed very rapidly; thus it is concluded that secondary vortexes which have axes of rotation parallel to the axis of the main vortex caused this mixing. The mixing may vary from one end of the tube to the other since a longer time was required to diffuse the dye in the right side than in the left side of the tube.



With radial outflow (suction distribution D), illustrated in Fig. 39, the region with large radial mixing appears to encompass most of the vortex tube. This mixing may be the result of secondary vortexes similar to those shown in Fig. 18 for the vortex tube with plain end walls. Because of the opacity of the suction end walls, it was impossible to secure a good photograph of these secondary vortexes for the present case.

[REDACTED]

REFERENCES


1. Anderson, Olof: Theoretical Solutions for the Secondary Flow in the End Wall of a Vortex Tube. UAC Research Laboratories Report R-2494-1. November 1961.
2. Anderson, Olof: Theoretical Effect of Mach Number and Temperature Gradient on Primary and Secondary Flow in a Jet-Driven Vortex. Air Force Systems Command Report RTD-TDR-63-1098, Prepared by UAC Research Laboratories. November 1963.
3. Owen, F. S., R. W. Hale, B. V. Johnson, and A. Travers: Experimental Investigation of Characteristics of Confined Jet-Driven Vortex Flows. UAC Research Laboratories Report No. R-2494-2, November 1961. Confidential.
4. Kendall, James M.: Experimental Study of a Compressible Viscous Vortex. JPL Technical Report No. 32-290. June 5, 1962.
5. Johnson, B. V., A. Travers, and R. W. Hale: Measurements of Flow Patterns in a Jet-Driven Vortex. UAC Research Laboratories Report No. RTD-TDR-63-1094, November 1963. Confidential.
6. Mack, Leslie M.: The Laminar Boundary Layer on a Disk of Finite Radius in a Rotating Flow. Part I: Numerical Integration of the Momentum-Integral Equations and Application of the Results to the Flow in a Vortex Chamber. JPL Technical Report No. 32-224, May 20, 1962.
7. Johnson, B. V.: Analysis of Secondary-Flow-Control Methods for Confined Vortex Flow. UAC Research Laboratories Report C-910091-1, September 1964. Confidential.
8. Weske, J. R. and T. M. Rankin: Generation of Secondary Motions in the Field of a Vortex. (University of Maryland) The Physics of Fluids, Vol. 6, No. 10, October 1963.

LIST OF SYMBOLS

A_j	Area of injection slot at vortex tube periphery, ft^2
L	Length of vortex tube, ft
Q_j	Volumetric flow rate of injection jet which drives vortex, ft^3/sec
Q_s	Volumetric flow rate through suction end walls, ft^3/sec
Q_t	Volumetric flow rate in thru-flow ducts, ft^3/sec
r	Local radius, ft (except where noted)
$Re_{r,p}$	Local radial Reynolds number in primary flow, $V_r r / \nu$, dimensionless
$Re_{r,s}$	Radial Reynolds number based on total suction flow rate, $Q_s / 2 \pi \nu L$, dimensionless
$Re_{r,t}$	Thru-flow radial Reynolds number, $Q_t / 2 \pi \nu L$, dimensionless
$Re_{r,l}$	Radial Reynolds number based on net flow at peripheral wall, $\frac{Q_t + Q_s}{2 \pi \nu L}$, dimensionless
$Re_{t,j}$	Tangential Reynolds number based on average inlet jet velocity, $V_j r_l / \nu = Q_j r_l / (A_j \nu)$, dimensionless
$U_{z,w}$	Wall suction velocity (positive toward wall), ft/sec
V_j	Average jet velocity, Q_j / A_j , ft/sec
V_r	Local radial velocity in primary flow, ft/sec
V_ϕ	Tangential component of velocity in primary flow, ft/sec
z	Distance measured in a direction parallel to the axis of the vortex tube from the axial midplane for basic vortex tube, ft
ν	Kinematic viscosity, ft^2/sec

Subscripts indicating radial stations

l	Outside radius of vortex tube
6	Outside radius for wall suction


10 Outside radius of thru-flow exhaust port

j Radius of injection jet which drives vortex (normally at radial station 1)

APPENDIX

SUPPLEMENTARY FLUID INJECTION STUDIES

In addition to the tests described in the main body of this report, a number of flow visualization tests using various fluid injection techniques were performed in the vortex tube with both plain and suction end walls. The studies were for the purpose of determining the effect on the vortex flow patterns of radial fluid injection through one to three ducts located in the peripheral wall of the vortex tube with plain end walls, tangential fluid injection through six ducts located in each of the suction end walls, and fluid injection through a porous tube positioned along the centerline of the vortex tube when it was equipped with the suction end walls. The above tests were qualitative in nature; therefore, only a short discussion of the results is presented.

Vortex Tube with Plain End Walls

The experimental apparatus for the studies of radial fluid injection through the peripheral wall consisted of three .090-in. dia injection ducts, one located at the midplane and the other two located 5 in. from each end wall. The ducts could be moved radially to obtain various immersion lengths into the vortex tube. Figure 40 shows a sequence of dye photographs for the flow condition tested without supplementary fluid injection and Figs. 41 through 44 demonstrate the effect on this dye pattern of the presence of the ducts with and without supplementary fluid injection through the peripheral wall.

In Fig. 41a the center duct was inserted radially a distance of 1 in. into the vortex tube with no fluid injection except for an initial dye injection pulse. The dye rapidly formed a cylindrical distribution similar to that shown in Fig. 40 with no duct inserted into the flow. The effect of inserting all three ducts 1 in. into the tube with no fluid injection is shown in Fig. 41b; the dye in the tube was from the previous run. It can be seen that the probes had essentially no effect on the pattern. Note that a dye pulse injected from the right end wall (3.25 min) assumed the shape of a cell like that which formed without the ducts. It appears that as long as the ducts are within the turbulent outer region (jet mixing region) away from the location of the radial stagnation surface marked by the dye (surface at which $V_r = 0$) the turbulence caused by the wakes from the ducts is damped and does not extend into the cell region.

Figure 42a illustrates the effect of inserting the center duct a distance of 1.5 in. into the vortex tube; in this case the duct extended into the cell region causing a gross disturbance and changing the dye pattern from a constant-diameter

[REDACTED]

cylinder to two shrinking, conical dye fronts caused by the radial inflow of fluid which has lost angular momentum due to the drag of the duct. In Fig. 42b, all three ducts are inserted 1.5 in. into the vortex tube with no supplementary injection through the ducts and the effect is to cause the vortex to separate into four cell regions.

Figure 43 (a, b and c) shows the effect of increasing amounts of supplementary flow through the center duct (1-in. insertion distance). In Fig. 42a, the supplementary injection of 0.072 gpm (equivalent to a thru-flow Reynolds number of 1.0) has caused a localized disturbance at the axial center of the dye cylinder (radial stagnation surface) and the cylinder has a radius 1/2 in. less than for the case without ducts. Note also that after 12.75 minutes the outer dye cylinder actually splits in two, showing that the disturbance affects a region of large radial extent. As shown in Figs. 43b and 43c, increasing the flow injection rate to .144 gpm and then .216 gpm, respectively, caused a conical shrinking dye front to form. The average radial velocity increased with the injection flow rate.

Figure 44 (a, b and c) demonstrates the effect of progressively increasing amounts of supplementary flow through three ducts (1-in. insertion). In Fig. 44a, the effect of injection at .072 gpm through each duct is to cause the vortex to separate into four regions, each of which has a shrinking cylindrical dye front. Figures 44b and 44c, obtained with injection rates of .144 and .216 gpm through each duct, show essentially the same result, but with two noticeable differences. A very turbulent cell is formed between the outside ducts and the end walls causing the dye in this region to leave the vortex rapidly. In the region between the two outer ducts a radial stagnation surface has formed at a radius of approximately 2 in.

It is interesting to note that the effect on the flow patterns of inserting the center duct 1.5 in. radially into the vortex tube without fluid injection (Fig. 42a) is very similar to the disturbance illustrated in Fig. 43c, where flow was injected through the center duct which was only inserted 1 in. into the flow. Both figures (42a and 43c) show a similar shrinking, conical dye front; however, the one in Fig. 42a has a slightly higher radial velocity.

Although the main effect of inserting the ducts into the flow (with and without fluid injection) is to cause radial inflow in the region of the ducts with a corresponding change in the flow patterns within the vortex tube, it should be noted that the flow inside a radius of approximately 3 in. in all the photographs appears to remain essentially laminar (compare with Fig. 40) except for the region near each end wall, which appears more turbulent. The outer, peripheral region (jet mixing region) remains very turbulent in all cases, as indicated by the diffuse dye clouds.

Vortex Tube with Suction End Walls

As reported in the main body of this report, the flow patterns for case 7 with suction distribution C (solid-body rotation) appear to be somewhat turbulent as shown by the diffuse dye patterns and undulations in the bottom photograph of Fig. 38. It was felt that an increase in the rotational velocities in the core region might stabilize the flow. An attempt was made to increase the rotational velocities by the tangential injection of fluid through each suction end wall.

Each suction end wall was fitted with six equally spaced, tangential injection ducts (0.125-in. dia) slanted at an angle of 14 deg relative to the end-wall surface and located at a radius of 2.5 in. Flow with total equivalent radial Reynolds numbers of 1 to 12 for all twelve ducts was injected into the end-wall boundary layers during tests with suction distribution C. Observation of the dye patterns resulting from the above configuration showed a slight increase in the rotational velocities in the core region; however, the stabilizing effect was insignificant and an increase in turbulence at the end walls was noted due to the injection.

The final series of tests with the suction end walls and supplementary fluid injection employed injection through a 1-in. dia porous tube located along the centerline of the vortex tube (see Fig. 3, configuration 2). These tests were performed to explore the general characteristics of flows with large radial outflow rates. Three suction distributions were used; equal suction rates from only the three outermost plenums (1 gpm, equivalent to a thru-flow Reynolds number of 13, from each plenum), suction from all the plenums at the maximum flow rates measurable with the installed meters, and no suction.

In the tests with suction from the three outer plenums, jet tangential Reynolds numbers from 100,000 to 300,000 and flow rates through the porous tube equivalent to thru-flow Reynolds numbers of 20 to 200 were employed. The dye patterns showed that the dye moved radially out very rapidly, was very diffuse (although the gross turbulent eddies appeared to be smaller than those observed in the tests with suction distributions D and E) and that a large turbulent mixing region existed.

The tests in which flow was withdrawn from all of the plenums in the suction end walls ($Re_{r,t} \cong 120$) were performed at a jet tangential Reynolds number of 100,000 and flow rates through the porous tube, equivalent to radial Reynolds numbers of 20 through 40. A unique instability was observed in these tests. Although dye was injected uniformly around the entire circumference of the porous tube, it moved radially away from the porous tube in two sheets on opposite sides of the porous tube, and these sheets rotated with the flow. At about $r = 2.5$ in. the sheets curled up to form secondary vortexes with axes parallel to the axis of rotation of the primary flow. These dye sheet-secondary vortex combinations extended the complete length of the vortex tube.

[REDACTED]

The tests with no flow withdrawn through the suction end walls were performed at a jet Reynolds number of 100,000 and flow, equivalent to radial Reynolds numbers of 3 to 7, was injected through the porous tube. This case is similar to case 4 reported in the main body of the report except that plain end walls were employed for case 4. The patterns observed in these tests appeared more stable than any other radial outflow case tested. The dye moved radially outward at a rate slower than with other radial outflow cases and remained in the vortex tube for approximately 90 minutes.

TABLE I
CONFIGURATIONS AND FLOW CONDITIONS
FOR TESTS IN 10-INCH DIAMETER WATER VORTEX TUBE

$$Re_{r,i} = Re_{r,t} + Re_{r,s}$$

CASE	END WALL CONFIGURATION	THRU-FLOW WITHDRAWAL OR INJECTION CONFIGURATION (SEE FIG. 3)	SUCTION DISTRIBUTION (SEE FIGS. 21 & 22)	$Re_{r,t}$	$Re_{r,s}$	$Re_{r,i}$	$Re_{t,i}$	V_j FT/SEC
1	PLAIN END WALLS	1	—	60	—	60	118,600	3.16
2		1	—	30	—	30	118,600	3.16
3		1	—	0	—	0	102,800	3.16
4		2	—	-3	—	-3	102,800	3.16
5	SUCTION END WALLS	1	A	42.6	83.1	125.7	118,600	3.16
6		1	B	45.7	58.3	104.0	118,600	3.16
7		1	C	2.0	22.8	24.8	118,600	3.16
8		3	D	-3.0	19.3	16.3	118,600	3.16
9		3	E	-3.0	55.7	52.7	346,000	9.22

GEOMETRY OF VORTEX TUBE EMPLOYED IN TESTS

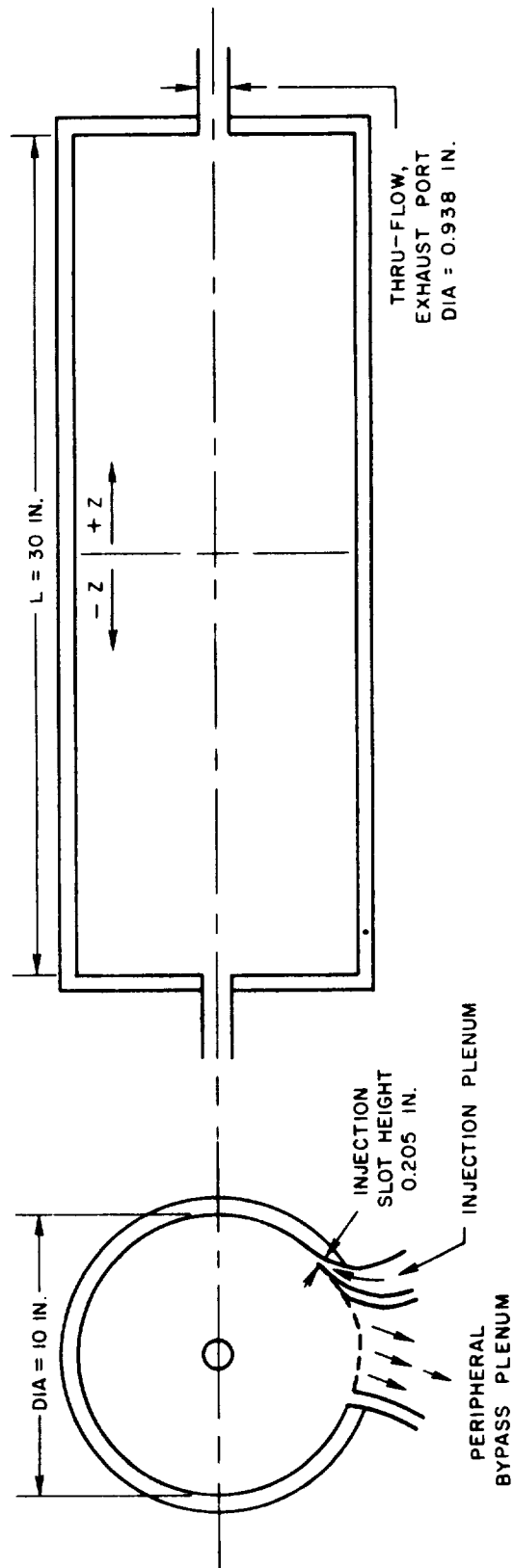
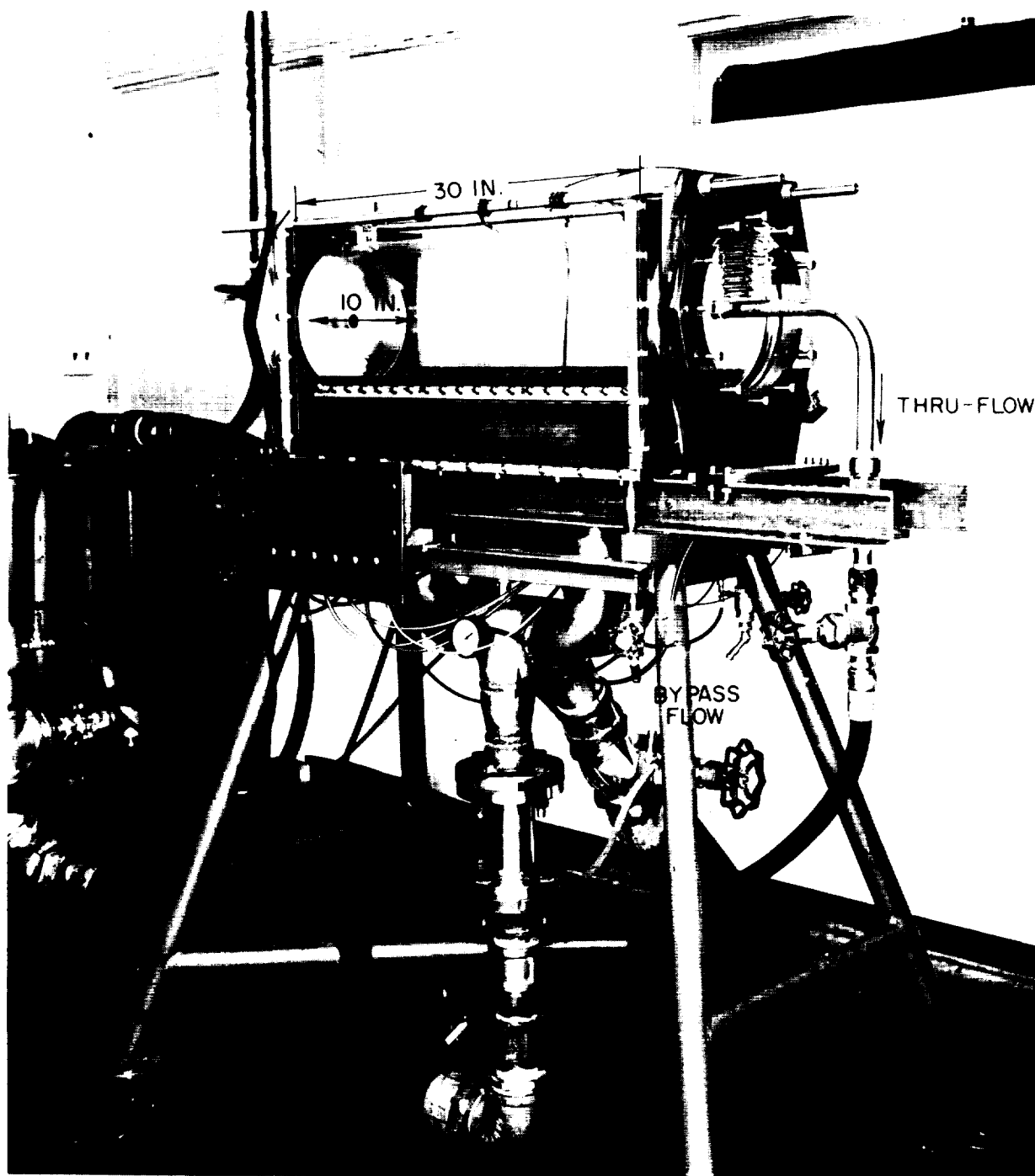


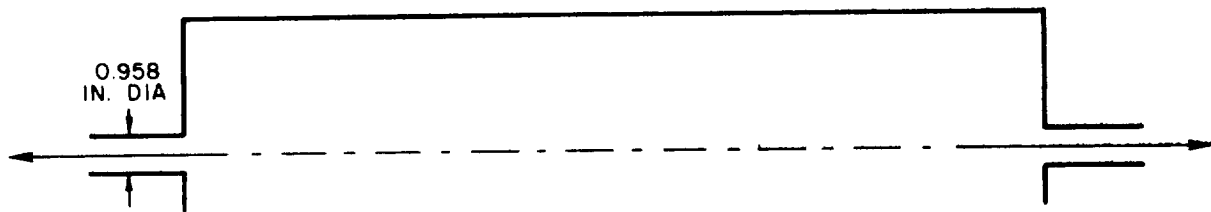
FIG. 1

FIG. 2

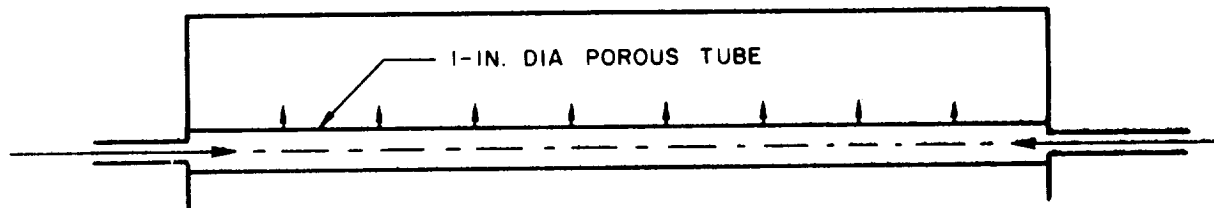
PHOTOGRAPH OF 10-INCH DIAMETER WATER VORTEX TUBE



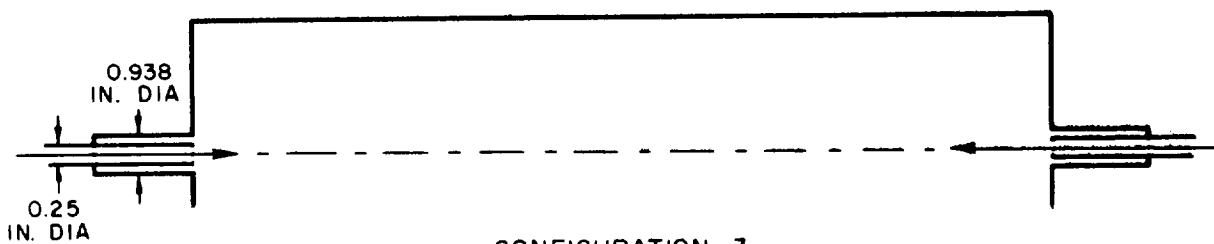
SKETCHES OF THRU-FLOW INJECTION AND WITHDRAWAL CONFIGURATIONS



CONFIGURATION 1



CONFIGURATION 2



CONFIGURATION 3

PHOTOGRAPHS OF SUCTION END WALLS

3/8 IN. PLENUM WIDTH



WITHOUT SCREEN



WITH SCREEN

OPTICAL SYSTEM USED TO OBTAIN DYE AND PARTICLE-TRACE PHOTOGRAPHS

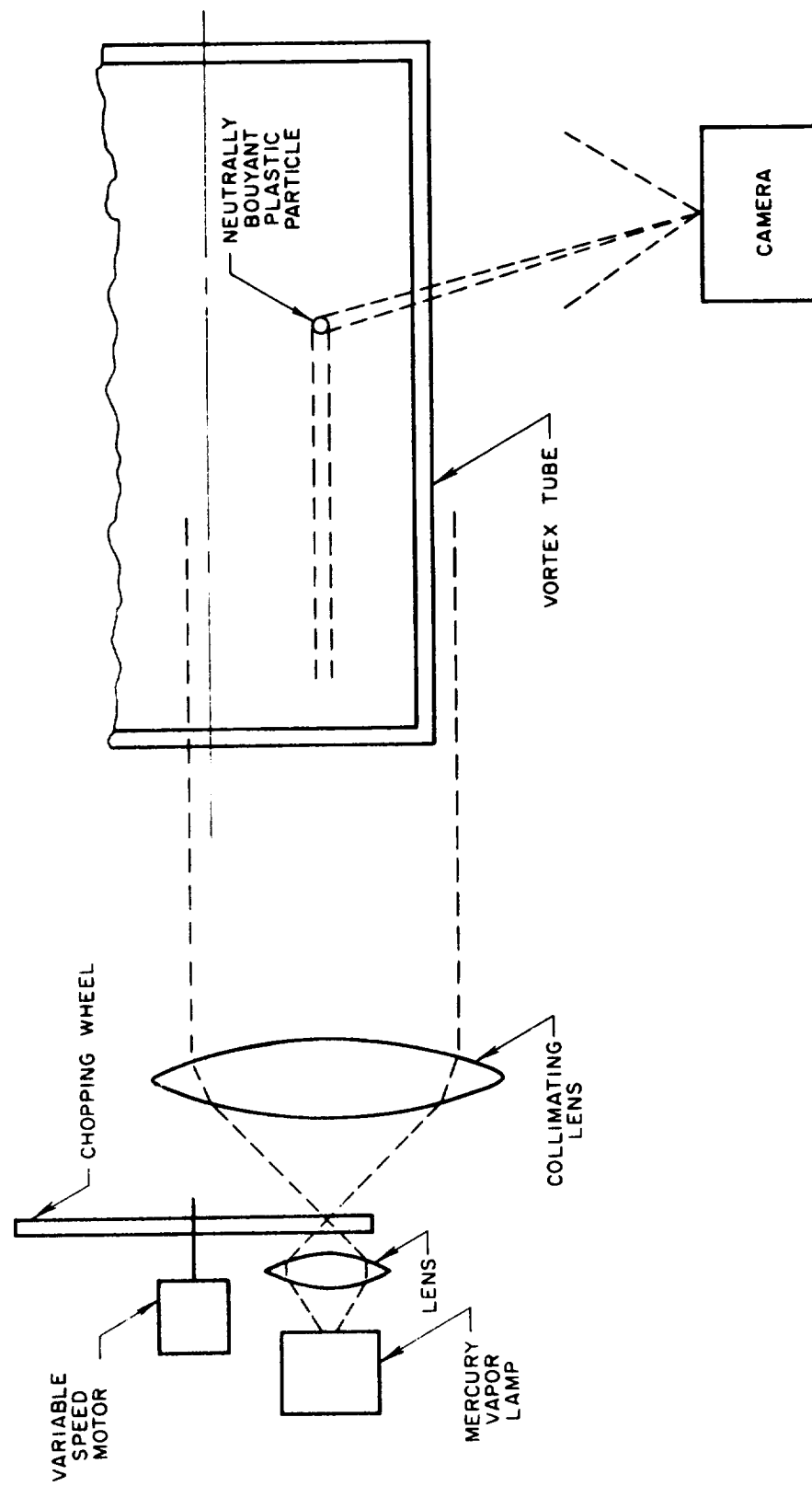
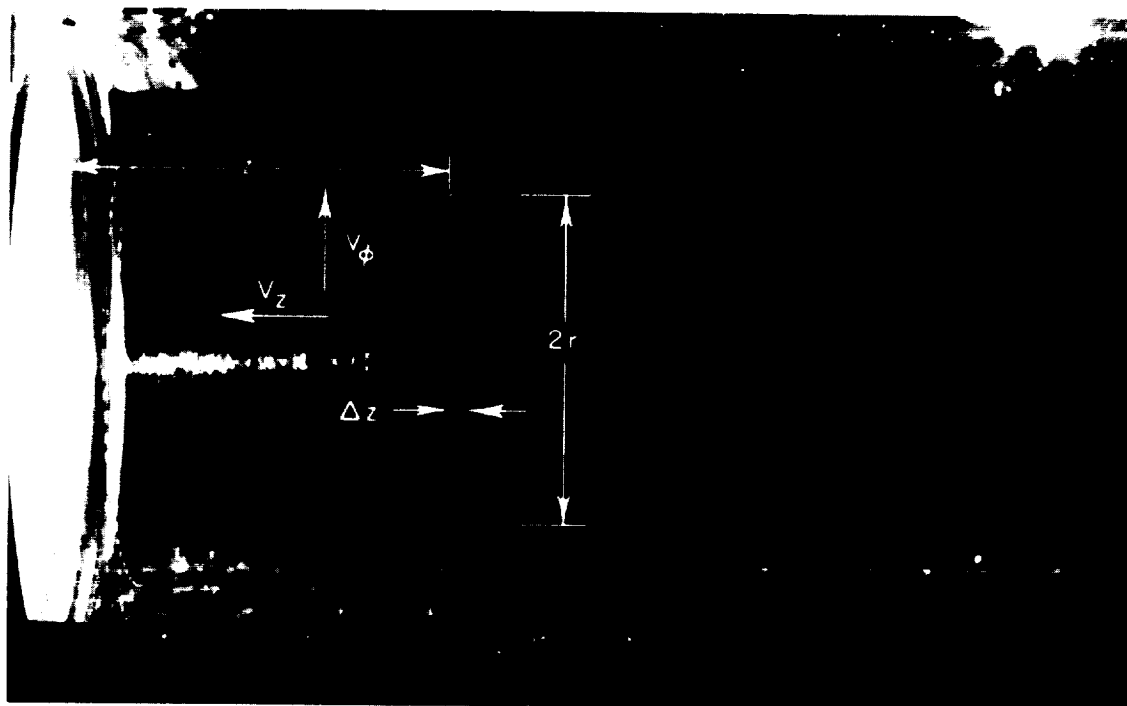
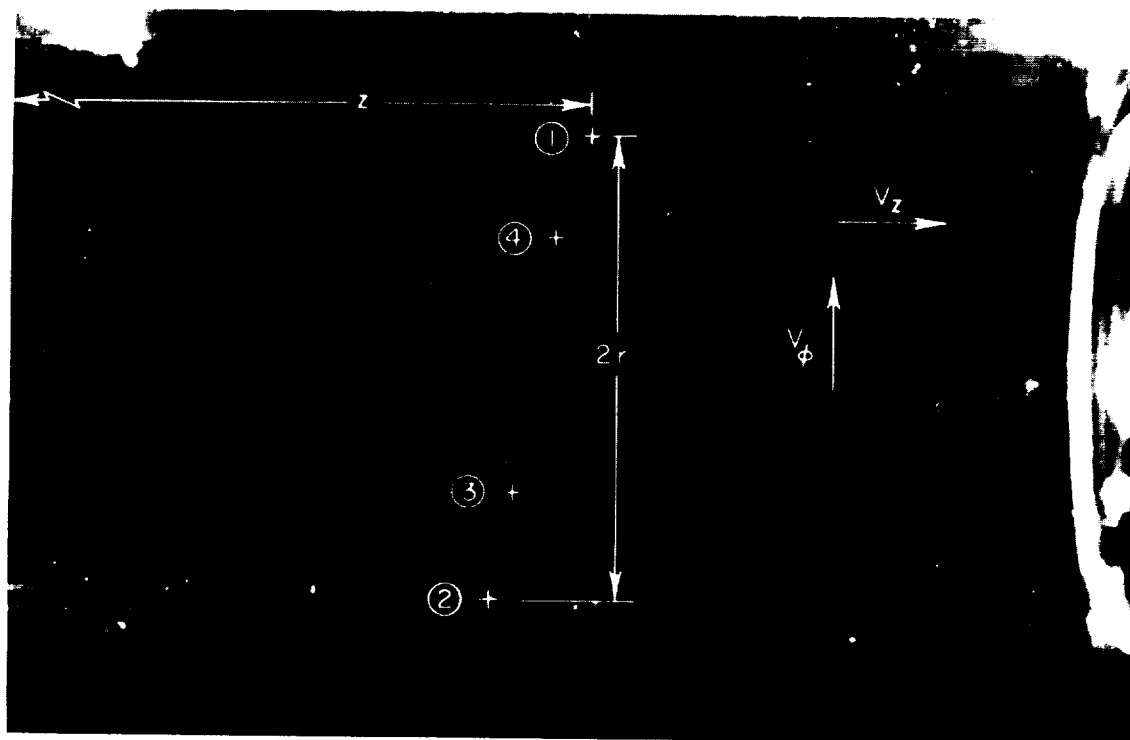
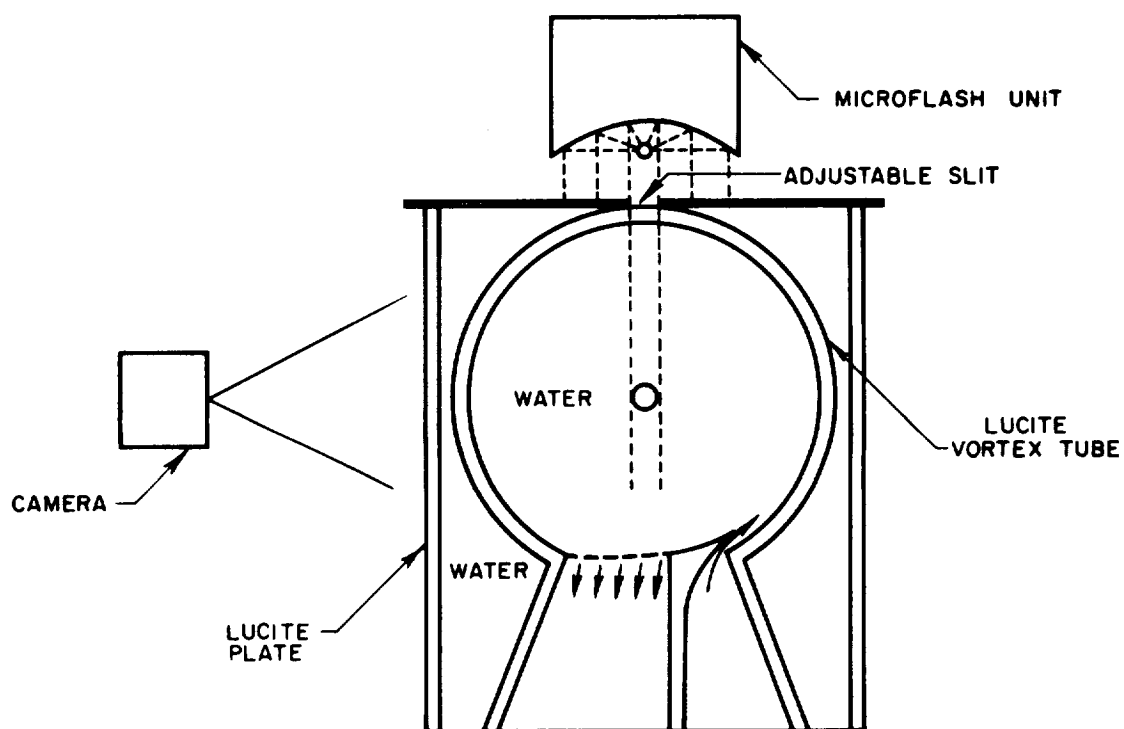


FIG. 5

TYPICAL PARTICLE - TRACE PHOTOGRAPHS



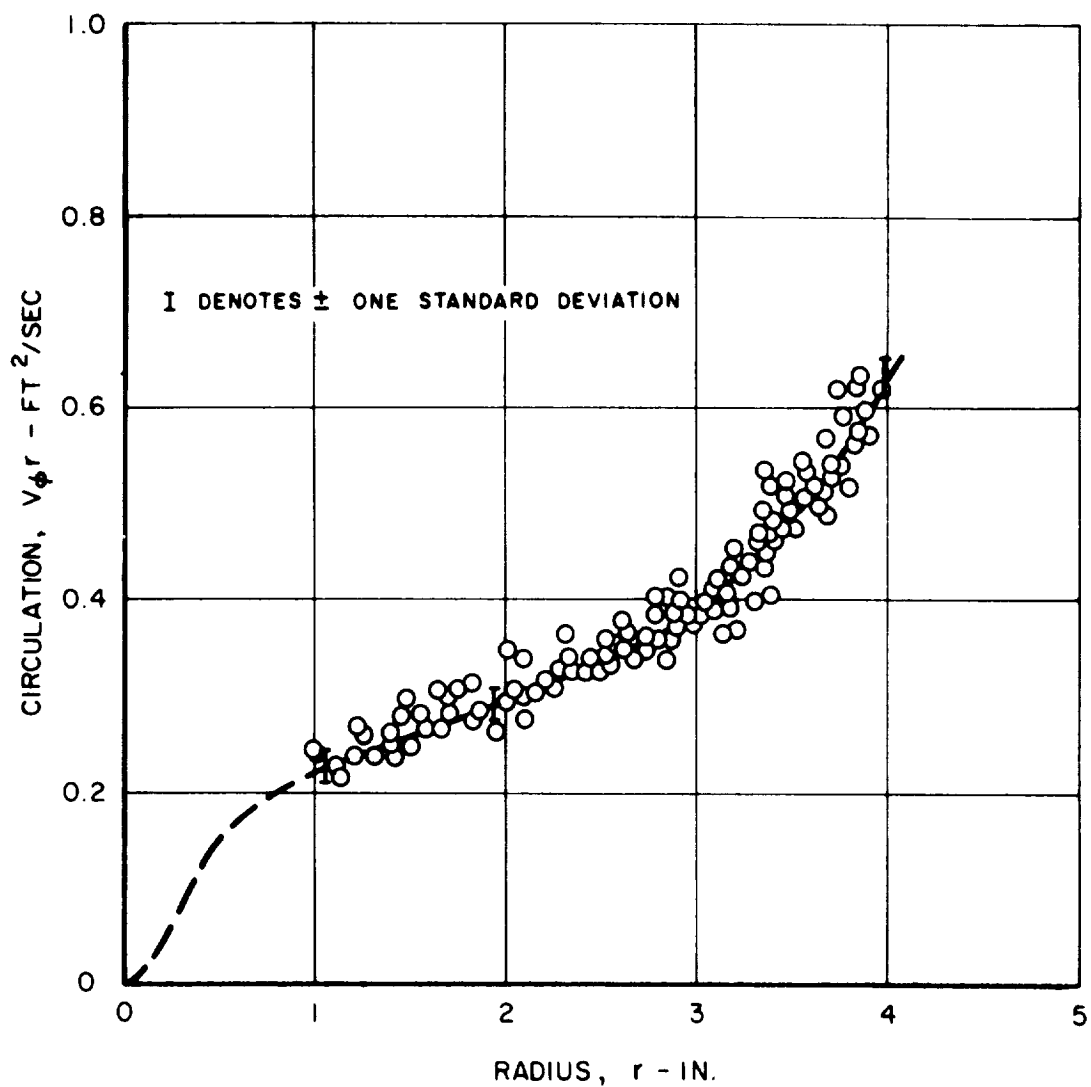
OPTICAL SYSTEM USED TO OBTAIN MICROFLASH DYE PHOTOGRAPHS



CIRCULATION PROFILE FOR VORTEX TUBE
WITH PLAIN END WALLS AND
THRU-FLOW REYNOLDS NUMBER OF 30

$$Re_{t,j} = 118,600$$

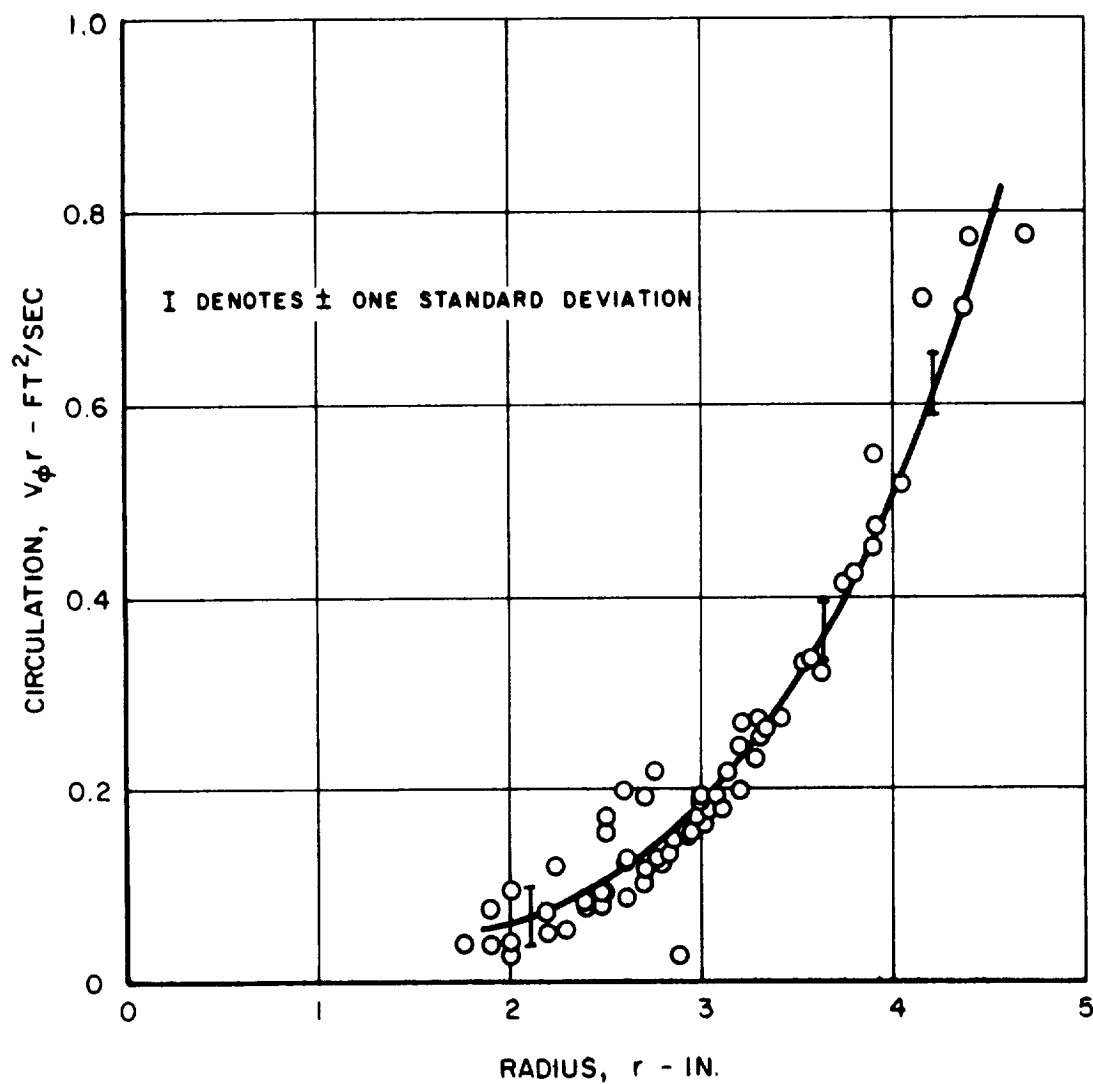
SEE TABLE I (CASE 2) FOR CONFIGURATION



CIRCULATION PROFILE FOR VORTEX TUBE
WITH PLAIN END WALLS AND
THRU-FLOW REYNOLDS NUMBER OF 0

$$Re_{t,j} = 102,800$$

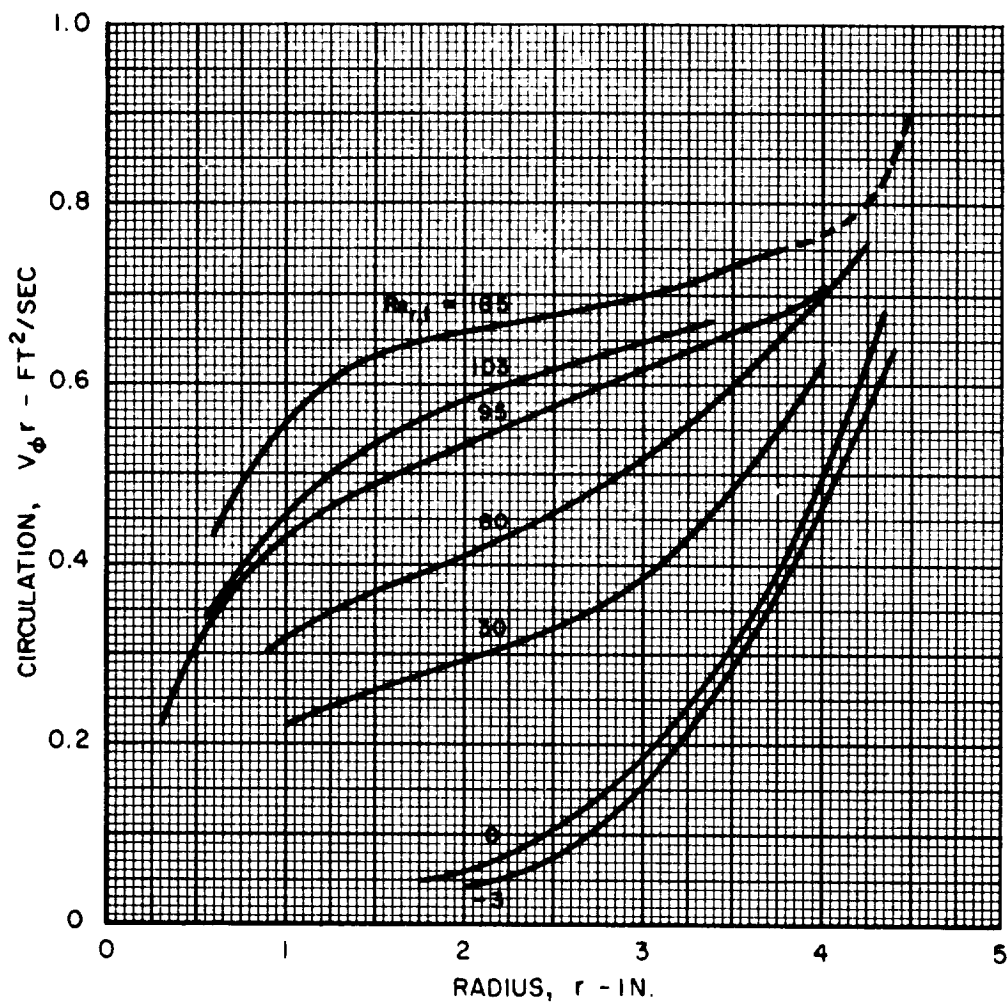
SEE TABLE I (CASE 3) FOR CONFIGURATION



CIRCULATION PROFILES FOR VORTEX TUBE WITH PLAIN END WALLS AND SEVEN THRU-FLOW REYNOLDS NUMBERS

CASE	$Re_{r,t}$	GEOMETRY	$Re_{t,j}$	V_j
4	-3	FLUID INJECTION THROUGH POROUS TUBE ALONG CENTERLINE	102,800	3.16 FT/SEC
3	0	NO THRU-FLOW	102,800	
2	30	THRU-FLOW BOTH ENDS	118,600	
1	60	THRU-FLOW BOTH ENDS	118,600	
	95	THRU-FLOW ONE END	117,500	
	103	THRU-FLOW BOTH ENDS	110,400	
	185	THRU-FLOW BOTH ENDS	122,400	

CURVES FOR $Re_{r,t} = 95, 103, \text{ AND } 185$ FROM REF. 5



TANGENTIAL VELOCITY PROFILES FOR VORTEX TUBE WITH PLAIN END WALLS AND SEVEN THRU-FLOW REYNOLDS NUMBERS

CASE	$Re_{r,t}$	GEOMETRY	$Re_{t,j}$	v_j
4	-3	FLUID INJECTION THROUGH POROUS TUBE ALONG CENTERLINE	102,800	3.16 FT/SEC
3	0	NO THRU-FLOW	102,800	
2	30	THRU-FLOW BOTH ENDS	118,600	
1	60	THRU-FLOW BOTH ENDS	118,600	
	95	THRU-FLOW ONE END	117,500	
	103	THRU-FLOW BOTH ENDS	110,400	
	185	THRU-FLOW BOTH ENDS	122,400	

CURVES FOR $Re_{r,t} = 95, 103, \text{ AND } 185$ FROM REF. 5

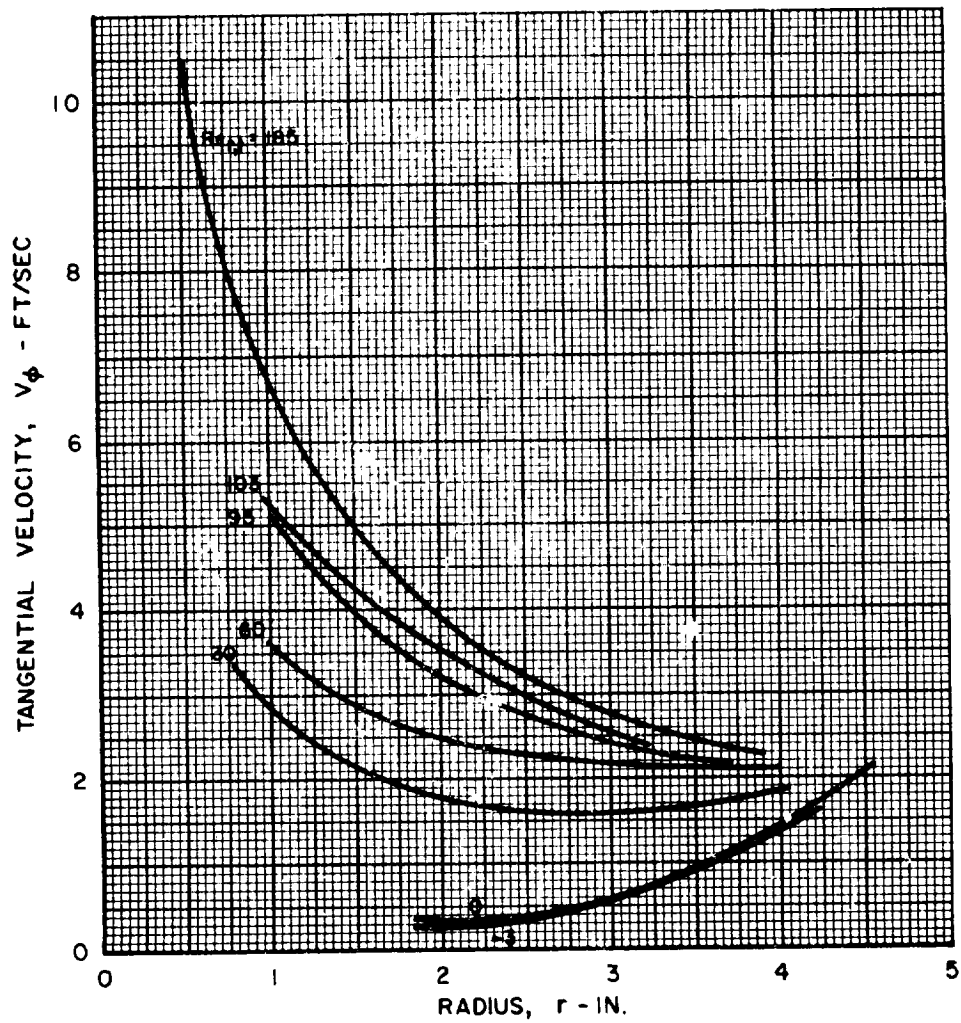


FIG. 12

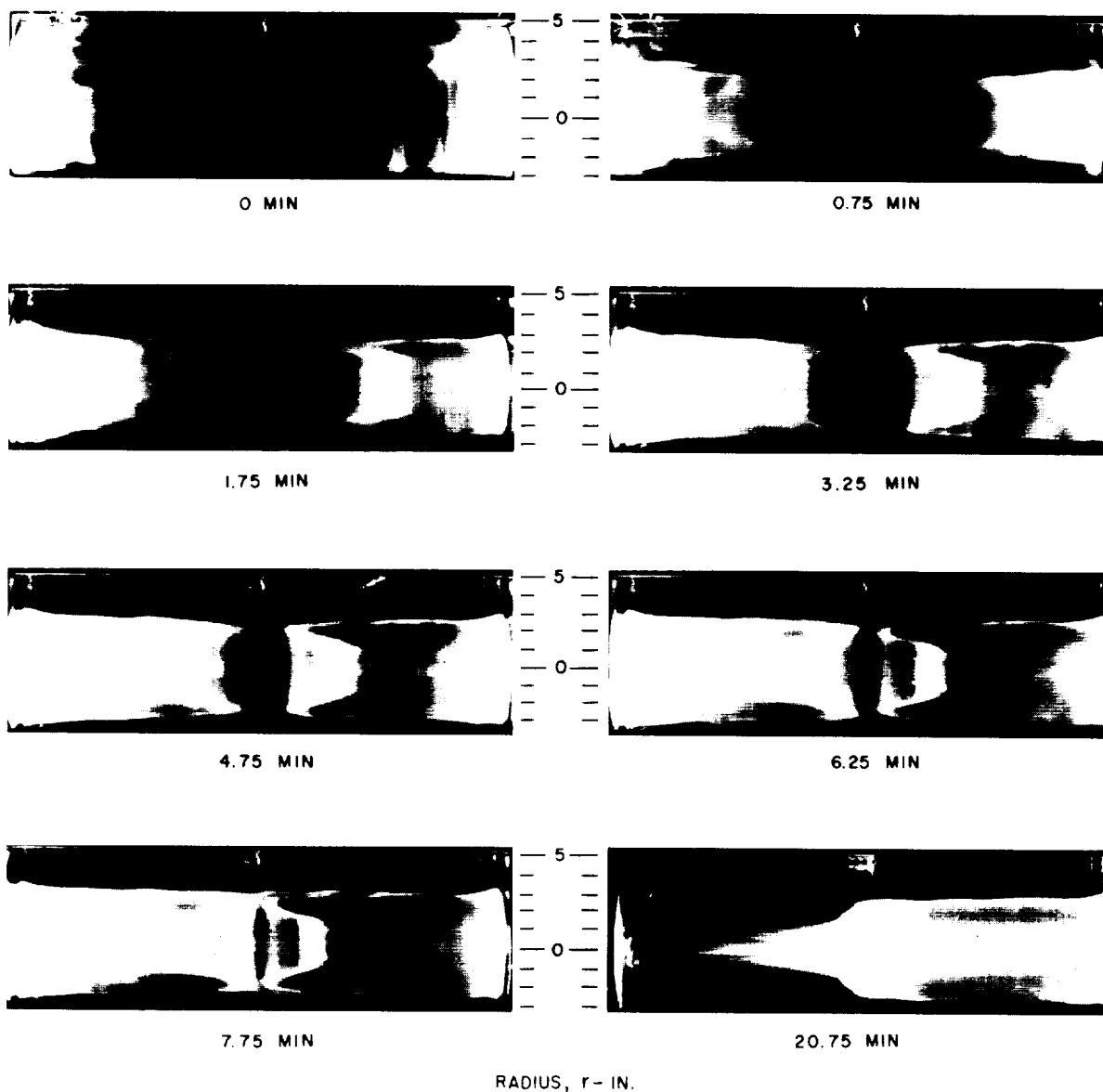
PHOTOGRAPHS OF DYE PATTERNS IN VORTEX TUBE WITH PLAIN
END WALLS AND THRU-FLOW REYNOLDS NUMBER OF 60

$$Re_{t,j} = 118,600$$

SEE TABLE I (CASE I) FOR CONFIGURATION

PHOTOGRAPHS TAKEN AT INDICATED TIMES AFTER CESSATION OF DYE INJECTION

LEFT AND RIGHT END WALL DYE INJECTION

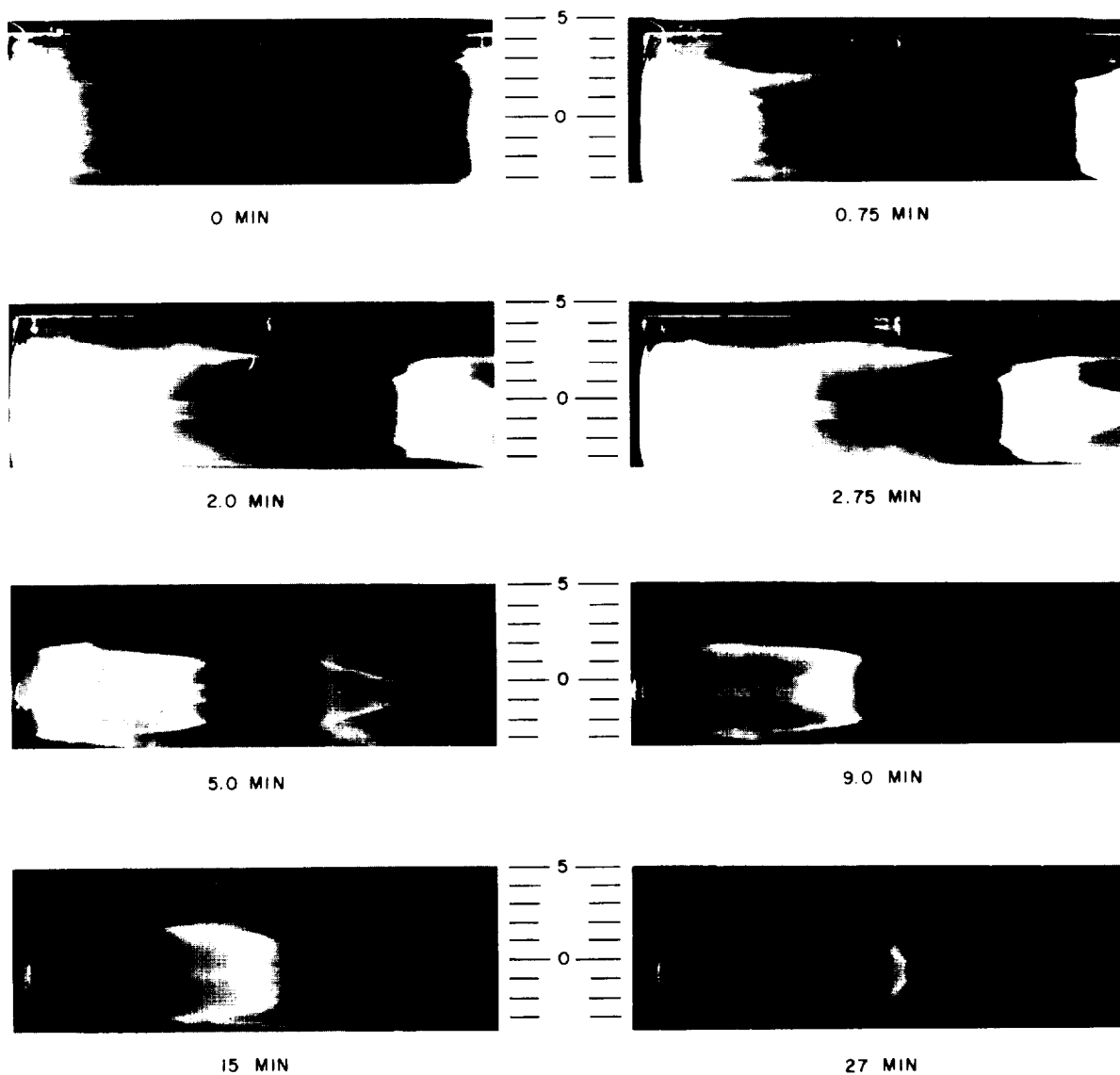


PHOTOGRAPHS OF DYE PATTERNS IN VORTEX TUBE WITH PLAIN END WALLS AND THRU-FLOW REYNOLDS NUMBER OF 30

$$Re_{t,i} = 118,600$$

SEE TABLE I (CASE 2) FOR CONFIGURATION
PHOTOGRAPHS TAKEN AT INDICATED TIMES AFTER CESSATION OF DYE INJECTION

LEFT AND RIGHT END WALL DYE INJECTION



RADIUS, r - IN.

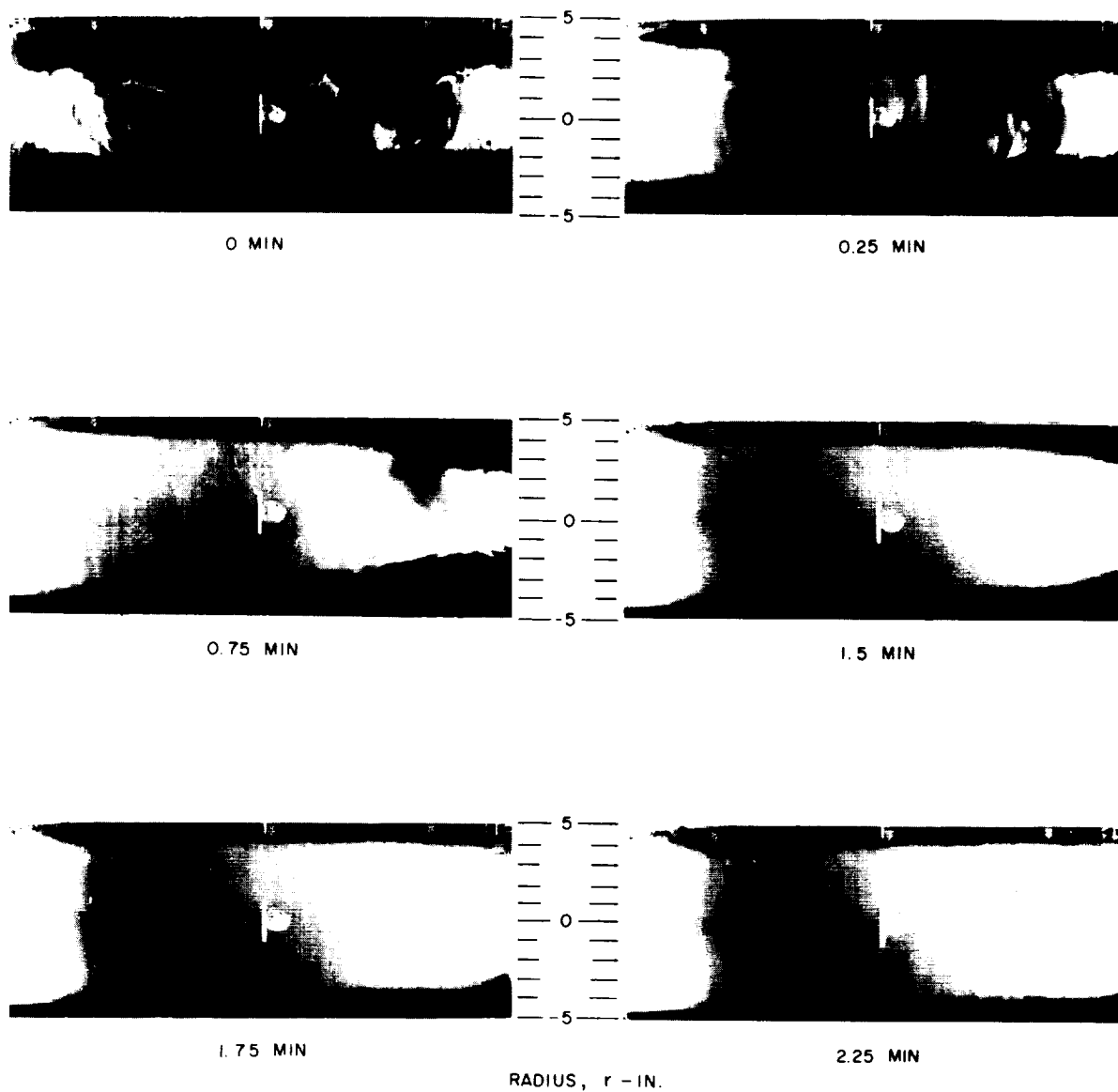
PHOTOGRAPHS OF DYE PATTERNS IN VORTEX TUBE WITH PLAIN END WALLS AND THRU-FLOW REYNOLDS NUMBER OF -3

$$Re_{t,j} = 102,800$$

SEE TABLE I (CASE 4) FOR CONFIGURATION

PHOTOGRAPHS TAKEN AT INDICATED TIMES AFTER CESSATION OF DYE INJECTION

DYE INJECTION THROUGH POROUS TUBE ALONG CENTERLINE

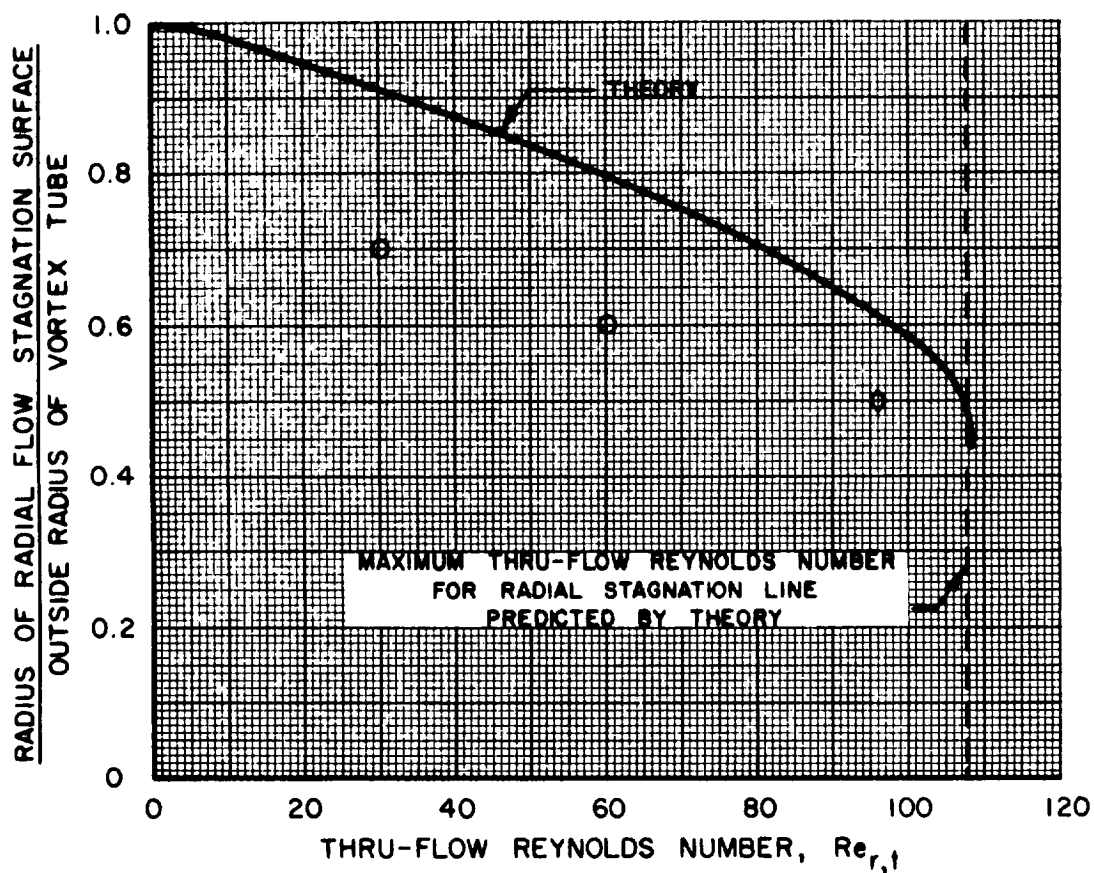


VARIATION OF RADIAL STAGNATION RADIUS WITH THRU-FLOW REYNOLDS NUMBER

$$Re_{t,j} = 118,000$$

THEORETICAL CURVE CALCULATED USING THE COMPUTATIONAL PROCEDURES
DISCUSSED IN REF. 2 WITH AN EFFECTIVE TANGENTIAL REYNOLDS
NUMBER OF 80,000 AT RADIUS r_1

- DATA FROM THIS REPORT (CASES 1 AND 2)
◇ DATA FROM REF. 5

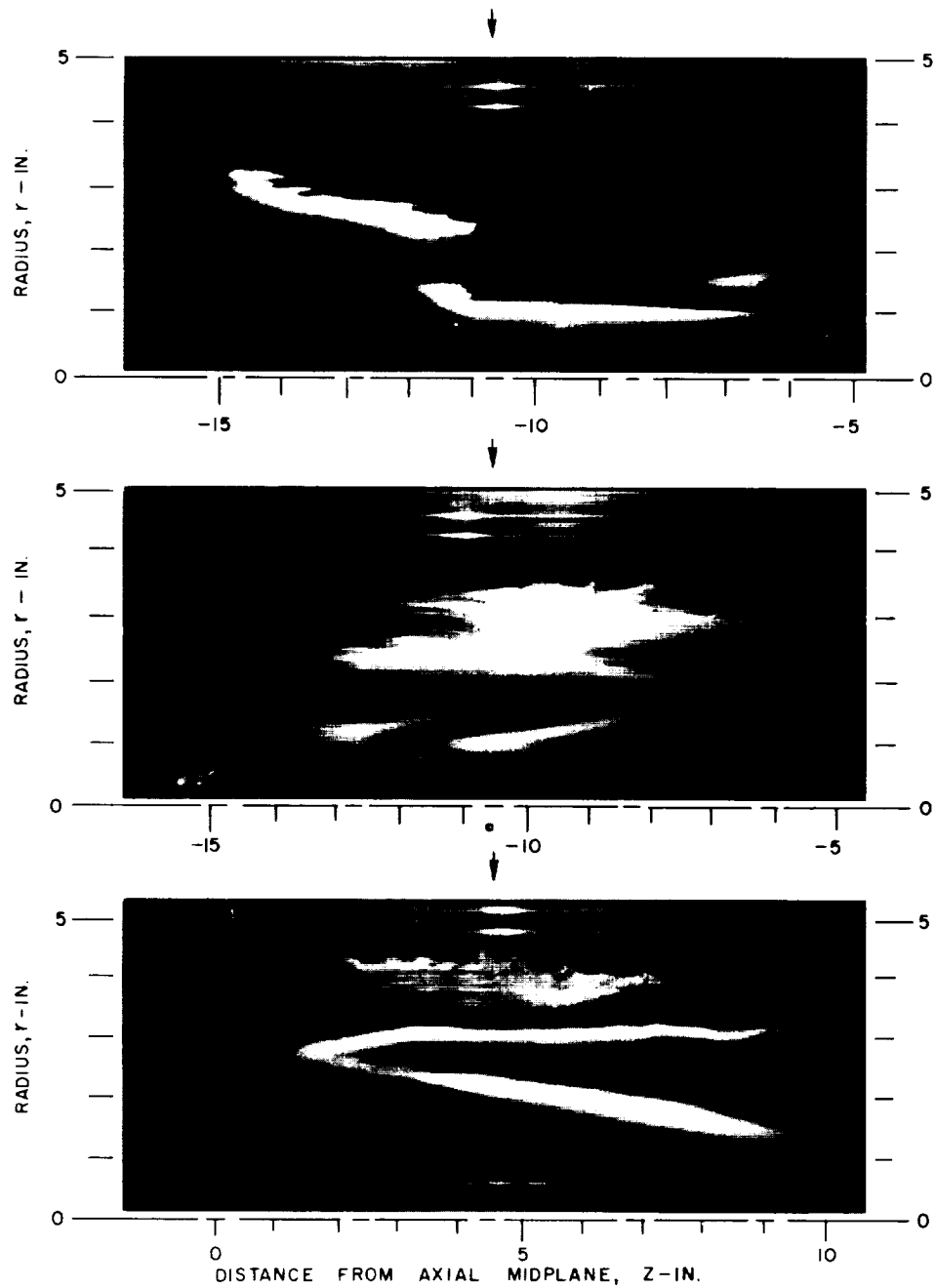


MICROFLASH PHOTOGRAPHS OF DYE PATTERNS WITH
PLAIN END WALLS AND THRU-FLOW REYNOLDS NUMBER OF 60

$$Re_{t,j} = 118,600$$

SEE TABLE I (CASE I) FOR CONFIGURATION

→ DIRECTION OF ILLUMINATION

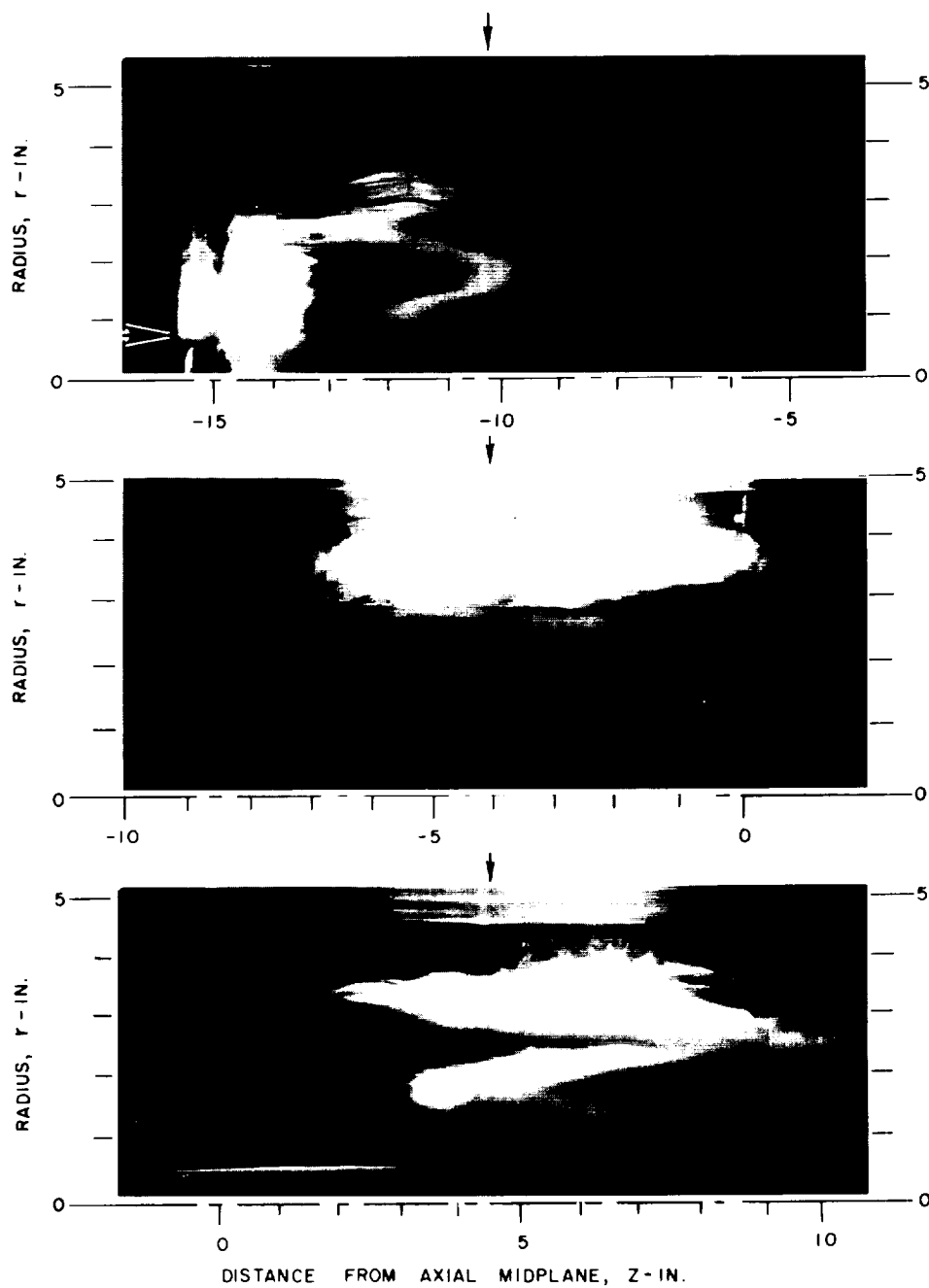


MICROFLASH PHOTOGRAPHS OF DYE PATTERNS WITH PLAIN END WALLS AND THRU-FLOW REYNOLDS NUMBER OF 30

$$Re_{t,j} = 118,600$$

SEE TABLE I (CASE 2) FOR CONFIGURATION

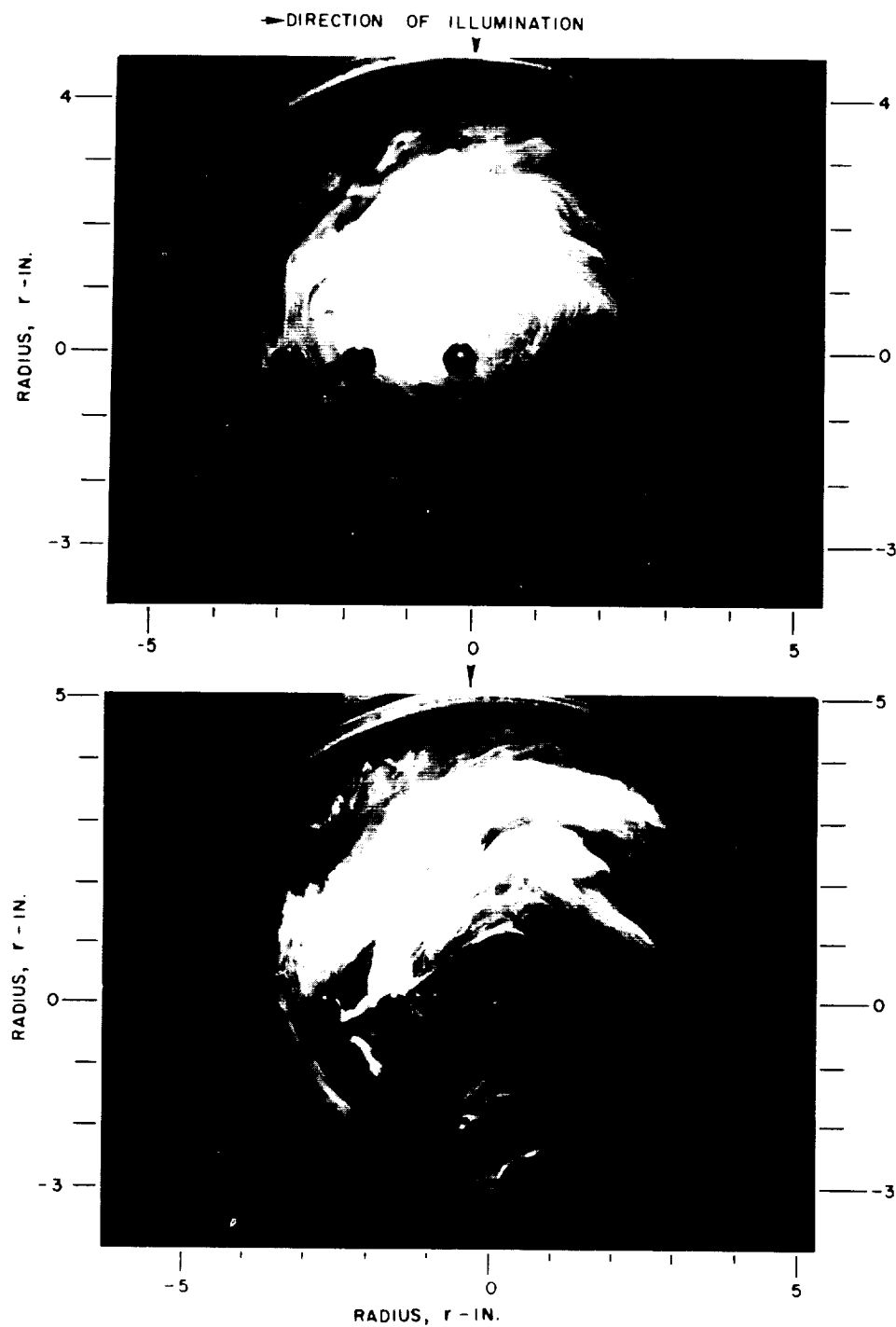
—► DIRECTION OF ILLUMINATION



MICROFLASH PHOTOGRAPHS OF DYE PATTERNS WITH PLAIN
END WALLS AND THRU-FLOW REYNOLDS NUMBER OF 0

$$Re_{t,j} = 102,800$$

SEE TABLE I (CASE 3) FOR CONFIGURATION

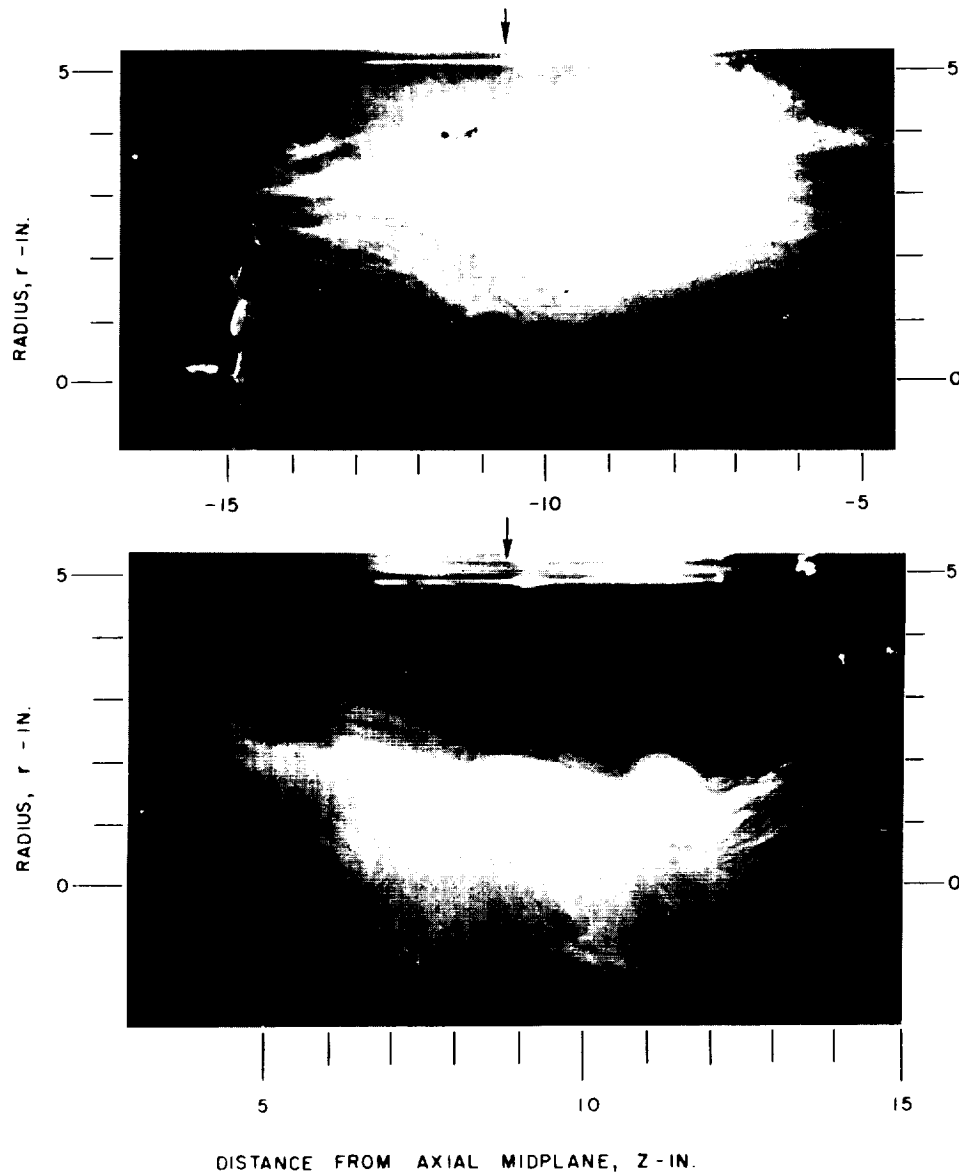


MICROFLASH PHOTOGRAPHS OF DYE PATTERNS WITH PLAIN END WALLS AND THRU-FLOW REYNOLDS NUMBER OF 0

$$Re_{t,i} = 102,800$$

SEE TABLE I (CASE 3) FOR CONFIGURATION

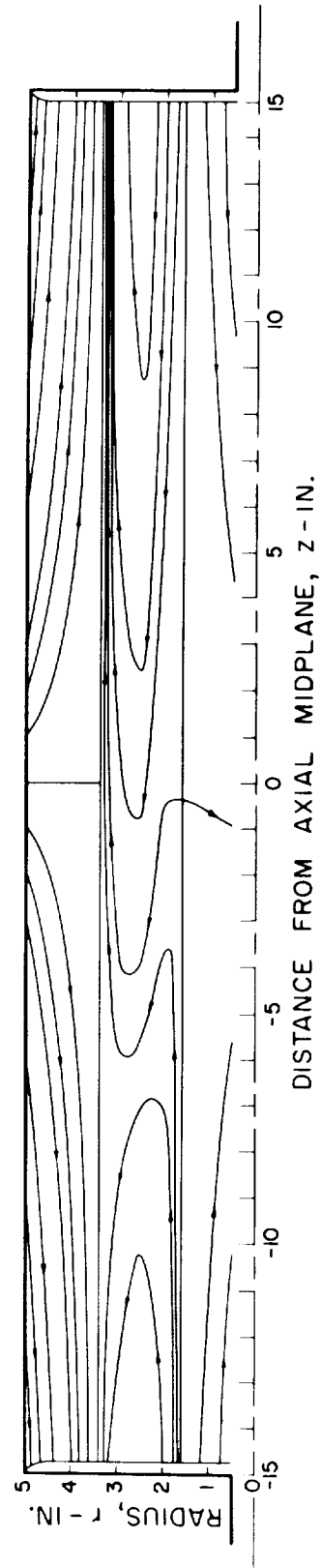
→ DIRECTION OF ILLUMINATION



STREAMLINE SKETCH OF VORTEX TUBE WITH PLAIN END WALLS
AND THRU-FLOW REYNOLDS NUMBER OF 30

$$Re_{t,j} = 118,600$$

SEE TABLE I (CASE 2) FOR CONFIGURATION



STREAMLINE SKETCH OF VORTEX TUBE WITH PLAIN END WALLS AND THRU-FLOW REYNOLDS NUMBER OF 0

$$Re_{t,j} = 102,800$$

SEE TABLE I (CASE 3) FOR CONFIGURATION

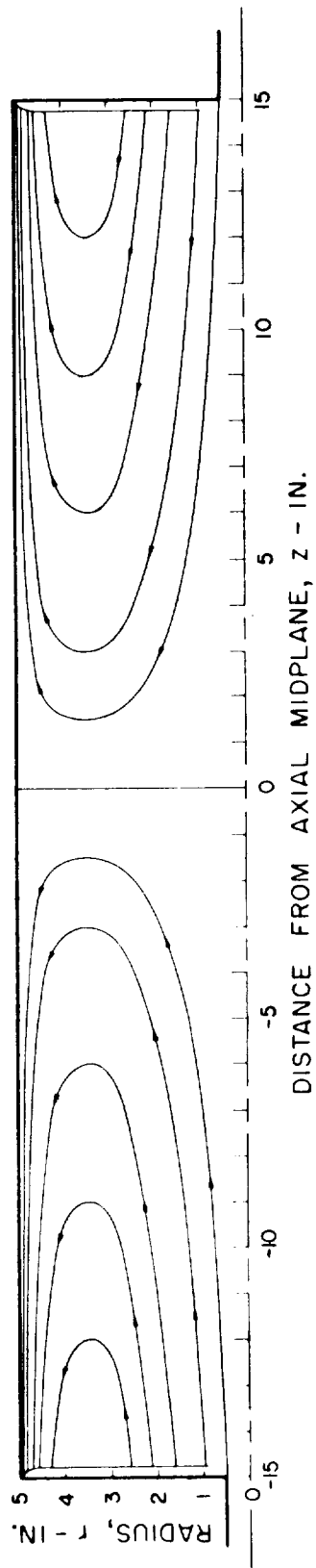


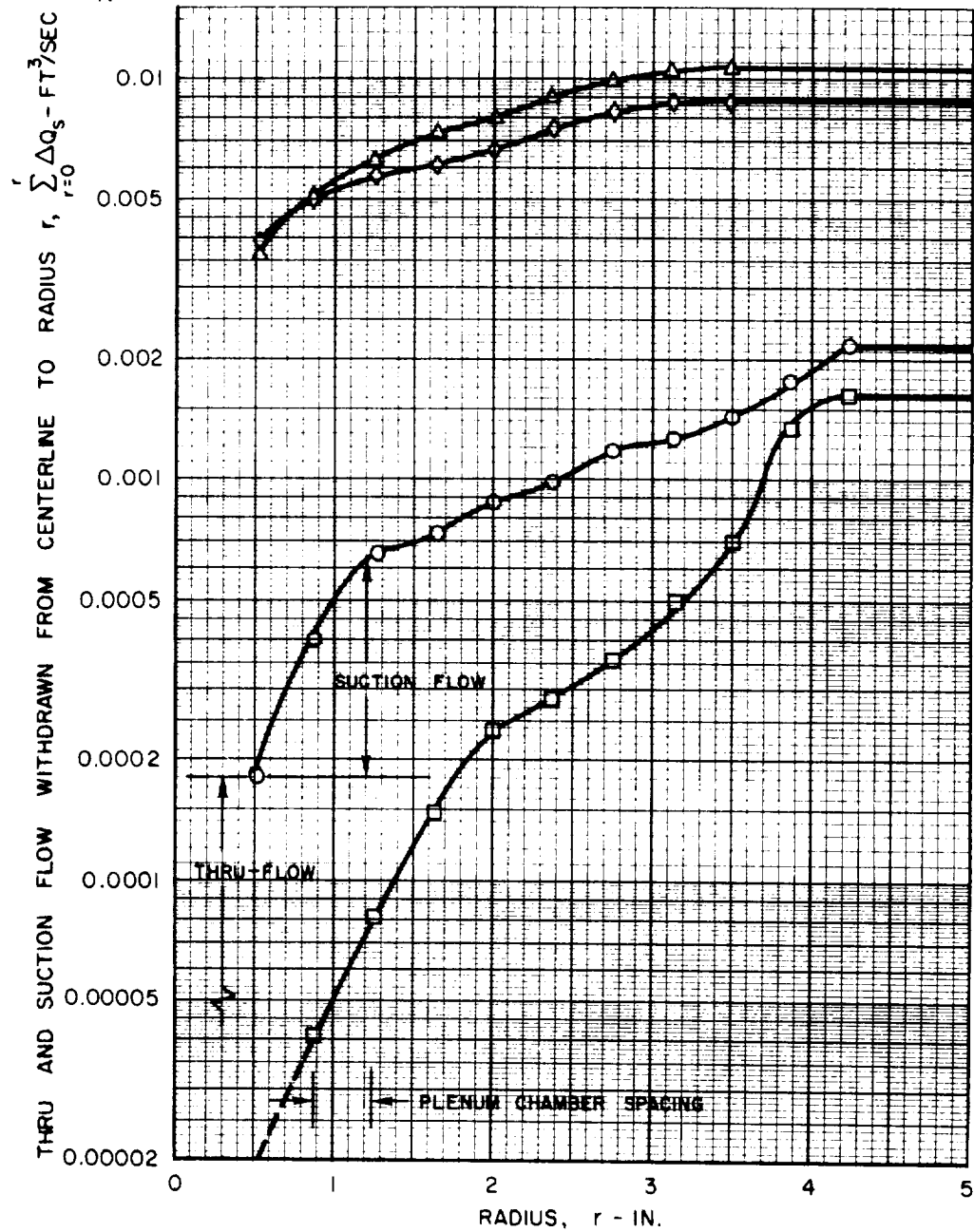
FIG. 20

DISTRIBUTION OF FLOW WITHDRAWN THROUGH THE END WALLS FOR SUCTION DISTRIBUTIONS A, B, C AND D

SYMBOL	CASE	SUCTION DISTRIBUTION	DESIRED PRIMARY FLOW CHARACTERISTIC	$Re_{r,t}$	$Re_{r,s}$
Δ	5	A	RADIAL FLOW IN	43	83
\diamond	6	B	RADIAL FLOW IN	46	58
\circ	7	C	SOLID-BODY ROTATION	2	23
\square	8	D	RADIAL FLOW OUT	-3	19

 $Re_{t,j} = 118,600$ $V_j = 3.16$ FT/SEC

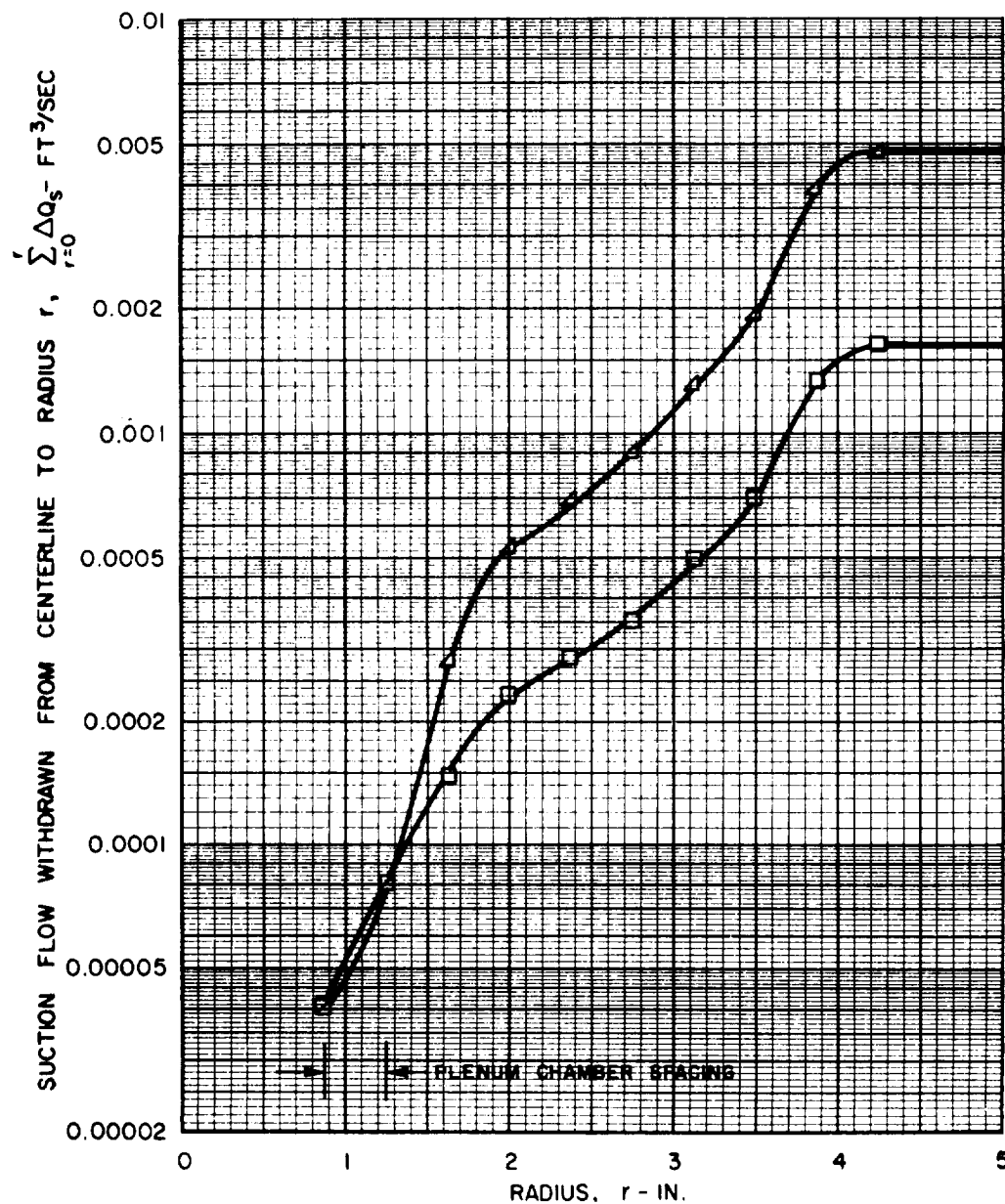
SEE TABLE I FOR CONFIGURATION



DISTRIBUTION OF FLOW WITHDRAWN THROUGH THE END WALLS FOR SUCTION DISTRIBUTIONS D AND E

SYMBOL	CASE	SUCTION DISTRIBUTION	DESIRED PRIMARY FLOW CHARACTERISTIC	$Re_{t,j}$	$Re_{t,t}$	$Re_{t,s}$	V_j - FT/SEC
□	8	D	RADIAL FLOW OUT	118,600	-3	19	3.16
Δ	9	E	RADIAL FLOW OUT	346,000	-3	56	9.22

SEE TABLE I FOR CONFIGURATION

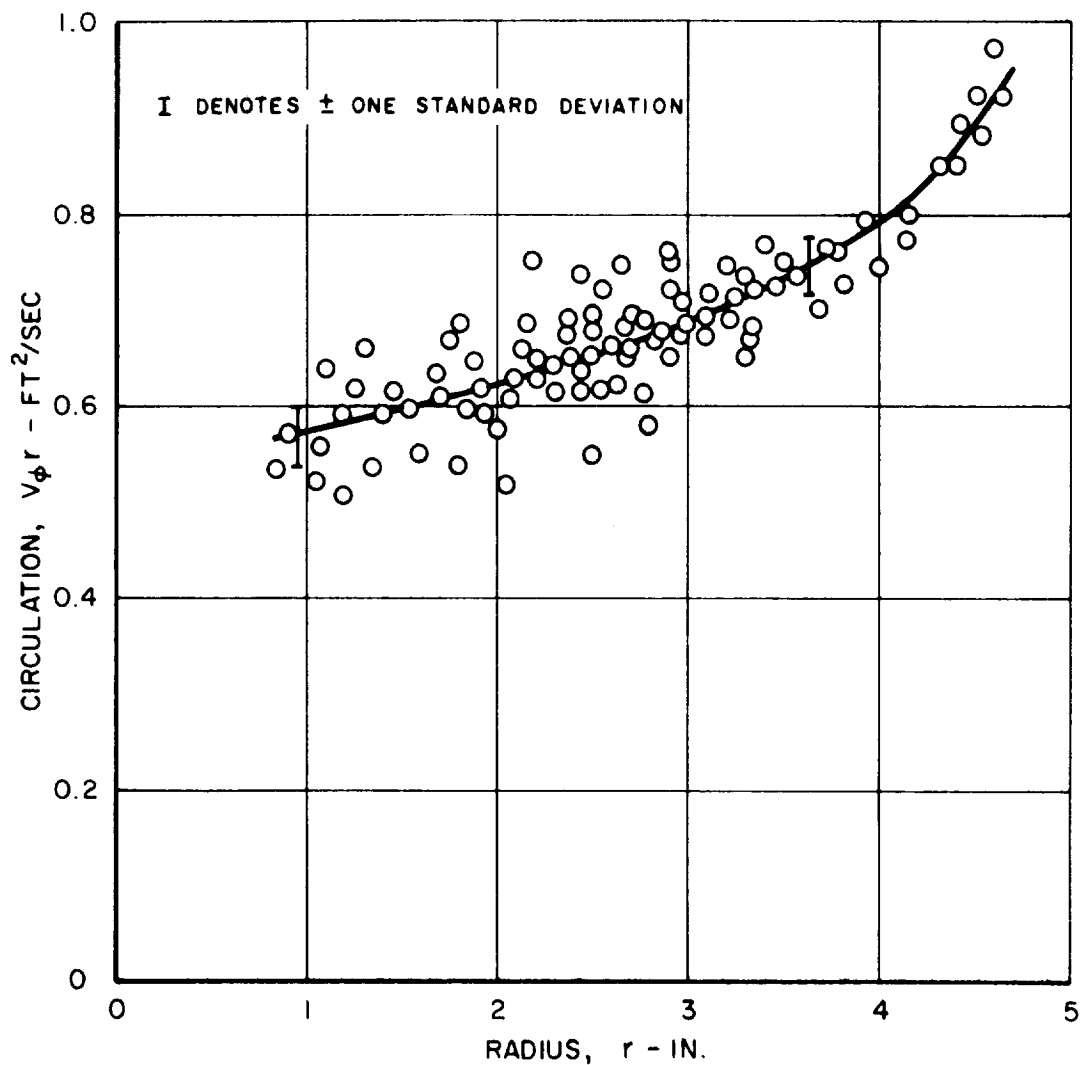


CIRCULATION PROFILE FOR VORTEX TUBE
WITH SUCTION DISTRIBUTION B AND
THRU-FLOW REYNOLDS NUMBER OF 45.7

SEE FIG. 21 FOR SUCTION FLOW DISTRIBUTION

$$Re_{t,j} = 118,600$$

SEE TABLE I (CASE 6) FOR CONFIGURATION

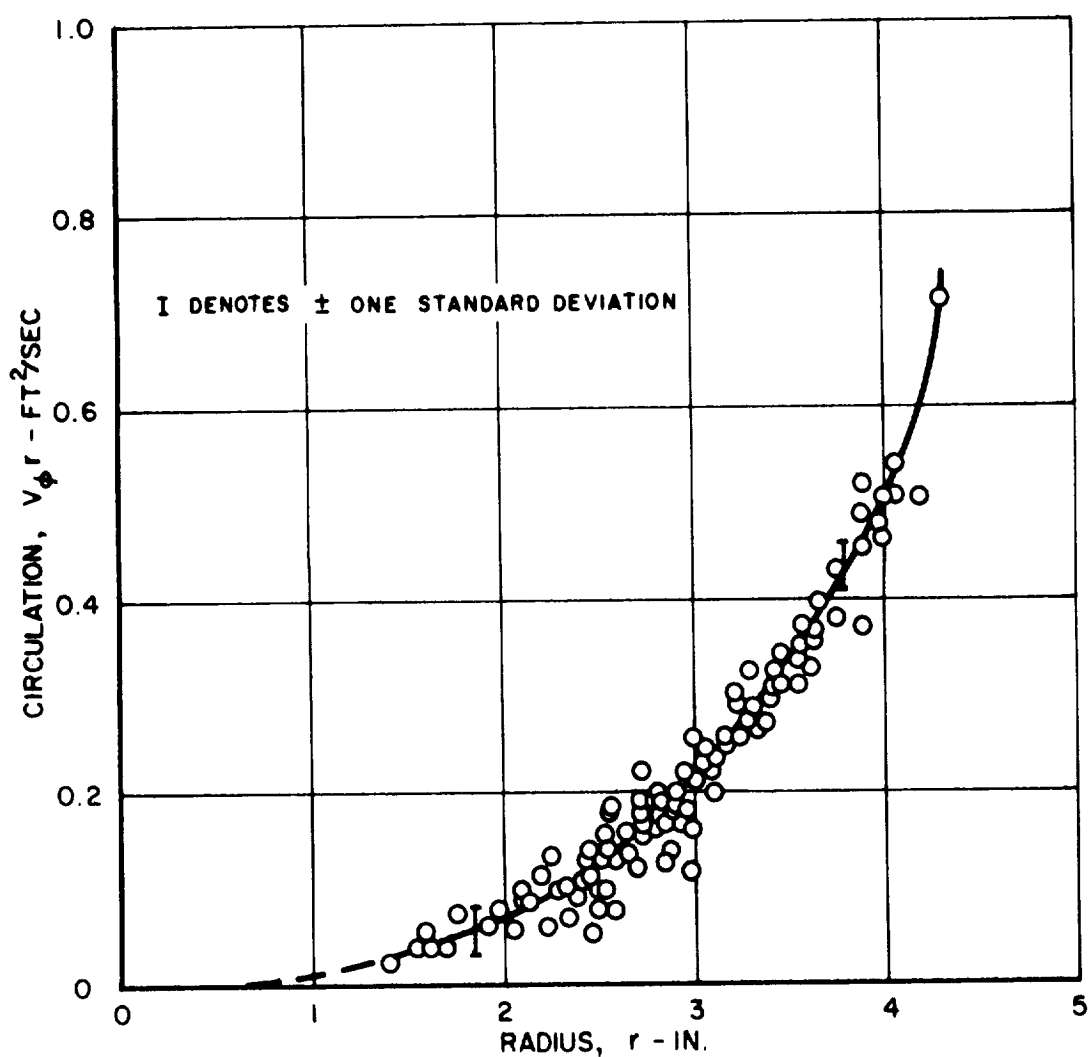


CIRCULATION PROFILE FOR VORTEX TUBE WITH SUCTION DISTRIBUTION D AND THRU-FLOW REYNOLDS NUMBER OF -3

SEE FIG. 21 FOR SUCTION FLOW DISTRIBUTION

$$Re_{t,j} = 118,600$$

SEE TABLE I (CASE 8) FOR CONFIGURATION



CONFIDENTIAL

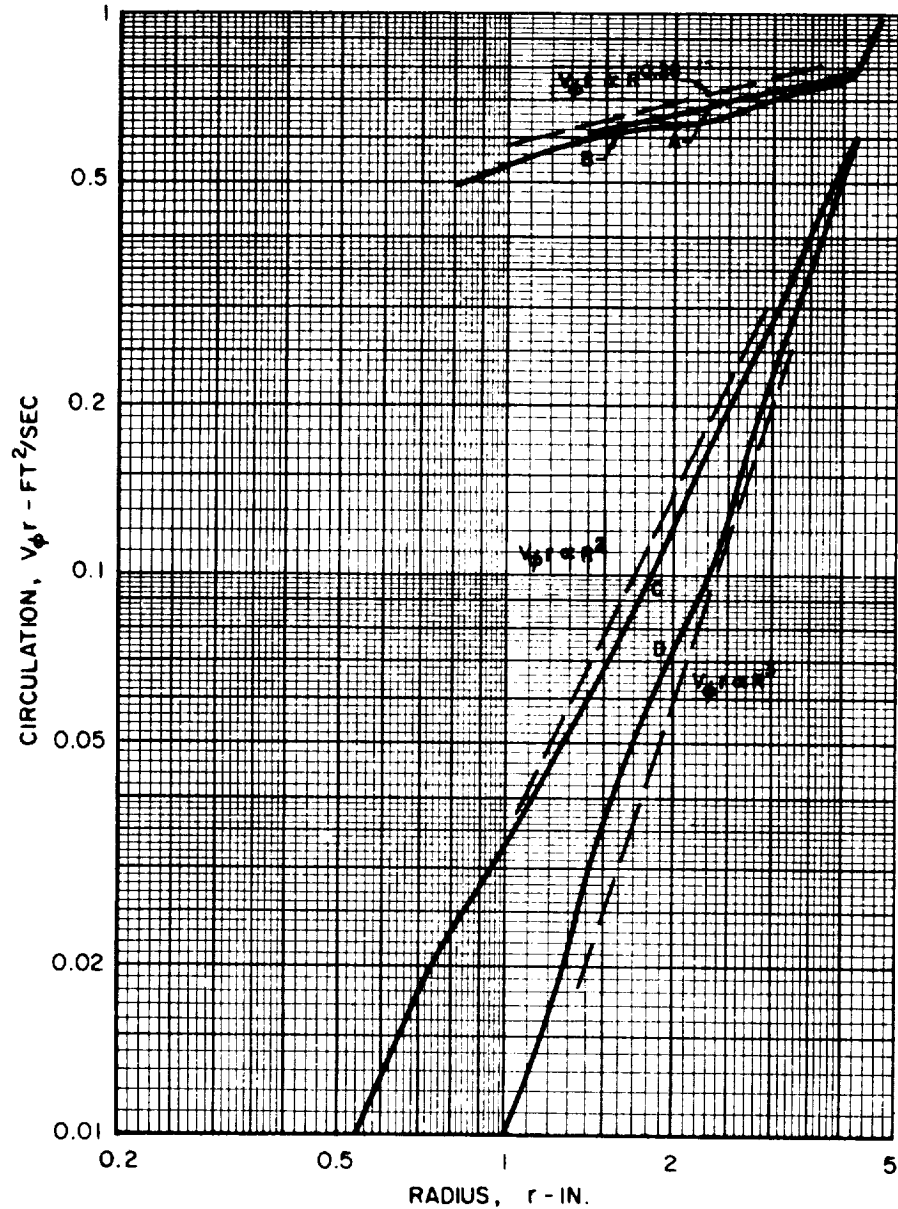
CIRCULATION PROFILES FOR VORTEX TUBE WITH SUCTION DISTRIBUTIONS A, B, C AND D

$$Re_{t,j} = 118,600$$

SUCTION DISTRIBUTION	CASE	$Re_{r,t}$	APPROXIMATE η_r	INDICATED $Re_{r,p}$ (SEE TEXT)
A	5	43	0.25	—
B	6	46	0.25	—
C	7	2	2	0
D	8	-3	3	-1.0

SEE FIG. 21 FOR SUCTION FLOW DISTRIBUTION

SEE TABLE I (CASES 5, 6, 7, 8) FOR CONFIGURATION



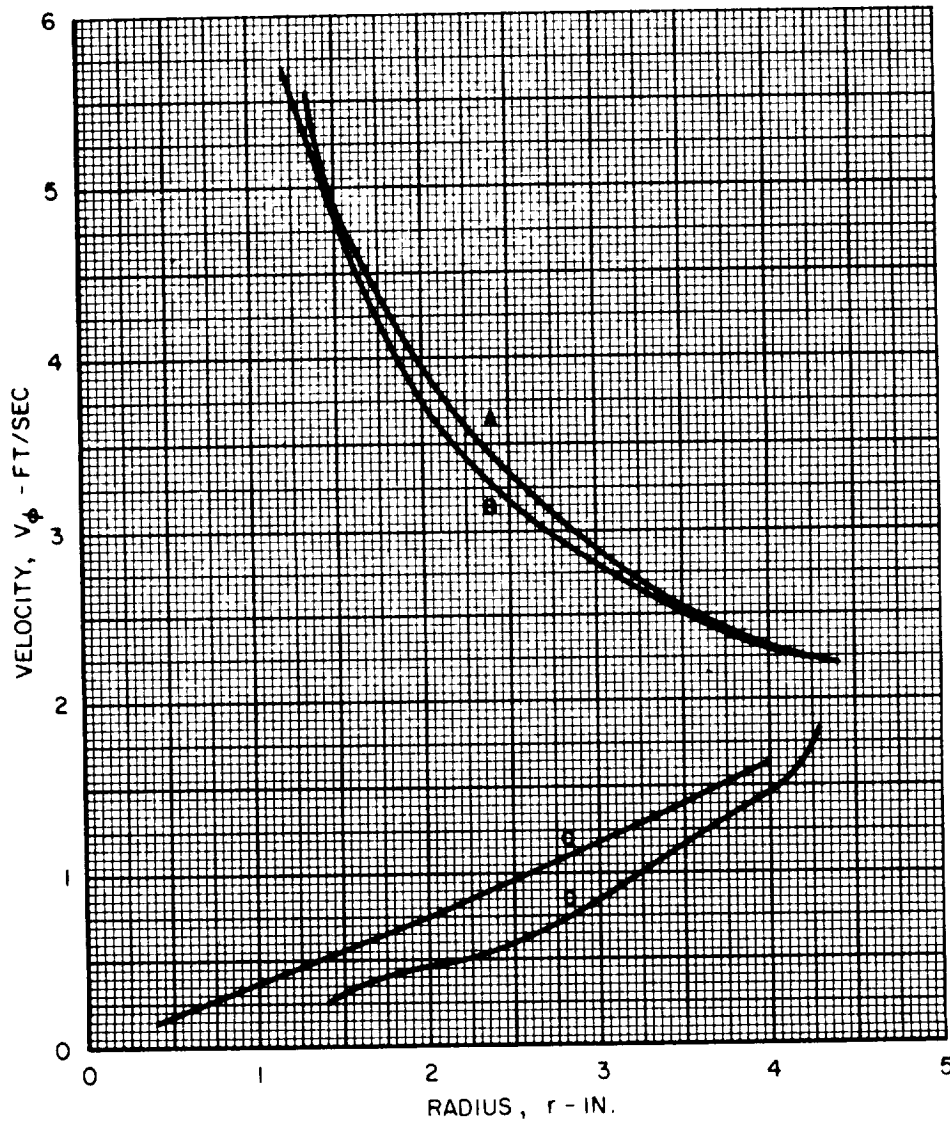
CONFIDENTIAL

**TANGENTIAL VELOCITY PROFILES FOR VORTEX TUBE
WITH SUCTION DISTRIBUTIONS A, B, C AND D**

$Re_{t,j} = 118,600$

SUCTION DISTRIBUTION	CASE	$Re_{r,t}$
A	5	43
B	6	46
C	7	2
D	8	-3

SEE FIG. 21 FOR SUCTION FLOW DISTRIBUTION
SEE TABLE I FOR CONFIGURATION

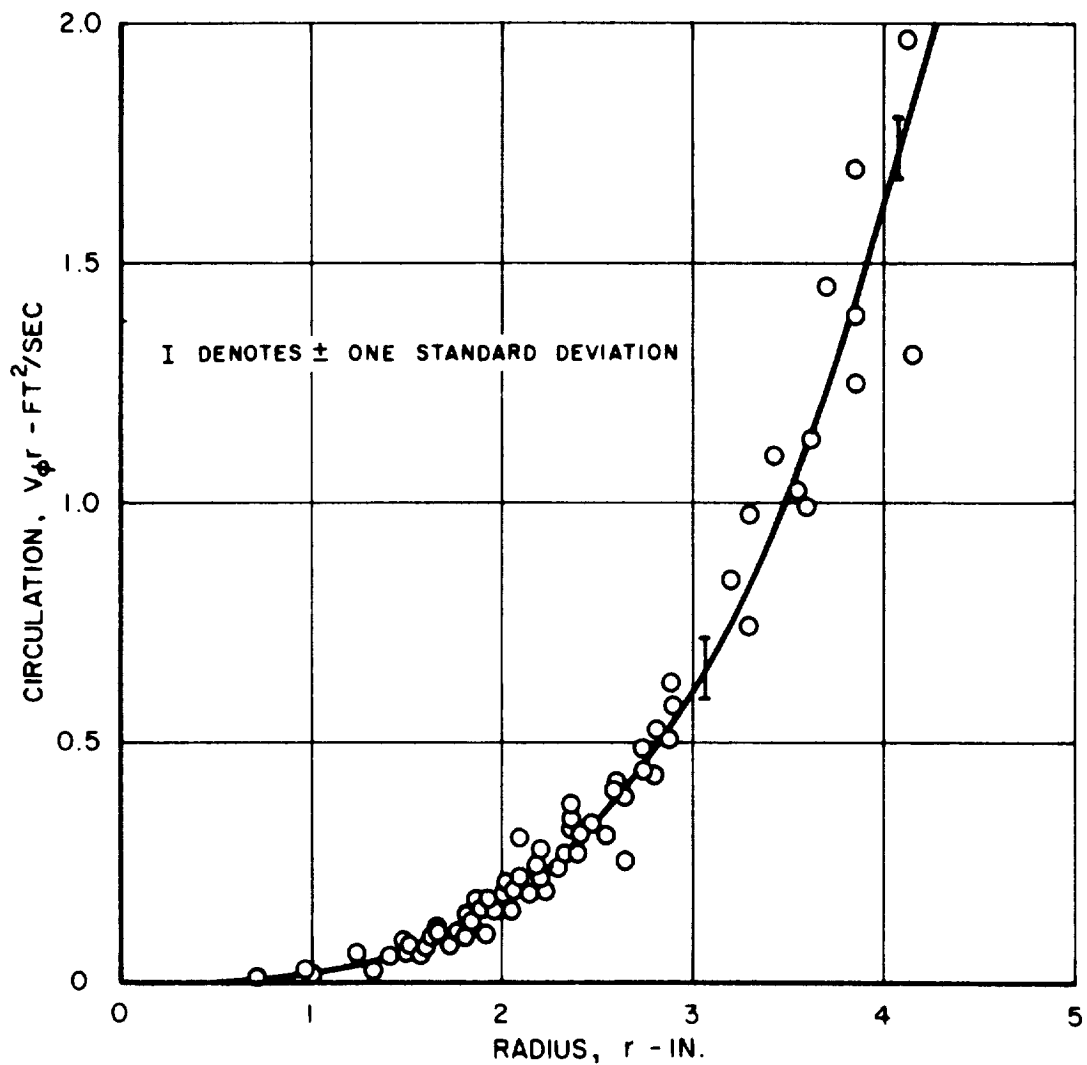


CIRCULATION PROFILE FOR VORTEX TUBE
WITH SUCTION DISTRIBUTION E AND
THRU-FLOW REYNOLDS NUMBER OF -3

SEE FIG. 22 FOR SUCTION FLOW DISTRIBUTION

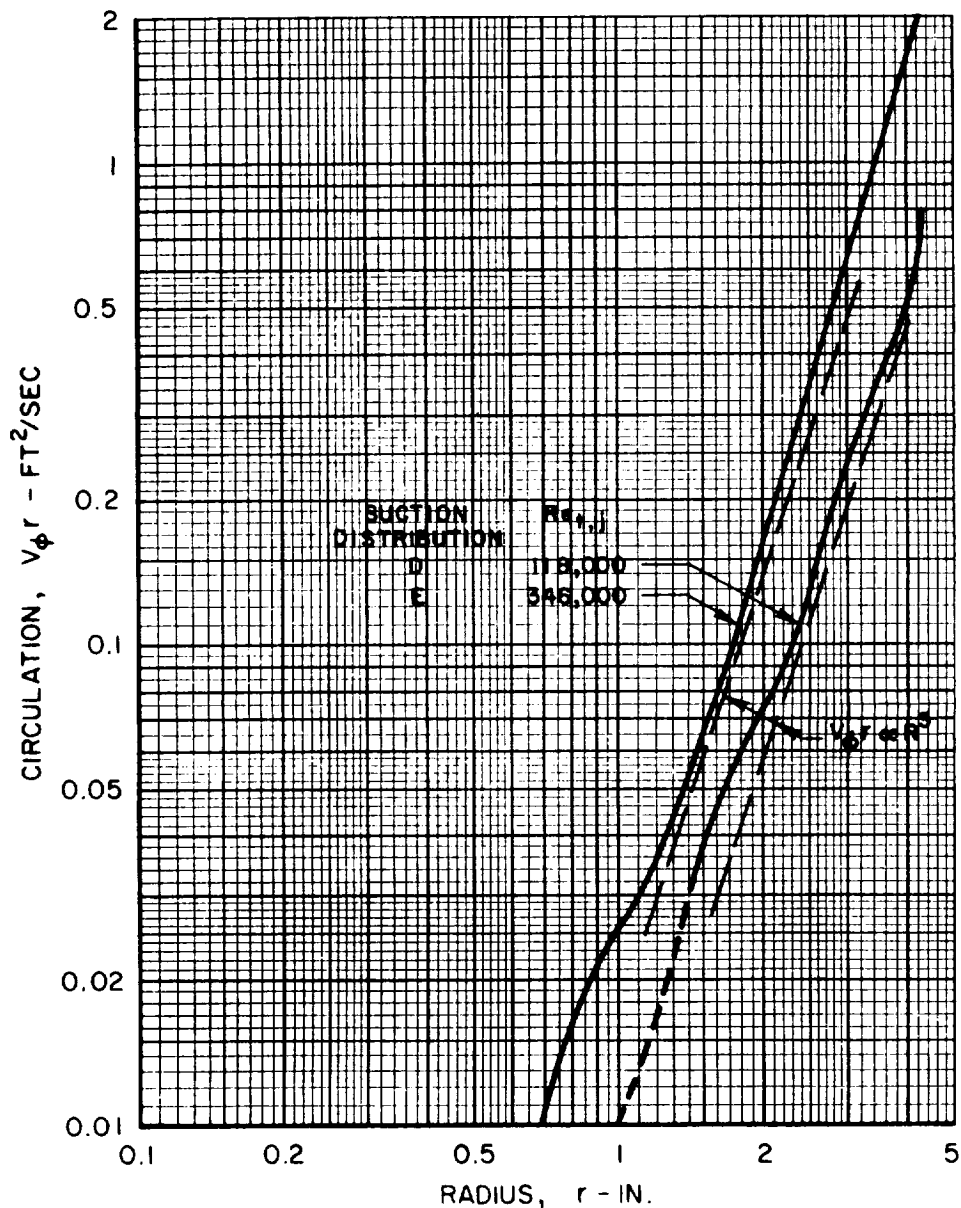
$$Re_{t,j} = 346,000$$

SEE TABLE I (CASE 9) FOR CONFIGURATION



CIRCULATION PROFILES FOR VORTEX TUBE WITH JET REYNOLDS NUMBERS OF 118,600 AND 346,000 AND SUCTION END WALLS

SEE FIG. 22 FOR SUCTION FLOW DISTRIBUTION
SEE TABLE I (CASES 8 AND 9) FOR CONFIGURATION

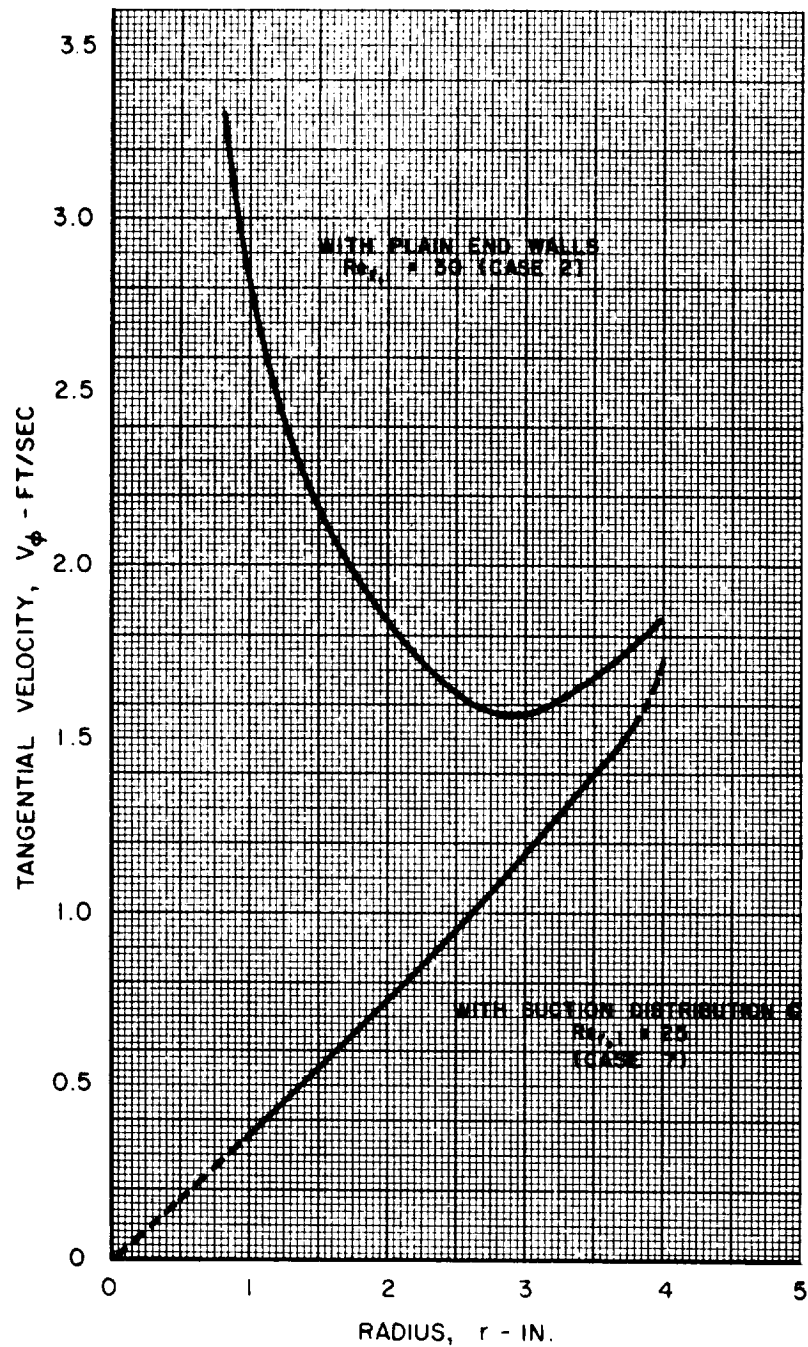


EFFECT OF END-WALL SUCTION ON TANGENTIAL VELOCITY PROFILE

$$Re_{t,j} = 118,600$$

SEE FIG. 21 FOR SUCTION FLOW DISTRIBUTION

SEE TABLE I FOR CONFIGURATION

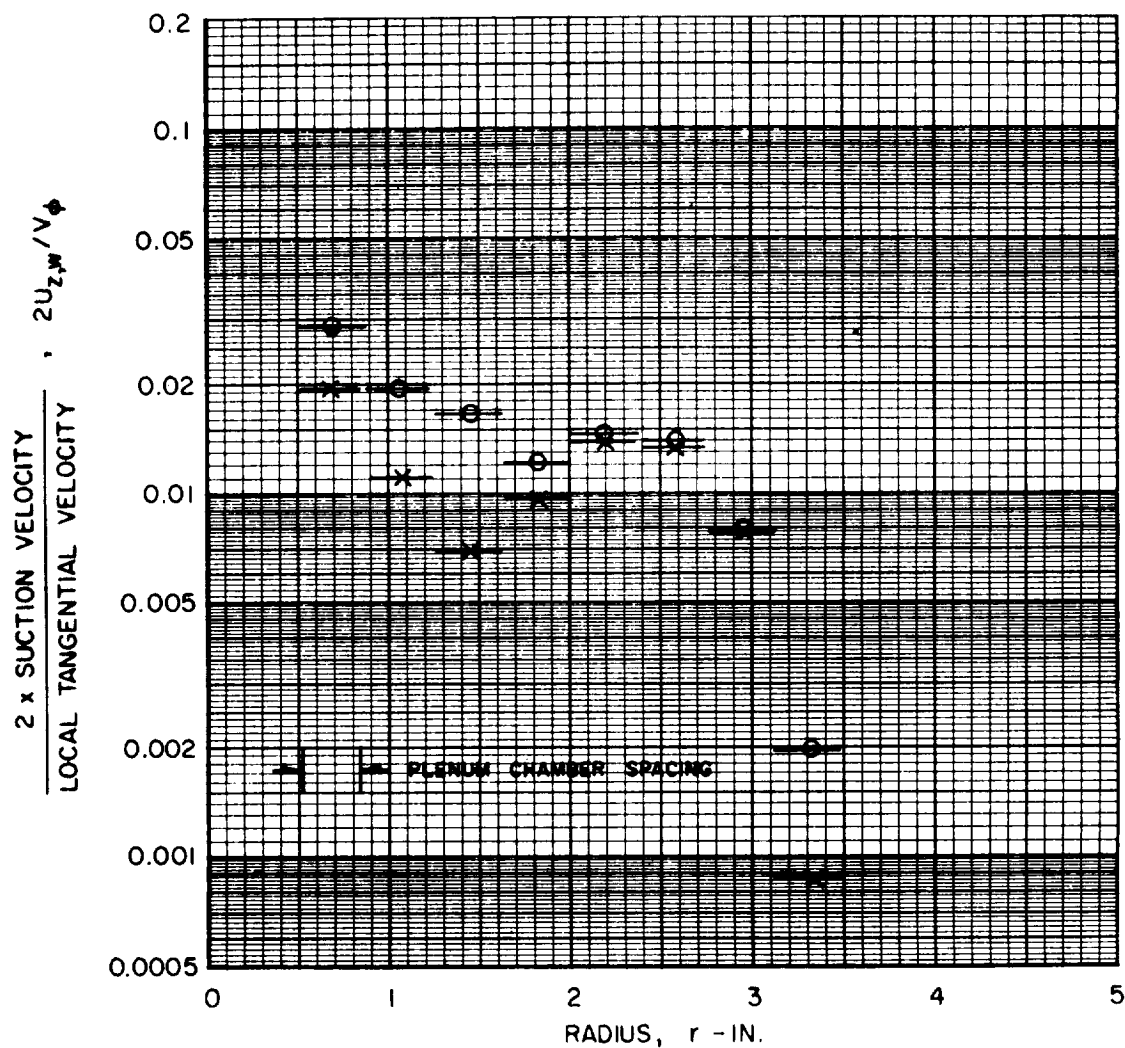


VARIATION OF THE RATIO OF END-WALL SUCTION VELOCITY TO LOCAL TANGENTIAL VELOCITY WITH RADIUS FOR SUCTION DISTRIBUTIONS A AND B

$$Re_{t,j} = 118,600$$

SYMBOL	CASE	SUCTION DISTRIBUTION
O	5	A
X	6	B

SEE FIG. 21 FOR SUCTION FLOW DISTRIBUTION
SEE TABLE I (CASES 5 AND 6) FOR CONFIGURATION

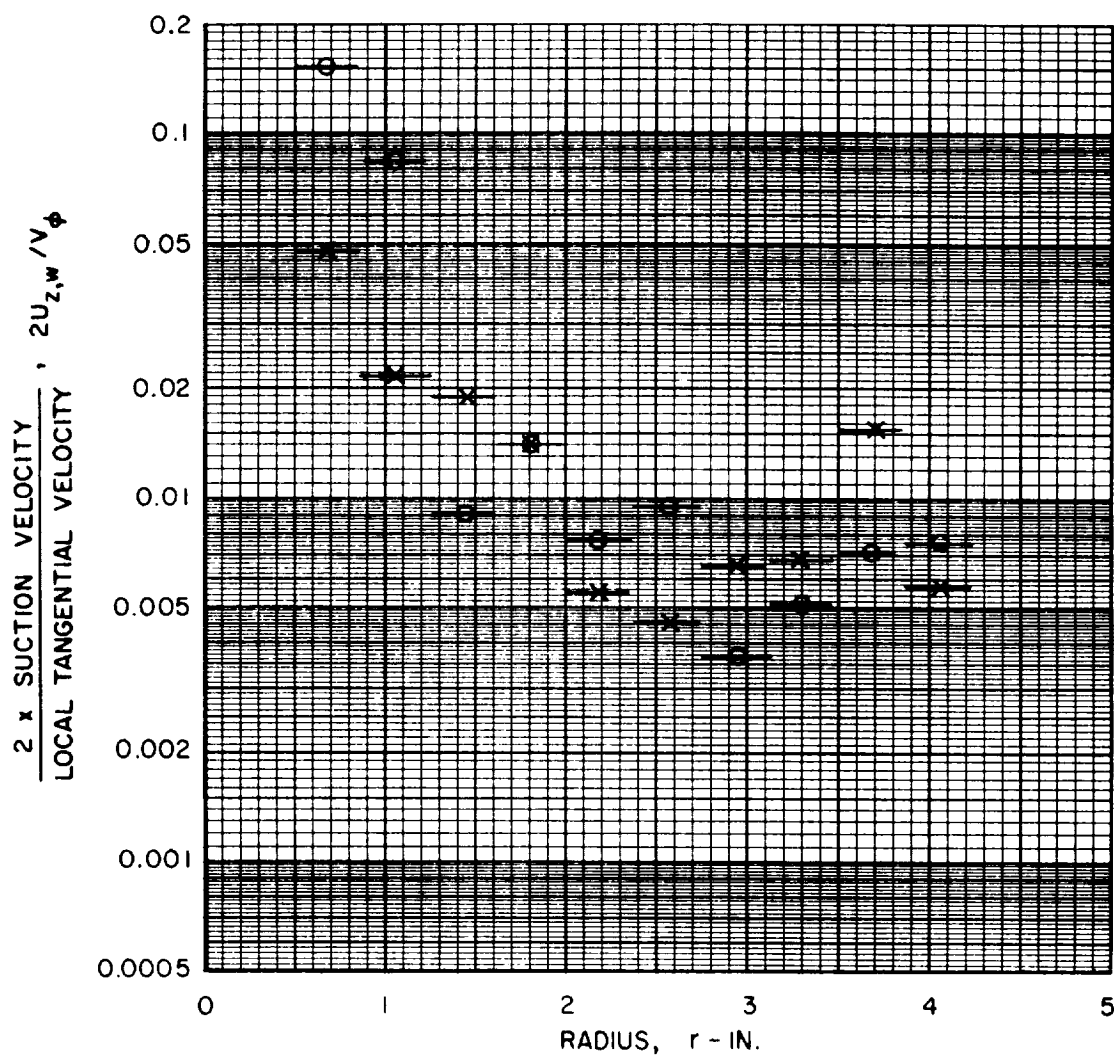


VARIATION OF THE RATIO OF END-WALL SUCTION VELOCITY TO LOCAL TANGENTIAL VELOCITY WITH RADIUS FOR SUCTION DISTRIBUTIONS C AND D

$$Re_{t,j} = 118,600$$

SYMBOL	CASE	SUCTION DISTRIBUTION
O	7	C
X	8	D

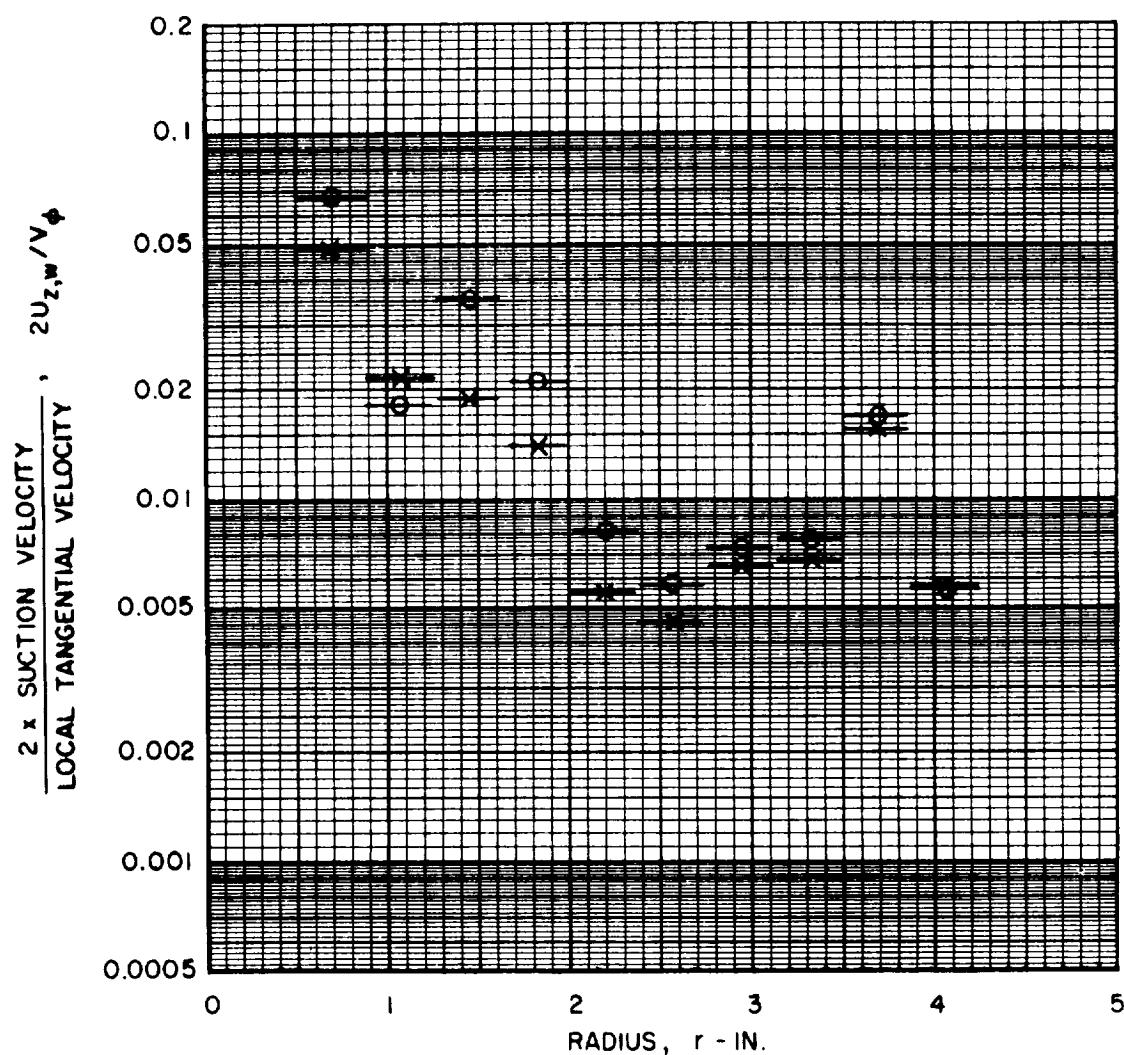
SEE FIG. 21 FOR SUCTION FLOW DISTRIBUTION
SEE TABLE I (CASES 7 AND 8) FOR CONFIGURATION



VARIATION OF THE RATIO OF END-WALL SUCTION VELOCITY
TO LOCAL TANGENTIAL VELOCITY WITH RADIUS FOR
SUCTION DISTRIBUTIONS D AND E

SYMBOL	CASE	SUCTION DISTRIBUTION	$Re_{1,j}$
X	8	D	118,600
O	9	E	346,000

SEE FIG. 22 FOR SUCTION FLOW DISTRIBUTION
SEE TABLE I (CASES 8 AND 9) FOR CONFIGURATION



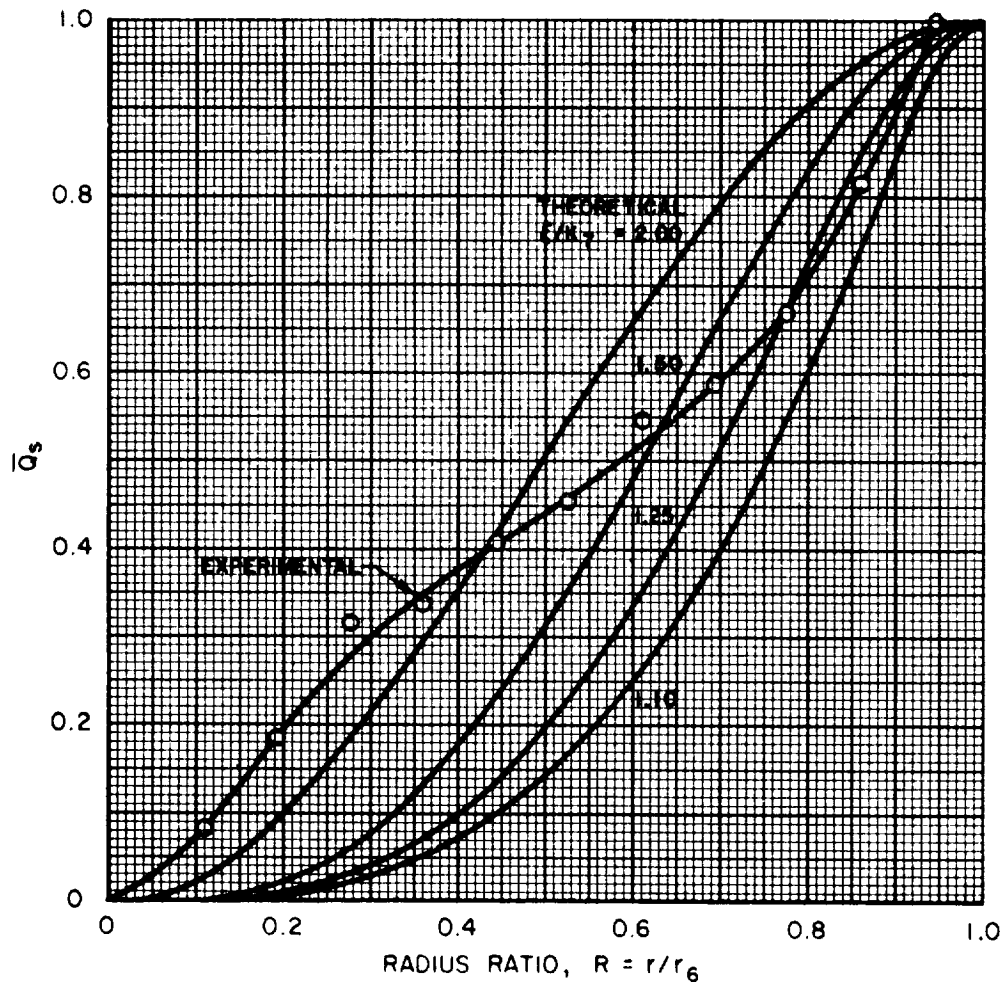
COMPARISON OF EXPERIMENTAL AND THEORETICAL DISTRIBUTION OF FLOW WITHDRAWN THROUGH END WALLS FOR SOLID-BODY ROTATION (SUCTION DISTRIBUTION C)

ANALYTICAL RESULTS FROM REF. 7

$$\bar{Q}_s \text{ (THEORY)} = \frac{\text{SECONDARY FLOW IN END-WALL BOUNDARY LAYER}}{\text{SECONDARY FLOW IN END-WALL BOUNDARY LAYER AT RADIUS } r_6}$$

$$\bar{Q}_s \text{ (EXPERIMENTAL)} = \frac{\text{SUCTION FLOW WITHDRAWN FROM CENTERLINE TO RADIUS } r}{\text{TOTAL THRU AND SUCTION FLOW WITHDRAWN FROM WALL}}$$

$$r_6 = 4.5 \text{ IN.}$$

SEE PAGE 12 FOR DEFINITION OF ξ AND K_7 

PHOTOGRAPHS OF DYE PATTERNS FOR VORTEX TUBE WITH SUCTION DISTRIBUTION B AND THRU-FLOW REYNOLDS NUMBER OF 45.7

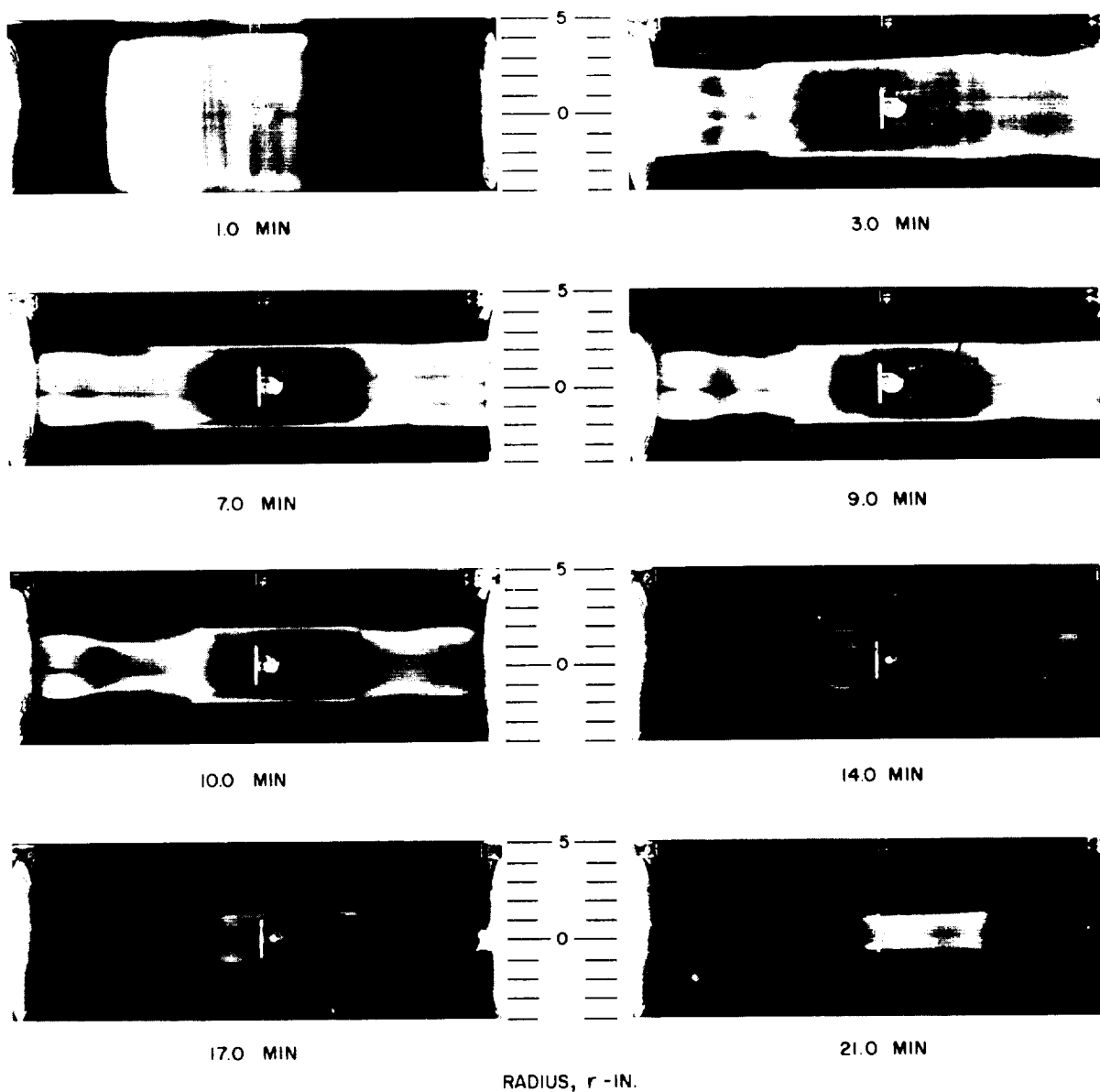
$$Re_{t,j} = 118,600$$

SEE TABLE I (CASE 6) FOR CONFIGURATION

SEE FIG. 21 FOR SUCTION FLOW DISTRIBUTION

PHOTOGRAPHS TAKEN AT INDICATED TIMES AFTER CESSATION OF DYE INJECTION

PERIPHERAL DYE INJECTION AT MIDPLANE



PHOTOGRAPHS OF DYE PATTERNS FOR VORTEX TUBE WITH SUCTION DISTRIBUTION C AND THRU-FLOW REYNOLDS NUMBER OF 2

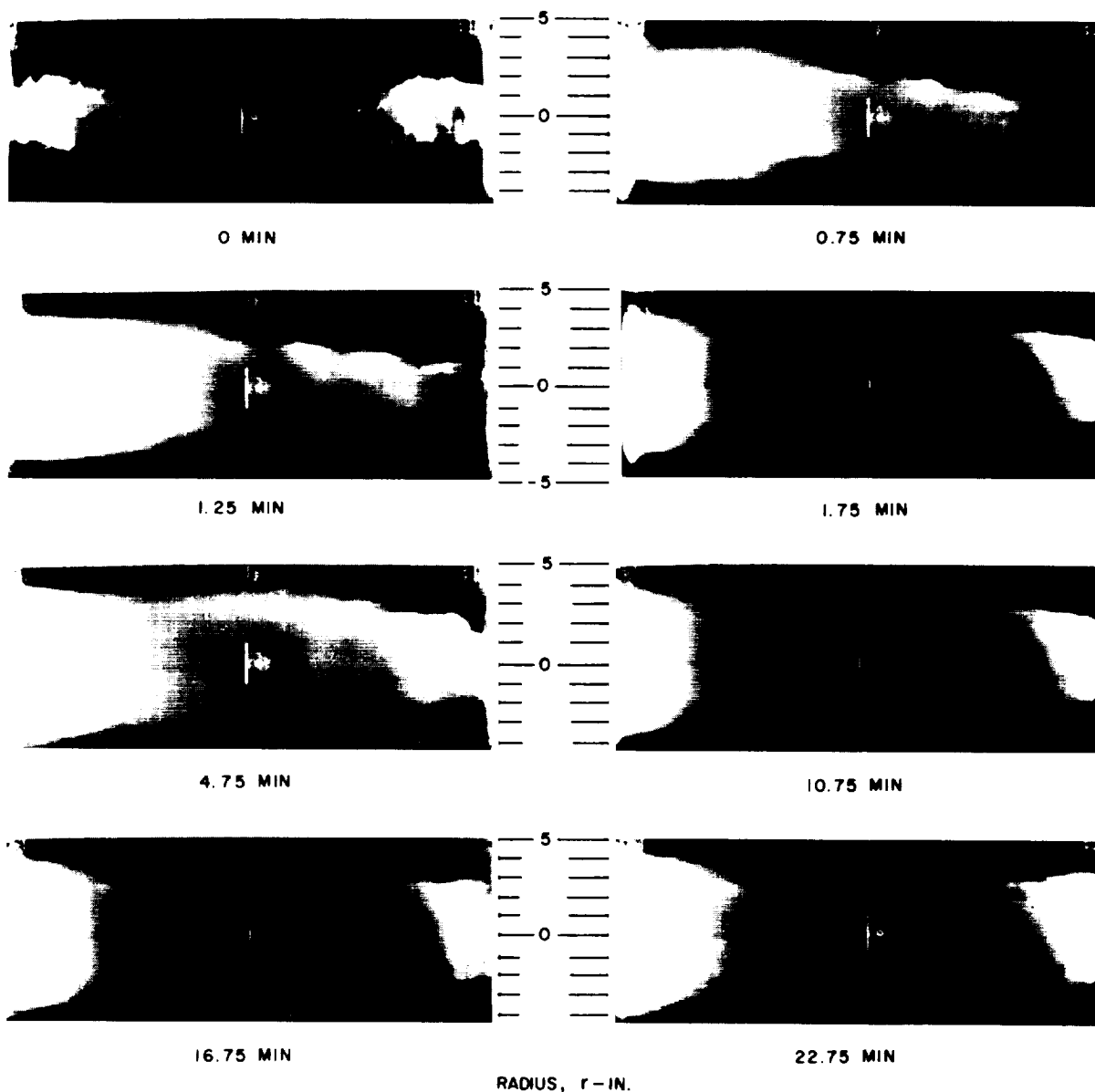
$$Re_{t,j} = 118,600$$

SEE TABLE I (CASE 7) FOR CONFIGURATION

SEE FIG. 21 FOR SUCTION FLOW DISTRIBUTION

PHOTOGRAPHS TAKEN AT INDICATED TIMES AFTER CESSATION OF DYE INJECTION

DYE INJECTION THROUGH 1/4 - IN. DIA PORTS LOCATED AT CENTER OF EACH END WALL



PHOTOGRAPHS OF DYE PATTERNS FOR VORTEX TUBE WITH SUCTION DISTRIBUTION D AND THRU-FLOW REYNOLDS NUMBER OF -3

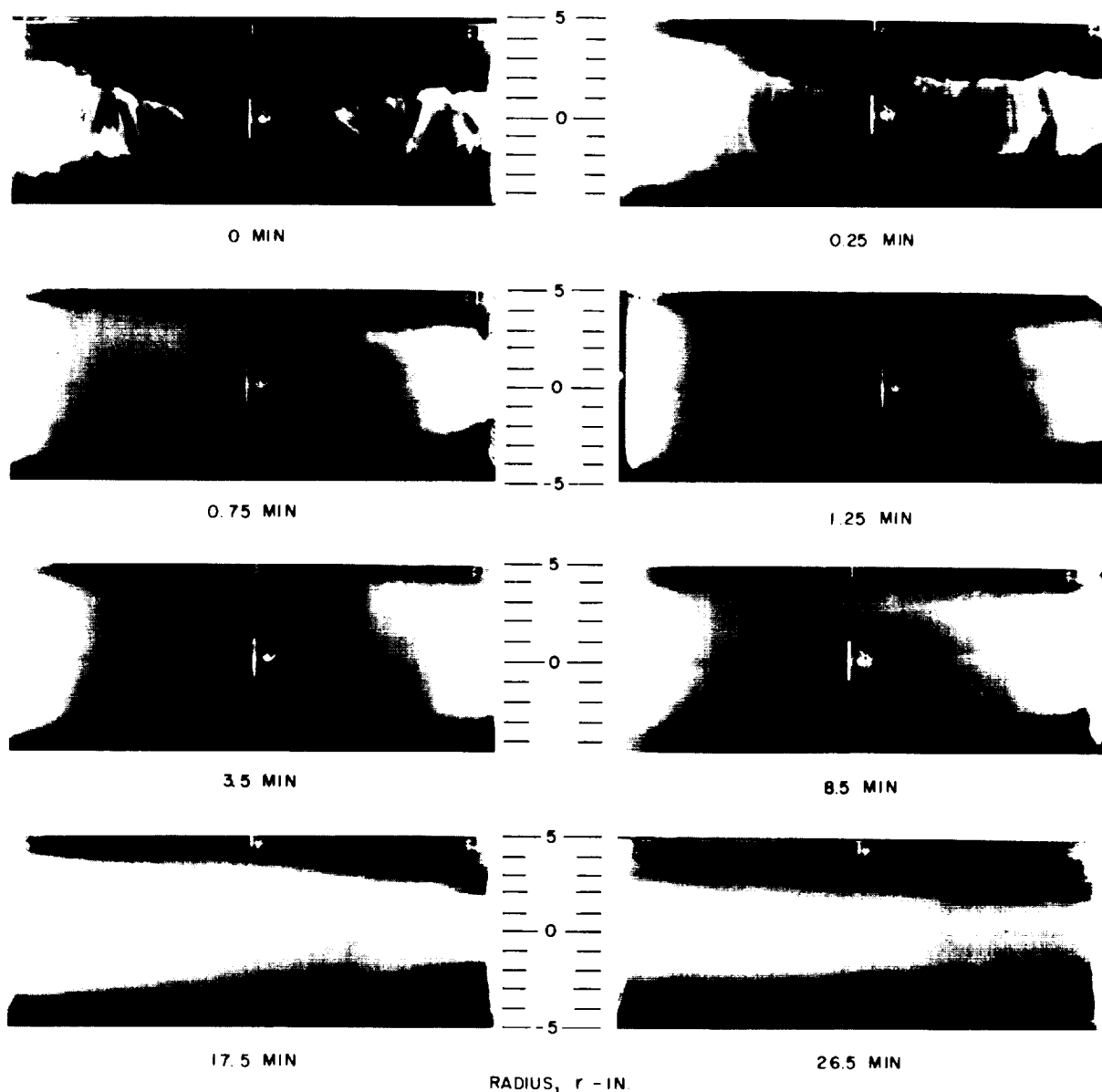
$$Re_{t,j} = 118,600$$

SEE TABLE I (CASE 8) FOR CONFIGURATION

SEE FIG. 21 FOR SUCTION FLOW DISTRIBUTION

PHOTOGRAPHS TAKEN AT INDICATED TIMES AFTER CESSATION OF DYE INJECTION

DYE AND FLUID INJECTION THROUGH 1/4-IN. DIA PORTS LOCATED AT CENTER OF EACH END WALL



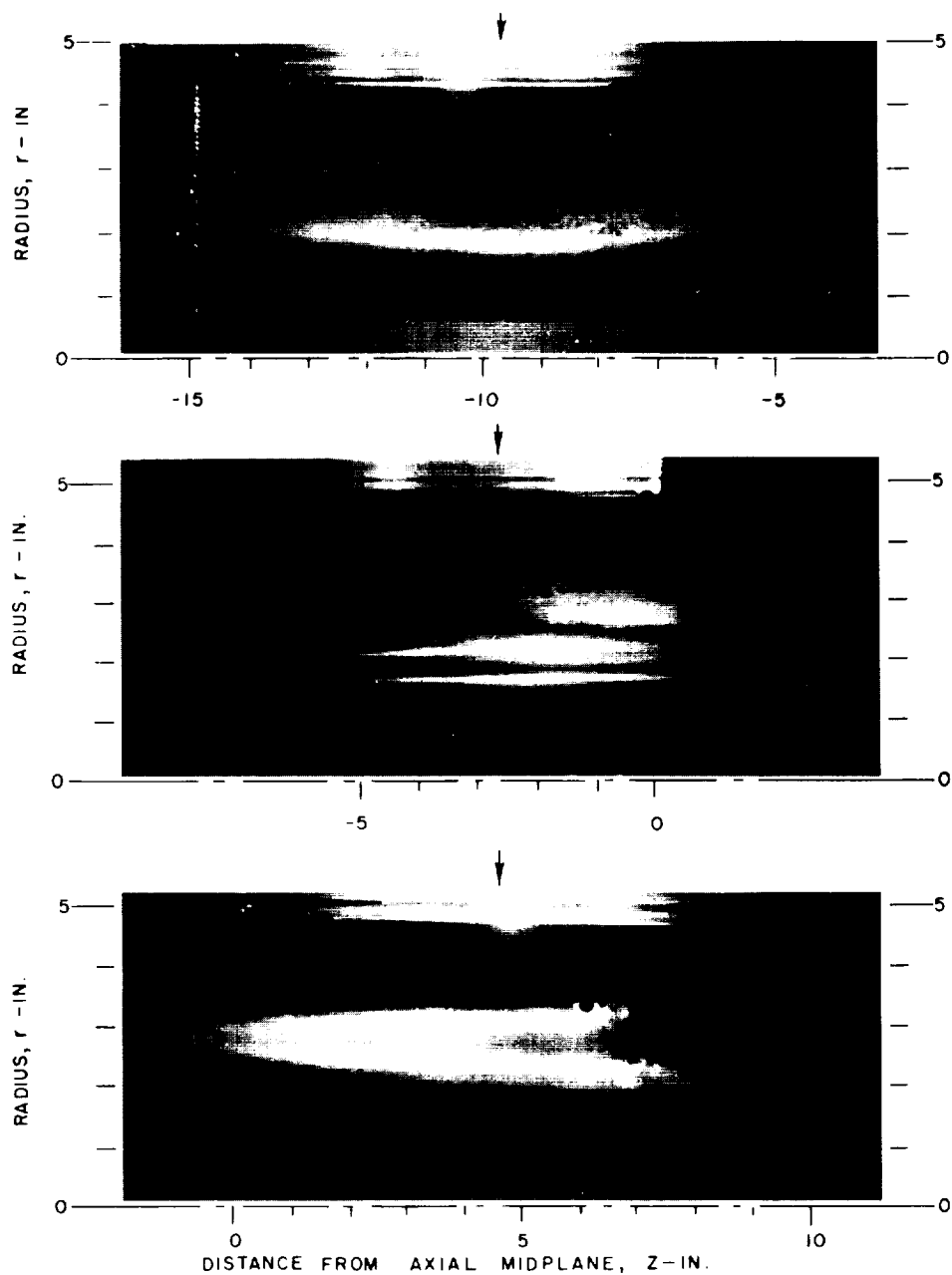
MICROFLASH PHOTOGRAPHS OF DYE PATTERNS WITH SUCTION DISTRIBUTION B AND THRU-FLOW REYNOLDS NUMBER OF 45.7

$$Re_{t,i} = 118,600$$

SEE TABLE I (CASE 6) FOR CONFIGURATION

SEE FIG. 21 FOR SUCTION FLOW DISTRIBUTION

→ DIRECTION OF ILLUMINATION



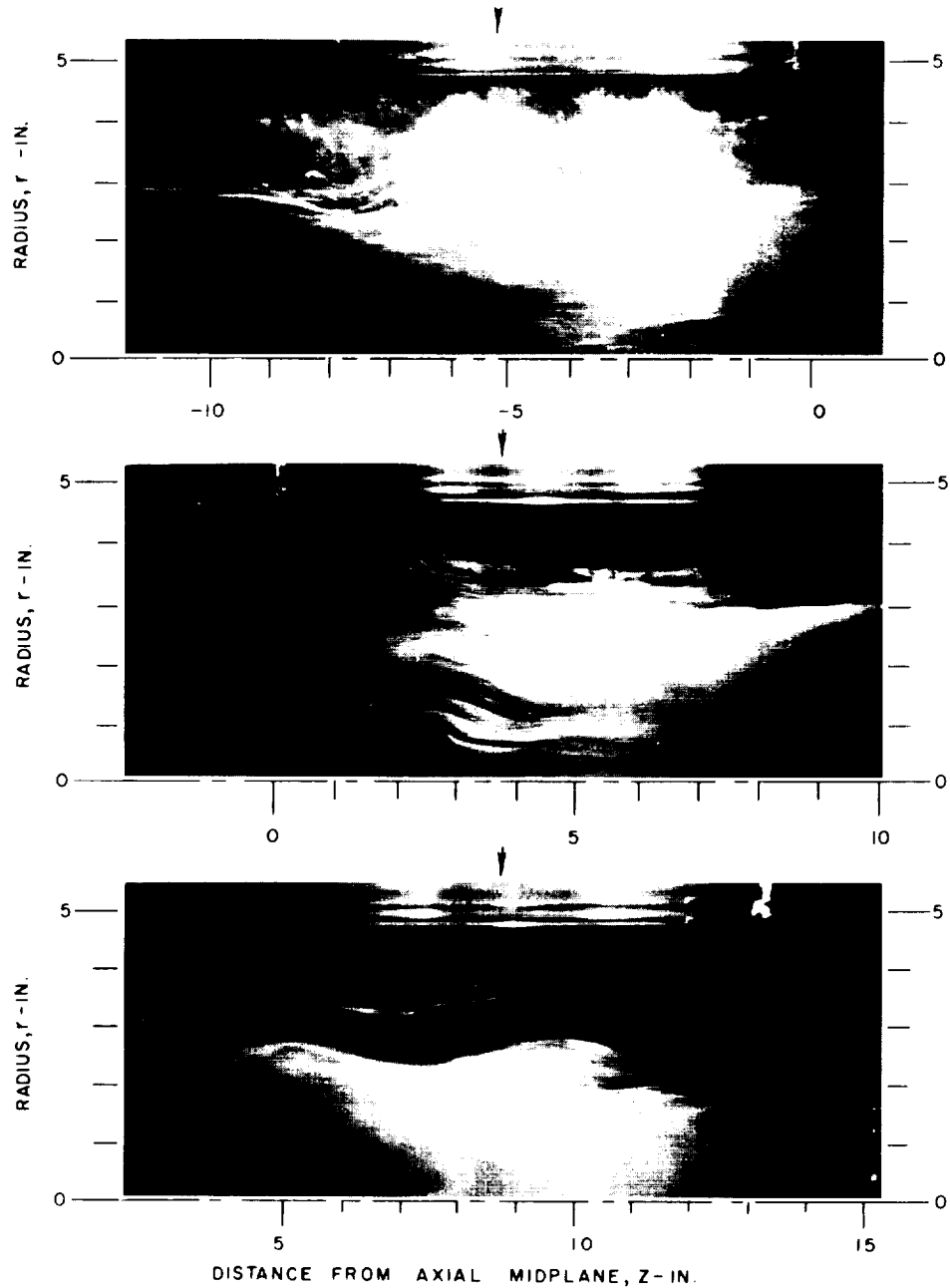
MICROFLASH PHOTOGRAPHS OF DYE PATTERNS WITH SUCTION DISTRIBUTION C AND THRU-FLOW REYNOLDS NUMBER OF 2

$$Re_{t,j} = 118,600$$

SEE TABLE I (CASE 7) FOR CONFIGURATION

SEE FIG. 21 FOR SUCTION FLOW DISTRIBUTION

—► DIRECTION OF ILLUMINATION



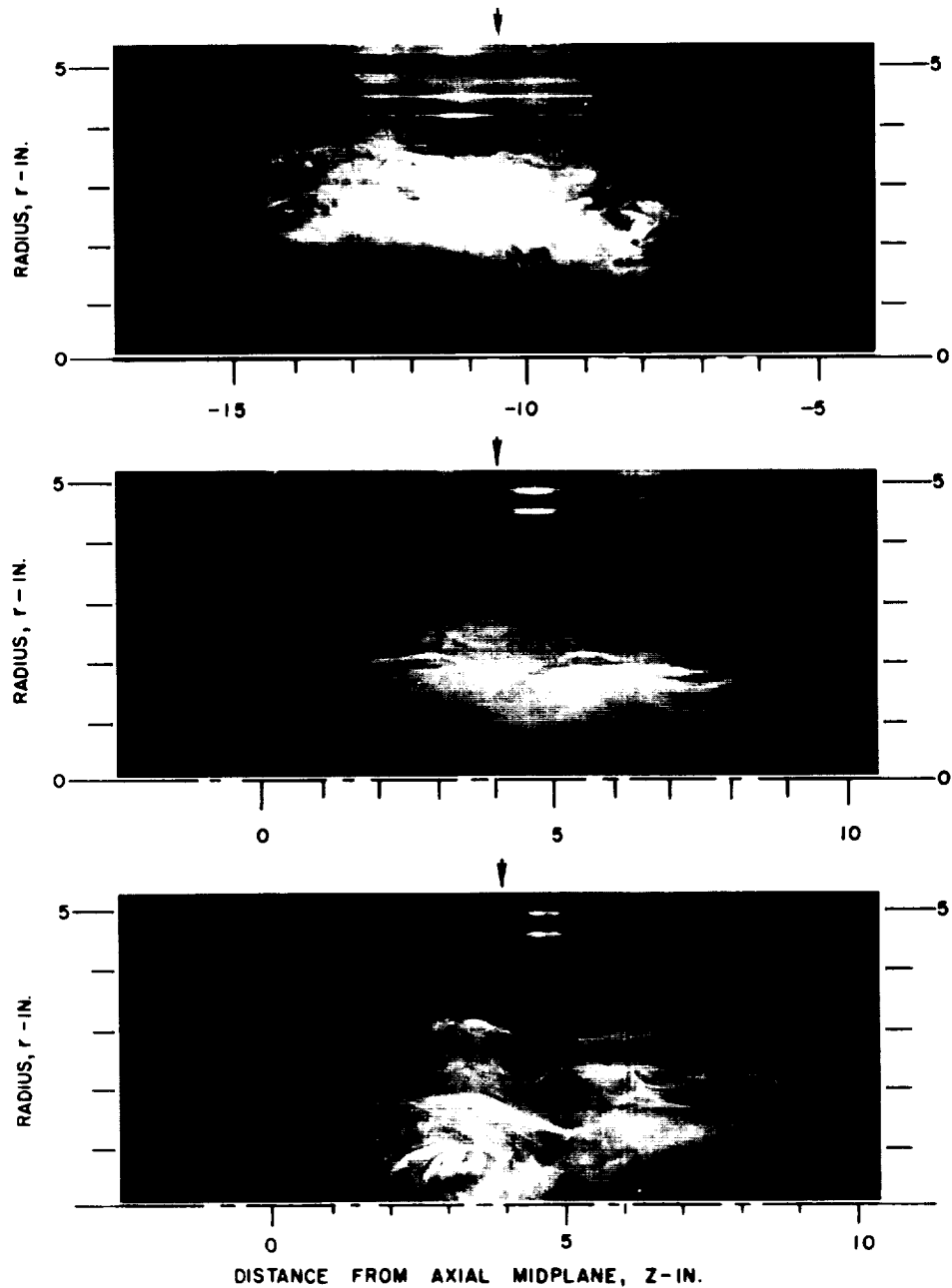
MICROFLASH PHOTOGRAPHS OF DYE PATTERNS WITH SUCTION DISTRIBUTION D AND THRU-FLOW REYNOLDS NUMBER OF -3

$$Re_{t,j} = 118,600$$

SEE TABLE I (CASE 8) FOR CONFIGURATION

SEE FIG. 21 FOR SUCTION FLOW DISTRIBUTION

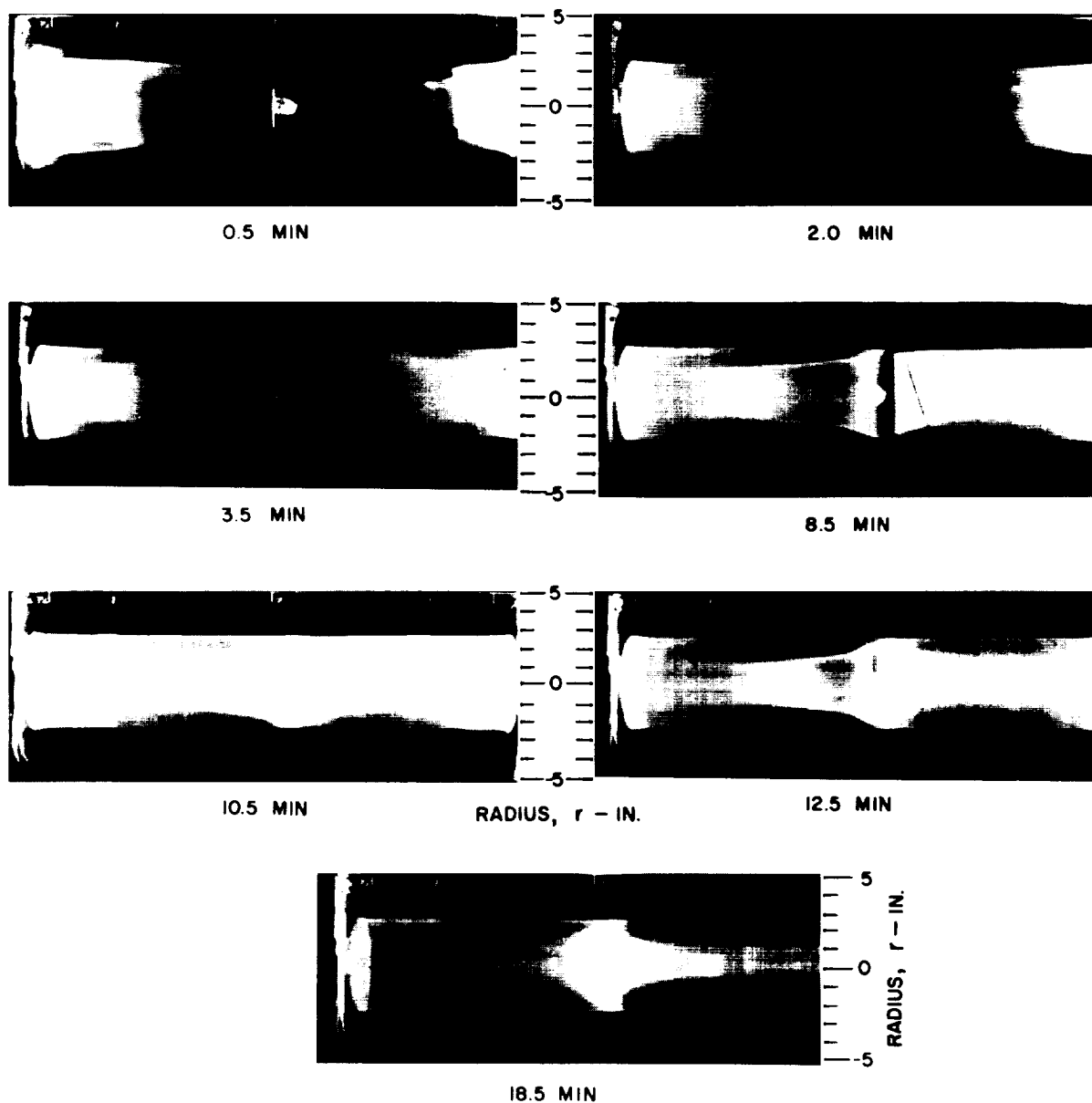
→ DIRECTION OF ILLUMINATION



PHOTOGRAPHS OF DYE PATTERNS IN VORTEX TUBE WITH PLAIN END WALLS AND THRU-FLOW REYNOLDS NUMBER OF 100

$$Re_{t,j} = 118,600$$

NO RADIAL FLUID INJECTION OR DUCTS INSERTED INTO VORTEX TUBE



PHOTOGRAPHS OF DYE PATTERNS WITH DUCTS INSERTED RADIALLY
1 INCH INTO VORTEX TUBE AND NO RADIAL FLUID INJECTION

$$Re_{t,j} = 118,600$$

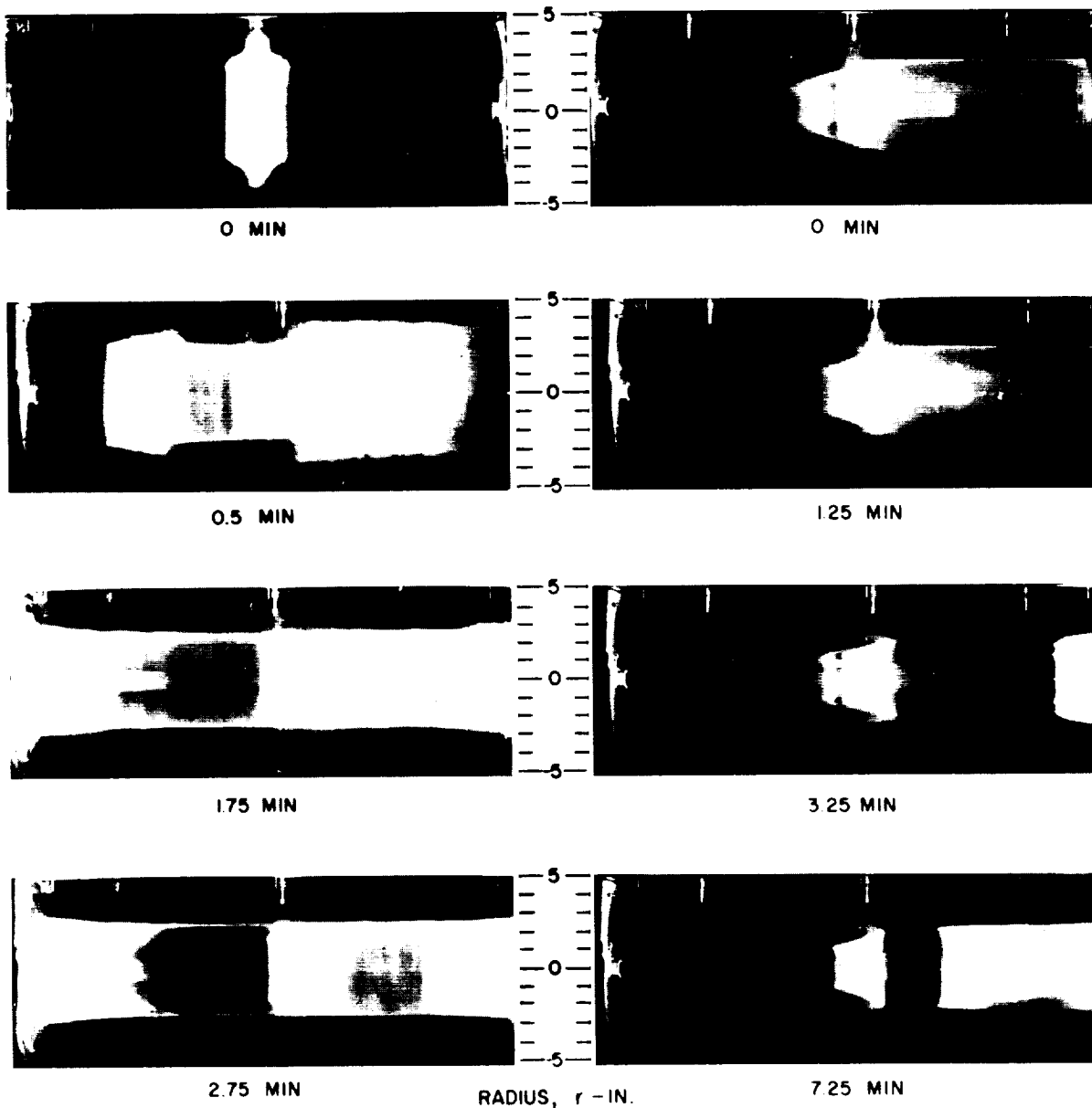
$$Re_{r,t} = 100$$

a

b

DUCT INSERTED AT MID-PLANE

DUCT INSERTED AT MID-PLANE
AND 5 IN. FROM EACH END WALL



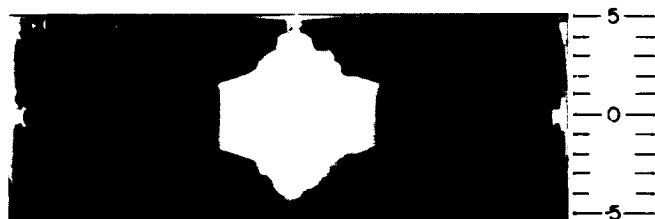
PHOTOGRAPHS OF DYE PATTERNS WITH DUCTS INSERTED RADIALLY
1.5 IN. INTO VORTEX TUBE AND NO RADIAL FLUID INJECTION

$$Re_{t,j} = 118,600$$

$$Re_{r,t} = 100$$

a

DUCT INSERTED AT MID-PLANE



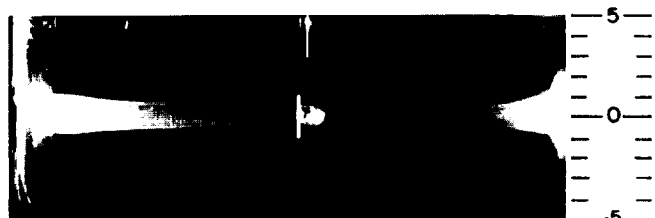
0 MIN



0.75 MIN



1.25 MIN

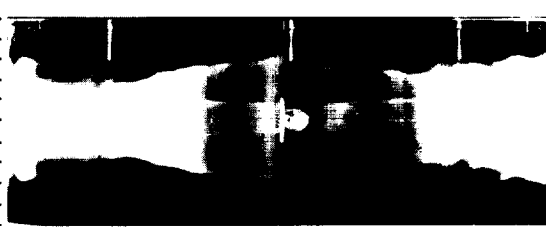


5.25 MIN

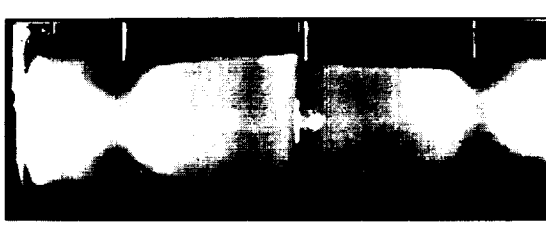
b

DUCTS INSERTED AT MID-PLANE
AND 5 IN. FROM EACH END WALL

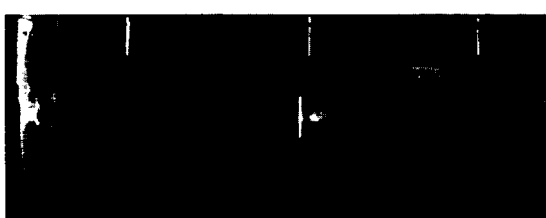
0 MIN



1.0 MIN



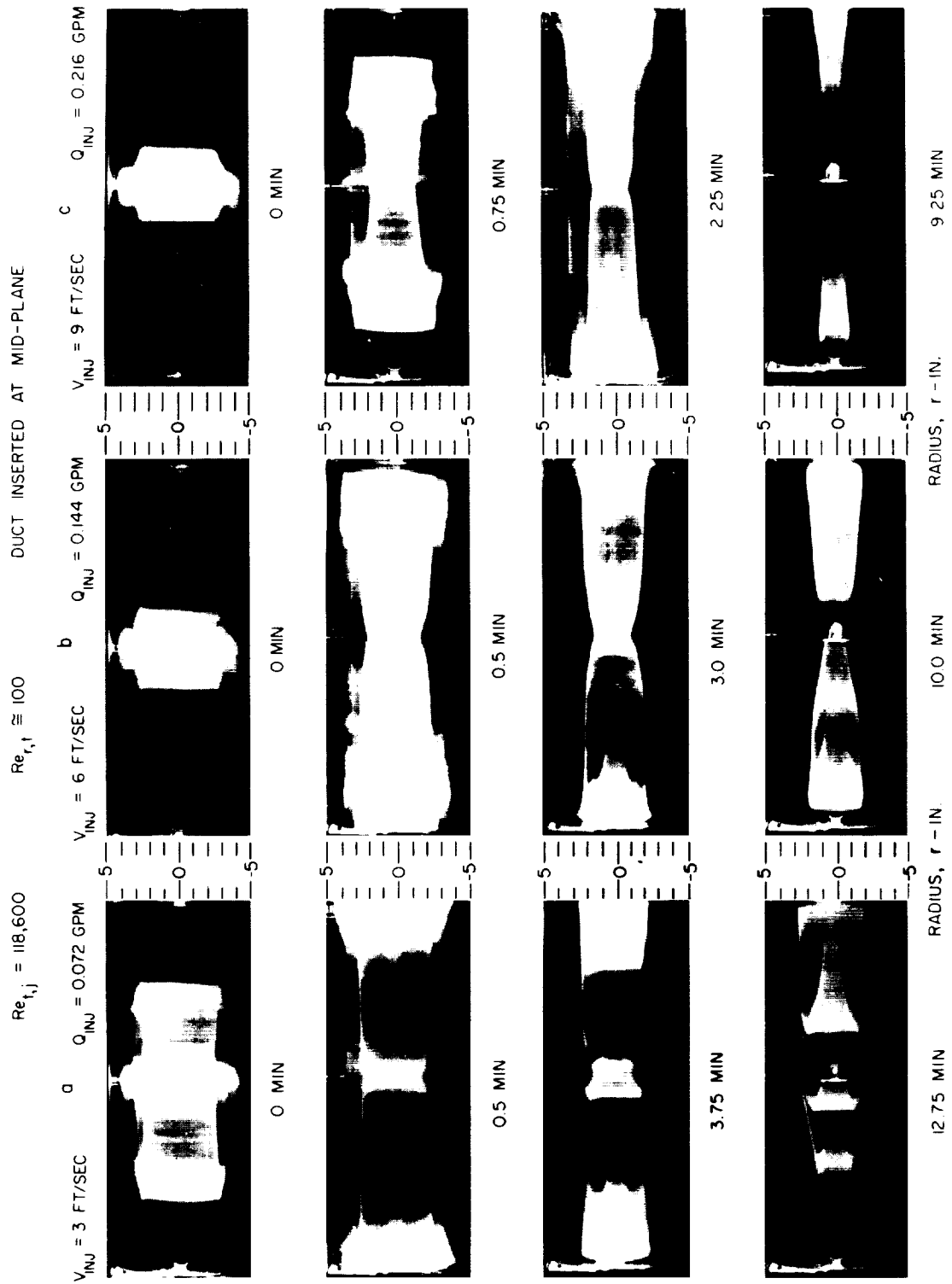
3.25 MIN



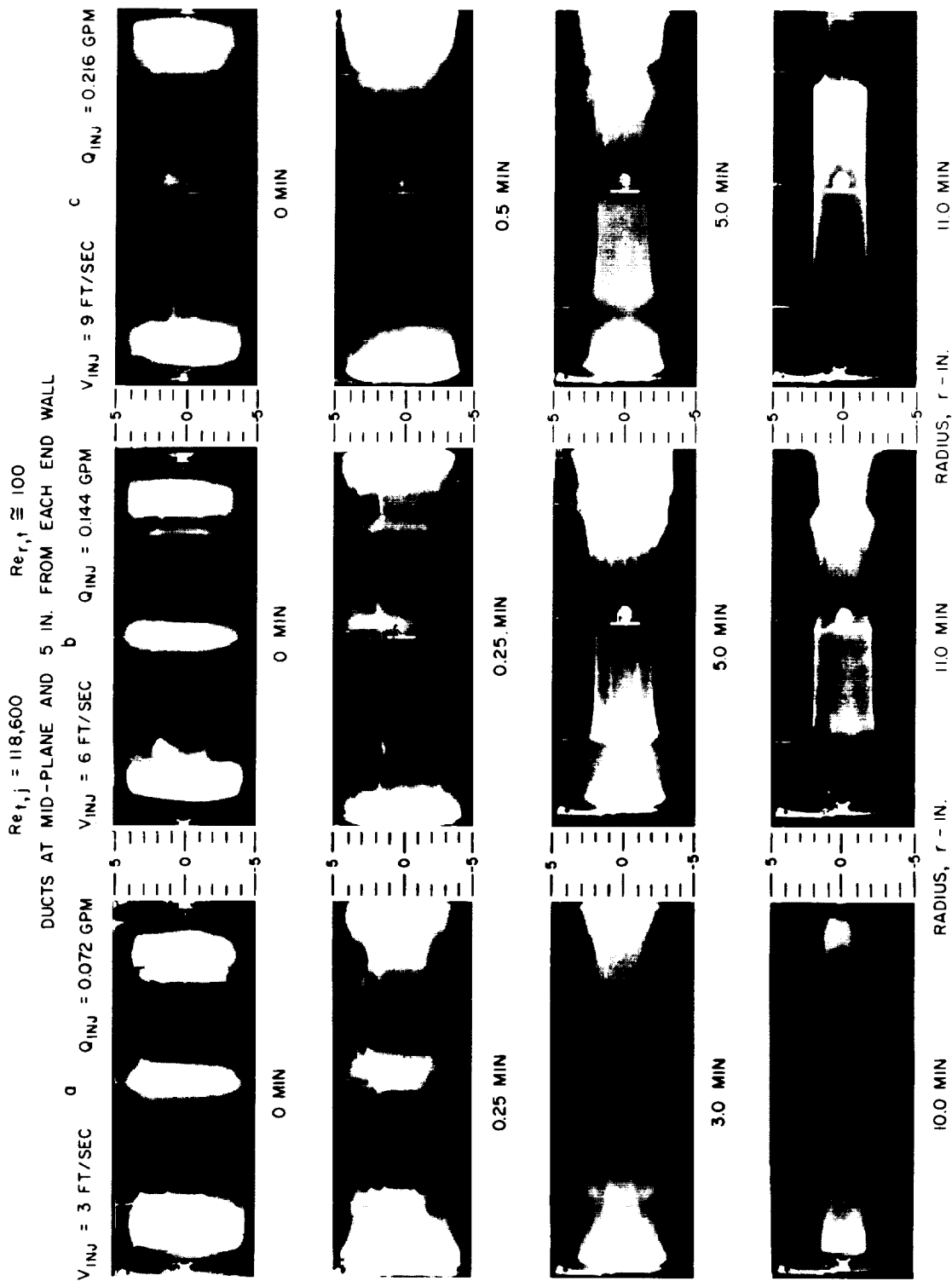
7.25 MIN

RADIUS, r - IN.

PHOTOGRAPHS OF DYE PATTERNS WITH A SINGLE DUCT INSERTED RADIALLY
1 INCH INTO VORTEX TUBE AND RADIAL FLUID INJECTION



PHOTOGRAPHS OF DYE PATTERNS WITH THREE DUCTS INSERTED RADIALLY 1 INCH INTO VORTEX TUBE AND RADIAL FLUID INJECTION



[REDACTED]

[REDACTED]